Estimation of the Life Cycle Greenhouse Gas Emissions of Bitumen-Derived Petroleum Fuels using Enhanced Solvent Extraction Incorporating Electromagnetic Heating (ESEIEH) and Toe-to-Heel Air Injection (THAI) Extraction Technologies

By

Mohsen Safaei

A thesis submitted in partial fulfillment of the requirements for the degree of

Master of Science

Department of Mechanical Engineering

University of Alberta

Abstract

There is increased focus on reduction of greenhouse gas (GHG) emissions to reduce global warming. Combustion of fossil fuels are a key contributor to emissions of GHG. Alberta is the largest hydrocarbon base in North America due to its oil sands deposit. Bitumen from oil sands is refined to produce transportation fuels. Current process of extraction of bitumen through surface mining and steam assisted gravity drainage (SAGD) methods are GHG intensive. National and global initiatives for GHG reduction have triggered the focus on development of cleaner and more efficient bitumen extraction technologies. Toe-to-heel air injection (THAI) and enhanced solvent extraction incorporating electromagnetic heating (ESEIEH) are two emerging bitumen extraction technologies and are expected to emit lower GHG emissions than current recovery methods. THAI uses compressed air, while in ESEIEH, radio frequency (RF) energy along with solvent is used to recover bitumen. Since these methods are at the early stages of development, a detailed investigation and quantification of their GHG footprints over life cycle are necessary for decision making and policy formulation.

The goal of this research is to develop bottom-up models to quantify the energy use and GHG emissions in these two recovery methods in various production pathways and energy scenarios. The developed model for THAI is used to assess the energy and GHG emission intensity from bitumen extraction, upgrading, transportation, refinery, and final use in vehicles, while the ESEIEH model, because of the lack of data on the properties of the produced bitumen, examines only the recovery process. The impacts of cogeneration, renewable electricity sources, and alternative configurations of surface facilities on ESEIEH emissions are explored. Sub-process mass-based allocation is used

to allocate the refinery emissions to the transportation fuels. A Monte Carlo simulation was used to perform the uncertainty analysis on the models to arrive at the most realistic range of GHG emissions.

The GHG emissions in ESEIEH range from 10 to 88 kg CO_2eq/bbl of bitumen. The wide range is mainly due to the electricity source, as electricity comprises 77% of the total energy required. Antenna efficiency and the reservoir's cumulative electricity-to-oil ratio (cEOR) had the greatest effect on overall GHG emissions in ESEIEH. Well-to-combustion (WTC) emissions in THAI range from 111-116 gCO_2eq/MJ of gasoline, 114-117 gCO_2eq/MJ of diesel, and 106-112 gCO_2eq/MJ of jet fuel depending on the pathway and input range considered for the uncertainty analysis. The combustion of transportation fuels in the vehicle engine shows the highest WTC emissions with a share of 63-69% followed by the extraction stage with 22-25%. The air-to-oil ratio (AOR) and CO_2 content of the produced gas have the largest effect on GHG emissions results in THAI. The SAGD GHG emissions from various studies were compared with this study's results and revealed that GHG emissions from THAI are in the same range as from SAGD.

The results of this study can help both government and the oil sands industry make emissions-reduction decisions. The results highlight which additional data is required from industry to increase the accuracy of GHG emissions estimates.

Preface

This thesis is the original work by Mohsen Safaei under the supervision of Dr. Amit Kumar. Chapter 2 will be submitted as Safaei, M., Oni, A.O., Gemechu, E.D., Kumar, A., “Evaluation of energy consumption and GHG emissions of bitumen extraction in the Enhanced Solvent Extraction Incorporating Electromagnetic Heating process” to a peer-reviewed journal. Chapter 3 is prepared for submission to a peer-reviewed journal as Safaei, M., Oni, A.O., Gemechu, E.D., Kumar, A., “Well-to-combustion greenhouse gas emissions assessment of bitumen recovery using the toe-to-heel air injection method.” I was responsible for the concept formulation, data collection, analysis, model development, and manuscript composition. Dr. Abayomi Olufemi and Dr. Eskinder Gemechu assisted in the model development and manuscript edits. Dr. Amit Kumar was the supervisory author and was involved with concept formulation, evaluation, assessment of results, and manuscript edits.

To my lovely parents, family, and friends for their support and encouragement.

Mohsen Safaei

September 2018

Acknowledgments

I would like to acknowledge the NSERC/Cenovus/Alberta Innovates Associate Industrial Research Chair in Energy and Environmental Systems Engineering and the Cenovus Energy Endowed Chair in Environmental Engineering for providing financial support for this project. I am grateful to the representatives from Cenovus Energy Inc., Suncor Energy Inc., Alberta Innovates (AI), Environment and Climate Change Canada (ECCC) and Natural Resources Canada (NRCan), Dr. Alex Turta (AT EOR Consulting Inc.), Dr. Malcolm Greaves (University of Bath), and Chris Patterson (Devon Canada) for their input and comments on this study.

I am deeply thankful to my supervisor, Dr. Amit Kumar, who gave me this wonderful opportunity to conduct my research in his group. His in-depth knowledge of the topic and valuable feedback on my work broadened my horizon on energy issues globally and helped me to improve my analytical and presentation skills. I greatly admire Dr. Kumar's ability to supervise the research and help students whenever necessary.

Additionally, I would like to acknowledge my examining committee members for their interest and time for my research and their valuable comments on my work. I express my sincere gratitude to Dr. Abayomi Olufemi Oni and Dr. Eskinder Gemechu, the postdoctoral fellows whom I had the privilege to work with. Thank you so much for your time and valuable input in my work and reviewing my papers, models, and thesis. Your feedback and comments helped me to significantly improve the quality of this work. I would like to also thank Astrid Blodgett for editing this work.

I acknowledge and thank my friends in the Sustainable Energy Research Group, Ali Alizade, Anil Katta, Elvis Ibdan, Giovanni Di Lullo, Madhumita Patel, Mohammad Ikthair Hossain Soiket, Ankit Gupta, Saeidreza Radpor, and Tanveer Hassan Mehedi for all the wonderful memories during these two years.

I also appreciate the continuous emotional support of my close friends, Hosein Bahari, Arian Velayati, Saeid Adabjo, Mansour Saffar, Nima Khakpoor, Farzad Ahmadi, Mehdi Nosrati, and Jessica Abella. Thank you so much for always being available and helping me to overcome the challenges I faced during living abroad.

I must confess that I could not have accomplished 19 years of schooling without the care, support, and continuous motivation of my wonderful parents and siblings.

Above all, I thank God for all the help He gave me during my life. Whenever I felt hopeless and disappointed, I felt Him touching my heart and showing me the right pass and the solution.

Table of Contents

Abstract ii

Preface iv

Acknowledgments vi

Table of Contents viii

List of Figures xi

List of Tables xiii

Abbreviations xv

Chapter 1: Introduction 1

1.1 Background 1

1.2 Literature review and research gaps 4

1.3 Research motivations 6

1.4 Research objectives 7

1.5 Scope and limitation of the thesis 8

1.6 Organization of the thesis 9

Chapter 2: Evaluation of energy and GHG emissions' footprints of bitumen extraction using Enhanced Solvent Extraction Incorporating Electromagnetic Heating technology 10

2.1 Introduction 10

2.2 Method 15

2.2.1 Process description 16

2.2.2 Simulation of the ESEIEH process 21

2.2.3 Scenarios for assessment of GHG emissions 26

2.2.4 Sensitivity and uncertainty analyses 27

2.3 Results 28

2.3.1 Extraction process 30

2.3.2 Separation process 31

2.4 Discussion 33

2.4.1 Extraction and separation process 33

2.4.2 The impact of electricity sources on the ESEIEH process 36

2.5 Conclusion 40

Chapter 3: Life cycle assessment of bitumen-derived transportation fuels from toe-to-heel air injection extraction technology 42

3.1 Introduction 42

3.2 Method 46

3.2.1 Goal and scope definition 47

3.2.2 Process description and data acquisition 49

3.2.3 Model development 54

3.2.4 Sensitivity and uncertainty analyses 63

3.3 Results and discussion 68

3.3.1 Extraction and surface facilities 68

3.3.2 Upgrading 70

3.3.3 Refinery 72

3.3.4 Crude transportation 76

3.3.5 The WTC comparative assessment results 77

3.3.6 Uncertainty analysis 78

3.3.7 Comparison of life cycle GHG emission of THAI with SAGD and Surface Mining 81

3.4 Conclusion 82

Chapter 4: Conclusion and Recommendations for Future Work 83

4.1 Conclusion 83

4.2 Greenhouse Gas Footprint of ESEIEH Method for Bitumen Extraction 83

4.4 Greenhouse Gas Footprint of (THAI) for Bitumen Extraction 85

4.4 comparison of WTC GHG emissions of transportation fuel production from THAI process with SAGD and surface mining 87

4.5 Recommendations for Future Work 87

Bibliography 89

Appendix A 116

Appendix B 122

List of Figures

Fig. 2.1. Schematic diagram of the ESEIEH process 14

Fig. 2.2. Schematic of transportation fuel production using the bitumen extraction through the ESEIEH process 16

Fig. 2.3. Schematic diagram of the ESEIEH extraction and separation process 17

Fig. 2.4. The impact of electricity sources on the ESEIEH process (Pathway II) 38

Fig. 2.5. Uncertainty analyses of the difference sources of electricity on the ESEIEH process (Pathway II) 38

Fig. 2.6. Tornado plots. (a) Current Alberta electricity mix, (b) 2030 Alberta electricity mix, (c) Cogeneration, (d) Biomass..... 39

Fig. 3.1. High level diagram of the THAI process 45

Fig. 3.2. Cradle-to-grave schematic of transportation fuel production from bitumen..... 49

Fig. 3.3. Unit operations involved in extraction units for bitumen extraction in the THAI process 50

Fig. 3.4. Process flow diagram of the upgraders for processing THAI-based bitumen…… 52

Fig. 3.5. Deep conversion refinery configuration for processing of THAI-based bitumen..... 53

Fig. 3.6. Shares of energy use and GHG emissions in different unit operations in crude extraction in the THAI process..... 69

Fig. 3.7. GHG emissions contribution from different unit operations in delayed coking (DCU) and hydroconversion (HCU) upgraders..... 72

Fig. 3.8. Share of energy use in refining of bitumen, delayed coker SCO, and hydroconversion SCO 74

Fig. 3.9. GHG emissions associated with refining bitumen and SCO..... 76

Fig. 3.10. Tornado plots for the WTC emissions in the production of gasoline in different pathways. (a): Pathway 1; (b): Pathway 2; (c): Pathway 3 79

Fig. 3.11. Uncertainty in WTC GHG emissions in the production of transportation fuels from THAI 80

List of Tables

Table 2.1: Input data in the model for evaluation of energy consumption and GHG emissions in bitumen extraction via ESEIEH ……..... 21

Table 2.2: Input parameters and their distributions for uncertainty analysis for bitumen recovery using ESEIEH method 28

Table 2.3: Energy and GHG emissions of the ESEIEH process 30

Table 3.1: Input values for the calculation of energy use and GHG emissions in the extraction stage 55

Table 3.2: Input values for the calculation of energy use and GHG emissions in the upgrading stage 58

Table 3.3: Upgrader product specifications 59

Table 3.4: Input values for the calculation of energy use and GHG emissions in the refining stage 61

Table 3.5: Input values for the calculation of energy use and GHG emissions in the transportation, delivery, and distribution stages 62

Table 3.6: Range of variables considered for the sensitivity analysis 65

Table 3.7: Input parameter ranges and distribution for the Monte Carlo simulation 66

Table 3.8: Upgrader yields and utility consumption 70

Table 3.9: Refinery yields and utility consumption 73

Table 3.10: Breakdown of WTC emissions in the production of transportation fuels through different pathways (gCO2eq./MJ) 77

Abbreviations

ADU	Atmospheric distillation unit
AOR	Air-to-oil ratio
AGO	Atmospheric Gas Oil
API	American Petroleum Institute
AR	Atmospheric residue
bbl	Barrel
bpd	Barrels per day
cEOR	Cumulative electricity-to-oil ratio of the reservoir
CFS	Clean Fuel Standard
CH_4	Methane
CO_2	Carbon dioxide
cp	Centipoise
CSS	Cyclic steam stimulation
DC	Delayed coker
DCU	Delayed coking upgrader
DEA	Diethanolamine
DHT	Diesel hydrotreating unit
DR	Diluent ratio
EF	Emission factor
EM	Electromagnetic
ESEIEH	Enhanced Solvent Extraction Incorporating Electromagnetic Heating
FCC	Fluid catalytic cracking
FWKO	Free water knock out
gCO_2eq	Grams of carbon dioxide equivalents
GHG	Greenhouse gas
GHT	Gasoil hydrotreating unit
Gj	Gigajoule
GOR	Gas-to-oil ratio

GWP	Global warming potential
H_2S	Hydrogen sulfide
HC	Hydroconversion
HC	Hydrocracking
HCU	Hydroconversion upgrader
HT	Hydrotreater
HVGO	Heavy Vacuum Gas Oil
IPCC	Intergovernmental Panel on Climate Change
ISC	In situ-combustion
ISO	International Organization for Standardization
KHT	Kerosene hydrotreating unit
LCA	Life cycle assessment
LCFS	Low-Carbon Fuel Standard
LHV	Lower heating value
LPG	Liquefied petroleum gas
LVGO	Light Vacuum Gas Oil
MJ	Mega-joule
Mbpd	Million barrels per day
N_2O	Nitrous oxide
NG	Natural gas
NHT	Naphtha hydrotreating unit
P5	5th percentile
P95	95th percentile
PFS	Plant fuel system
R&D	Research and development
SAGD	Steam-assisted gravity drainage
SBR	Solvent based recovery
SCO	Synthetic crude oil
SGP	Saturated gas plant
SMR	Steam methane reforming
T&D	Transportation and distribution

TEG	Triethylene glycol
THAI	Toe-to-heel air injection
UGP	Unsaturated gas plant
VDU	Vacuum distillation unit
VR	Vacuum residue
WTC	Well-to-combustion

Chapter 1: Introduction

1.1 Background

The increase in global energy demand, limited availability of conventional fossil fuels and associated environmental concerns have led to the search for new energy sources. The oil sands are one of the promising energy sources to tackle this problem because of their abundance and the readiness of mature recovery and processing technologies. Alberta's oil sands, with 165.4 billion barrels of proven reserves, are the third largest crude resources in the world after those in Saudi Arabia and Venezuela [1]. Currently, Alberta produces 3.0 million barrels of bitumen per day (mbpd) and exports 64% of it to the United States [2, 3]. It is the largest hydrocarbon base in North America [1].

The oil sands are composed of mineral solids, water, and bitumen. Bitumen is separated from this mixture in order to produce synthetic crude oil (SCO) [4]. Bitumen can be extracted through surface mining and through in situ extraction methods. Current bitumen production through surface mining and in situ methods are 1.4 and 1.6 mbpd, respectively [1]. Unlike conventional oil, bitumen is almost immobile at room temperature because it is highly viscous [5]. Thus, viscosity reduction techniques are required to mobilize the bitumen and extract it from the reservoir. Viscosity reduction is critical for bitumen extraction from in situ. In addition, not every refinery can refine the bitumen because of its high sulfur, metal, and nitrogen content and low hydrogen-to-carbon ratio [6]. Experimental results have shown that bitumen viscosity drops significantly with an increase in the temperature [7]. Steam assisted gravity drainage (SAGD) and cyclic steam stimulation (CSS) are the current commercialized in situ methods; both use a

considerable amount of steam to deliver heat to the reservoir to mobilize the bitumen. Thus both are highly energy and greenhouse gas (GHG) emissions intensive [8]. In order to transport bitumen by pipeline, it needs to be mixed with lighter hydrocarbons, such as natural gas condensates or naphtha. The mixture is either sent directly to the refinery or directed to the upgrader unit where it is converted to a higher quality product called SCO through a series of chemical and physical processes [9]. Upgrading bitumen enables it to be processed in most refineries. It is generally more energy and emissions intensive to upgrade and refine bitumen than conventional crudes, mainly because of the high heat and hydrogen requirements for breaking its bonds and decreasing its impurities, respectively [10-13]. Because of these processes, bitumen recovery and upgrading are currently responsible for 9.8% of Canada's GHG emissions [14].

Growing understanding of the economic, health, and social impacts of climate change have triggered the implementation of regulations and policies to reduce global GHG emissions. The transportation sector is responsible for 20% of global GHG emissions [15] and, given this high share, there have been many attempts to reduce the GHG intensity of this sector as a solution to tackle the global climate change. The European Fuel Quality Directive [16] and the California Low-Carbon Fuel Standard (LCFS) [17] mandate reductions of 10% and 6%, respectively, on the life cycle GHG emissions of transportation fuels by 2020. The government of Canada is committed to reduce its GHG emissions by 30% compared to 2005 level by 2030 [18]. In addition, the Clean Fuel Standard (CFS) initiative of the government of Canada aims to reduce the GHG emissions from all fuels by 30 million tonnes in 2030 [19]. These targets and inherent large emissions intensity of

oil sands-derived transportation fuels have triggered the development of cleaner and more efficient bitumen recovery methods to satisfy global energy demand.

Emerging bitumen recovery methods aim to reduce water, energy, and associated GHG emissions in the extraction stage. In addition, there have been many efforts to improve the quality of the bitumen inside the reservoir to ease transportation and increase its commercial value. Enhanced Solvent Extraction Incorporating Electromagnetic Heating (ESEIEH) and Toe-to-Heel-Air-Injection (THAI) processes are two of these new recovery methods [20, 21]. In ESEIEH, radio frequency energy is used to heat the reservoir and solvent is added to the formation to further reduce bitumen viscosity and precipitate its heaviest components to partially upgrade its physical and chemical properties [20]. In THAI, a small portion of the reservoir is burned and the generated heat mobilizes the bitumen and thermally cracks its heavy residue, thus converting it to a lighter crude [22, 23]. Though these methods are expected to have lower environmental footprints than SAGD, there is a need to appropriately quantify the life cycle GHG emissions of these methods to understand the hotspots and improvements needed at each life cycle stage. The environmental footprints associated with solvent use, recovery, and electricity consumption in ESEIEH need to be assessed. Yet GHG emissions from reservoir combustion and handling the produced gas need to be quantified in the THAI process.

Life cycle assessment (LCA) is a widely used standardized environmental assessment tool used to evaluate the sustainability performance of a product that takes into account the material and energy requirements throughout the life cycle stages from extraction of natural resources to manufacturing, use, recycling, and final disposal [24-26]. According to the International Organization for Standard (ISO), LCA has four main stages: goal and

scope definition, life cycle inventory, life cycle impact assessment, and interpretation [25, 27]. In the first stage, the purpose of the study is stated and the system boundary, functional unit, assumptions, limitations, and allocation methods identified. The life cycle inventory is a list of all material and energy inputs and the associated emissions released in each life cycle. The impact assessment stage links the inventory results to a number of environmental problems such as the effects on global warming or human health. During the last stage, interpretation, the researcher seeks to identify the significant contributors to the overall results and energy, material, and environmental footprint reduction practices [24].

1.2 Literature review and research gaps

About 80% of the bitumen deposits in Alberta can be recovered through in situ methods [6]. Currently, bitumen production from in situ recovery in Alberta is about 1.6 mbpd (57% of total production) and this value is projected to reach 2.22 mbpd by 2030 [7]. Commercialized in situ recovery methods such as CSS and SAGD use large amounts of water and natural gas to produce steam for bitumen recovery [2]. The large energy requirements result in GHG emissions of 45-190 kg CO_2 eq. to extract one barrel of bitumen [3, 8]. The produced bitumen is also viscous and impure, thus it requires diluent to reduce its viscosity, to meet pipeline transportation specifications and upgrading, and to meet refinery specifications. [3]. In addition, the upgrading level (partial or full) influences how much of a resource such as hydrogen for hydrotreating and cracking is used in the refinery [9, 10]. Thus, new bitumen recovery technologies that could improve the environmental performance of petroleum fuels through their entire life cycle stages such as THAI, ESEIEH, and others are being investigated.

In the THAI method, pressurized or enriched air is injected into the reservoir to initiate combustion. The combustion heat reduces bitumen viscosity and burns its heavy components while improving bitumen quality [28]. Although THAI technology is not yet commercialized, there are three ongoing research and development (R&D) projects in Canada, China, and India [29]. Research shows that THAI recovery has a high oil recovery factor (up to 85%), significantly reduces bitumen viscosity, and increases its API [30]. Furthermore, the aromatics, resins, and asphaltene contents of bitumen are lowered [31], thus reducing the environmental burden during bitumen upgrading and refining. The application of THAI as a bitumen recovery method is promising and its environmental impacts associated with the entire life cycle stages of petroleum fuels derived from oil sands in terms of GHG emissions needs to estimate.

ESEIEH combines both electromagnetic heating and solvent extraction techniques. The antenna is placed horizontally in the reservoir to preheat the reservoir and solvent is then injected to further reduce viscosity. ESEIEH is considered to require a relatively lower solvent-to-oil ratio (SOR) and operate at a lower temperature than solvent-based and steam-based methods, respectively [20]. Furthermore, it could have a higher oil recovery factor than CSS and SAGD [32].

While there have been many studies on understanding these two processes and identifying areas for further improvement, there has been little work done on assessing the associated life cycle GHG emissions with these methods. Only Patterson [32] and Boone and colleagues [33] have made attempts to quantify the GHG emissions associated with bitumen recovery using the ESEIEH and THAI processes, respectively. The main issues with their studies are in the definition of the system boundaries and the

unclear and not transparent inputs, assumptions, and methods. In addition, these studies cannot assess the uncertainties in the overall results because of different operating conditions and reservoir properties. Furthermore, the studies are limited to the extraction stage and do not quantify the associated GHG emissions with the partially upgraded bitumen in the upgrading and refining stages.

There are different LCA models and studies relevant to the GHG emissions for transportation fuel production from the oil sands [10-13, 34-38]. The main problem with these models is that they are made for commercialized bitumen recovery methods and unable to simulate different recovery processes and analyze different feedstocks in the upgrader and refinery stages. Thus, a transparent LCA model that covers all the life cycle stages of transportation fuel production using ESEIEH and THAI and also identifies hotspots in the process and quantifies the uncertainties associated with different operating conditions and reservoir properties is needed. This model will provide a framework for policy makers both at industry and national levels to make emissions reduction and investment decisions and further develop climate policies. Additional detailed literature review is presented in chapters 2 and 3.

1.3 Research motivations

The following factors motivated this research:

- Current LCA models only report the life cycle GHG emissions of commercialized bitumen recovery techniques and are not capable of assessing the GHG emissions from emerging technologies. Thus, there is a need to develop an LCA model for those technologies.

- Current studies on new oil sands recovery methods focus only on the extraction stage and do not evaluate the impact of partially upgraded bitumen on the upgrading, refinery, and transportation stages.
- Current studies do not analyze the energy use and associated GHG emissions in each unit operation in the ESEIEH and THAI methods and therefore do not provide insights on the major energy consuming- and GHG emitting-units to identify areas for further improvement in the technologies before commercial development. There is a need for this analysis.
- Current LCA studies on emerging bitumen recovery methods report the results as point estimates and do not provide a range for the results based on different operating parameters and reservoir properties. A detailed uncertainty analysis based on ranges of different input parameters is required to obtain the most likely ranges for GHG emissions.

1.4 Research objectives

The overall objectives of this research are to determine the life cycle GHG emissions ranges of transportation fuel (gasoline, diesel, jet fuel) production from bitumen using THAI and ESEIEH and to compare the environmental footprints of these methods with SAGD and surface mining. The results of this study will provide insights into the performance of different technologies for policy makers and help them to implement emissions reduction policies. The specific objectives of this study are to:

- Develop a detailed, transparent, and theoretical LCA model for each life cycle stage involved in the production of transportation fuels from bitumen (extraction,

surface processing, transportation, upgrading, refining, and combustion) using the THAI and ESEIEH methods.

- Analyze the energy use and GHG emissions of different pathways for the production of transportation fuels.
- Perform a detailed sensitivity analysis to determine the sensitive inputs that significantly affect overall GHG emissions results.
- Determine the likely GHG emissions ranges for transportation fuel production in different production pathways by performing uncertainty analysis.

1.5 Scope and limitation of the thesis

This study evaluates the GHG emissions from crude extraction, upgrading (where necessary), refining, and the combustion of the produced fuel in vehicle engines. For the ESEIEH method, only the extraction stage is considered because there is very limited public data on bitumen properties produced by this method is available. This study does not include a techno-economic assessment of either methods. Since the quality of the oil produced by each technology differs, the two technologies cannot be compared at the extraction stage. Moreover, there is the need to analyze the life cycle stages from extraction to combustion, where the qualities of each product are similar. For upgrading and refining processes, this study only examines the delayed coker upgrader, hydroconversion upgrader, and deep conversion refinery. In calculating GHG emissions, only CO_2, CH_4, and N_2O are considered. Emissions attributed to infrastructure, equipment, and land use are not included in this study because of a lack of data.

1.6 Organization of the thesis

This is a paper-based thesis and is written in such a way that each chapter can be read independently. Thus, some assumptions and data are repeated between chapters. This thesis has four chapters as described below:

Chapter 2 provides information about the process model input parameters and describes the development of a LCA model to evaluate the GHG emissions associated with the material and energy requirements of the ESEIEH process. The chapter also presents the sensitivity and uncertainty results of GHG emissions from variations in operating parameters and reservoir properties and identifies the significant parameters.

Chapter 3 describes the assumptions, input data, and allocation methods used for the development of the LCA model for extraction, upgrading, refining, and transportation of bitumen produced in the THAI method. Energy use and GHG emissions in each life cycle stage are presented. Ranges of input data are also provided for the sensitivity and uncertainty analyses. Uncertainty results are presented and compared with the SAGD and surface mining emissions results from the literature.

Chapter 4 summarizes the key findings from chapters 2 and 3 and makes recommendations to improve this work.

Chapter 2: Evaluation of energy and GHG emissions' footprints of bitumen extraction using Enhanced Solvent Extraction Incorporating Electromagnetic Heating technology

2.1 Introduction

Conventional fossil fuels (crude oil, coal and natural gas) have been playing a dominant role in global energy supply. Petroleum production with approximately 100 million barrels per day (mbpd) makes up one-third of the world energy supply [39]. Majority of petroleum products are used as transportation fuels and contributed to 20% of global greenhouse gas (GHG) emissions [15]. Driven by population and economic growths, global energy consumption is projected to increase by 28% from 2015 level in 2040 [40]. The depletion of fossil fuel reserves is another pressing issue along with its climate change impact. With current production and consumption trends, it is only 20 (crude oil), 53 (natural gas) and 114 (coal) years before the world runs out of conventional fuels [41, 42]. Therefore, utilization of vast resources of unconventional crude reserves around the globe (2129.5 billion barrels) could be a potential solution to satisfy the world's energy demand for decades [42]. Oil sands are one of these unconventional sources that are composed of sands, water, and bitumen and are highly viscous and dense [5].

The oil sands reserves in Alberta, western Canadian province, with 165.4 billion barrels comprise 13.8% of the world's total proven oil reserves [40, 43]. At 3.0 mbpd, Alberta's bitumen production makes up 3% of the world's oil production [43, 44]. The production in Alberta is projected to reach 3.7 mbpd by 2030 [2].

Bitumen extraction is a challenging process due to its high viscous nature in which it exists in situ. It must be converted to a flowable form for easy mobility and processing. There are a number of bitumen extraction techniques, but cyclic steam stimulation (CSS) and steam assisted gravity drainage (SAGD) are the most widely used in situ methods [5]. In both the processes, pressurized high temperature steam is injected into a reservoir through injection wells; this transfers heat to the bitumen and reduces its viscosity [45]. The heated bitumen is extracted from in situ through production wells. Both CSS and SAGD use substantial amounts of natural gas and water to produce steam which is injected in-situ through the injection well [45, 46]. During this process a significant portion of the heat is lost inside the reservoir [47].

Oil sands recovery is GHG intensive. The sector is responsible for 9.8% of the total Canada's GHG emissions [14]. A few studies have been conducted to evaluate the energy and emission performances of different bitumen extraction technologies. Charpentier et al. [8] developed an life cycle assessment (LCA) model to estimate the energy use and GHG emissions in surface mining and SAGD processes based on a set of confidential data from the industry. Nimana et al [45] also developed an LCA model to evaluate the energy use and GHG emissions for the same bitumen recovery methods based on publicly available data. The study also examines the effect of cogeneration on bitumen recovery and concluded that GHG emissions in surface mining and SAGD could be reduced by 16-25% and 33-48%, respectively by implementation of cogeneration. Garcia et al. [48] evaluated the impact of capturing CO_2 from power and hydrogen production plants in reducing GHG emissions while and Bolea et al. [49] evaluated the impact of CO_2 capture during bitumen extraction. The GHG emission reduction

opportunities through the use of renewable energies in the SAGD process are analyzed by [50, 51]. Some studies investigated alternative energy saving opportunities and changing the current configuration of SAGD plants to reduce GHG emissions [52, 53]. While others evaluated the variability in GHG emissions during bitumen extraction in SAGD and CSS through statistical analysis [12, 54]. These two studies highlight that the discrepancy in output results are mainly due to different reservoir properties. Several improvement options in SAGD to predict the bitumen extraction emissions in the future was considered by [55] .

Existing literature on oil sands and relevant LCA models in the public domain ([56], [8], [57], [35],) focus on well-established and commercialized extraction technologies such as CSS and SAGD. There is a literature gap in evaluating the energy and GHG emission performances of emerging oil sands extraction technologies. Identifying the energy and environmental hot spots of extraction technologies at their early stage of development help the industry to take the required adjustment measure at a relatively lower cost than when the technologies are already in the market. This could also help policy makers to make more informed decisions and further facilitates the policy formulation.

The oil sands industry has been making efforts to develop alternative bitumen extraction and recovering technologies which can help the sector reduce its overall GHG emissions. A number of new technologies are at various stages of development, demonstration and deployment. These include Electromagnetic (EM) heating [58], solvent assisted extraction technique [59], and Enhanced Solvent Extraction Incorporating Electromagnetic Heating (ESEIEH) [20]. EM heating uses a radio frequency antenna that converts electricity to radio frequency energy. The antenna is placed inside a reservoir to

heat the bitumen by vaporizing the formation connate water [60]. The solvent-based extraction technique is based on injecting a light hydrocarbon-solvent as super-heated vapor into the reservoir. The solvent later rises, condenses and gives its latent heat to the bitumen [59]. Both EM heating and solvent-based extraction technologies have pros and cons. While both eliminate the water requirement and have high heat transfer efficiency [59-61], the low natural gas-to-electricity and then electricity-to-radio frequency conversion efficiencies mean EM's heating energy is not on par with SAGD or CSS [20]. In addition, solvent-based extraction has two major challenges. First, heat transfer from solvent to bitumen is affected by non-condensable gases inside the reservoir, thus special care must be taken to maintain the appropriate operating temperature and pressure to avoid solvent poisoning [62]. Second, solvent consumption and solvent loss are high, which affects the economic feasibility of the technology [33].

An overview of the ESEIEH process is presented in Fig. 2.1. ESEIEH combines the best features of both EM heating and solvent extraction techniques. The antenna is placed horizontally in the reservoir to preheat the reservoir, and light solvent is then injected to further reduce the viscosity [20]. ESEIEH is considered to require a relatively lower solvent-to-oil[1] ratio than solvent-based extraction and operates at a lower temperature than EM heating [20]. Furthermore, it could have a higher oil recovery factor[2] than CSS and SAGD [32].

[1] Solvent-to-oil ratio is an expression of the amount of solvent required at standard conditions and liquid state to extract one barrel of bitumen.
[2] The oil recovery factor is the amount of reservoir crude that can be recovered economically.

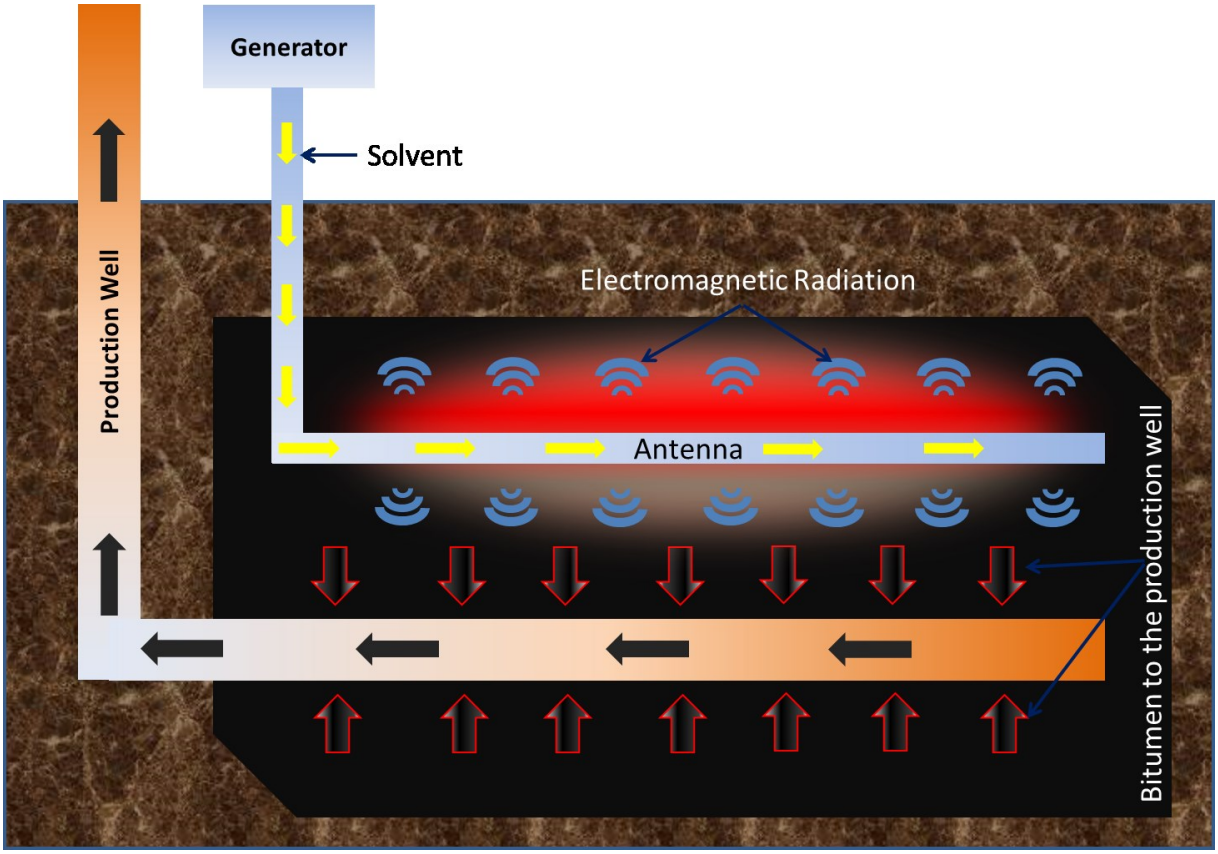

Fig. 2.1. Schematic diagram of the ESEIEH process

It is critical to understand the environmental footprint of ESEIEH in terms of GHG emissions. This will help in its comparison with in situ methods. Currently, there is very limited information in the peer-reviewed literature that quantify and characterize its environmental impacts through all the unit operations of extraction stage. Some preliminary estimates have been reported earlier [17, 18]. However, these studies do not address data transparency, nor fully define the system boundaries, the procedures and methods followed, and the assumptions and considerations made. This paper, therefore, aims to address this gap.

With the aim of addressing these research gaps, this paper strives to conduct a process-specific and comprehensive assessment of energy consumption and GHG emissions for the ESEIEH process by developing a data-intensive bottom-up model based on first engineering principle. The specific objectives of this research are to:

- Develop process model for the ESEIEH process;
- Develop a spread-sheet based model to characterize the energy and GHG emissions of the ESEIEH process;
- Identify the parameters that significantly impact the GHG emissions of the ESEIEH process;
- Evaluate different energy scenarios for improved performance of the ESEIEH process

2.2 Method

Fig. 2.2 illustrates the stages involved in production of transportation fuel from the ESEIEH process. The crude extracted from the reservoir is processed on the surface to separate the solvent and the formation water. The bitumen is then blended with lighter hydrocarbons such as natural gas distillates (diluent) to reduce the viscosity so that it can be transported via pipeline. The blended bitumen, known as dilbit, is either sent to the upgrader to be transformed into a higher quality crude (synthetic crude oil [SCO]) or sent directly to a refinery to produce transportation fuels [37].

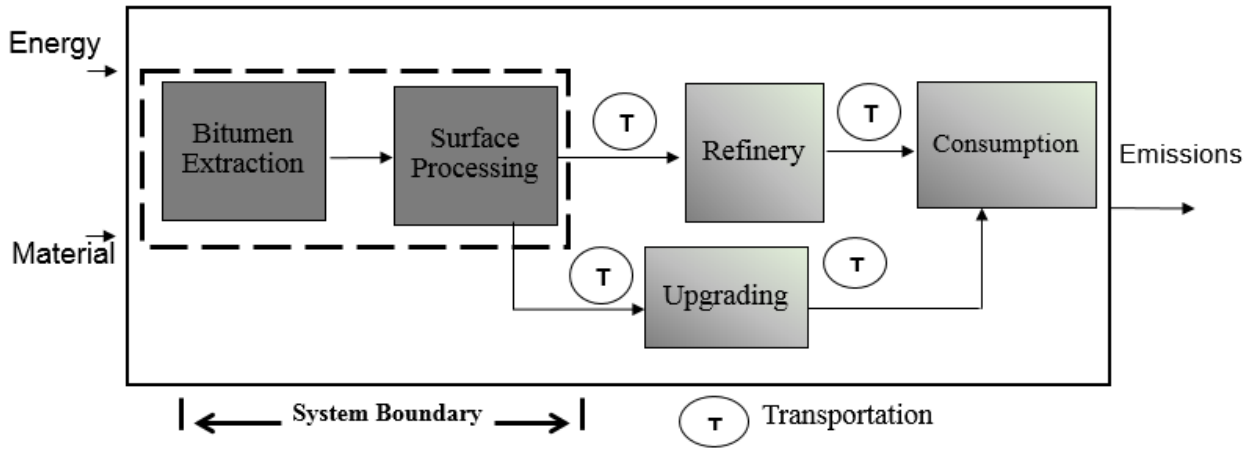

Fig. 2.2. Schematic of transportation fuel production using the bitumen extraction through the ESEIEH process

2.2.1 Process description

A detailed view of the extraction and separation of the ESEIEH process is provided in Fig. 2.3. The unit operations considered in each stage of extraction in the reservoir and separation at the surface are discussed below.

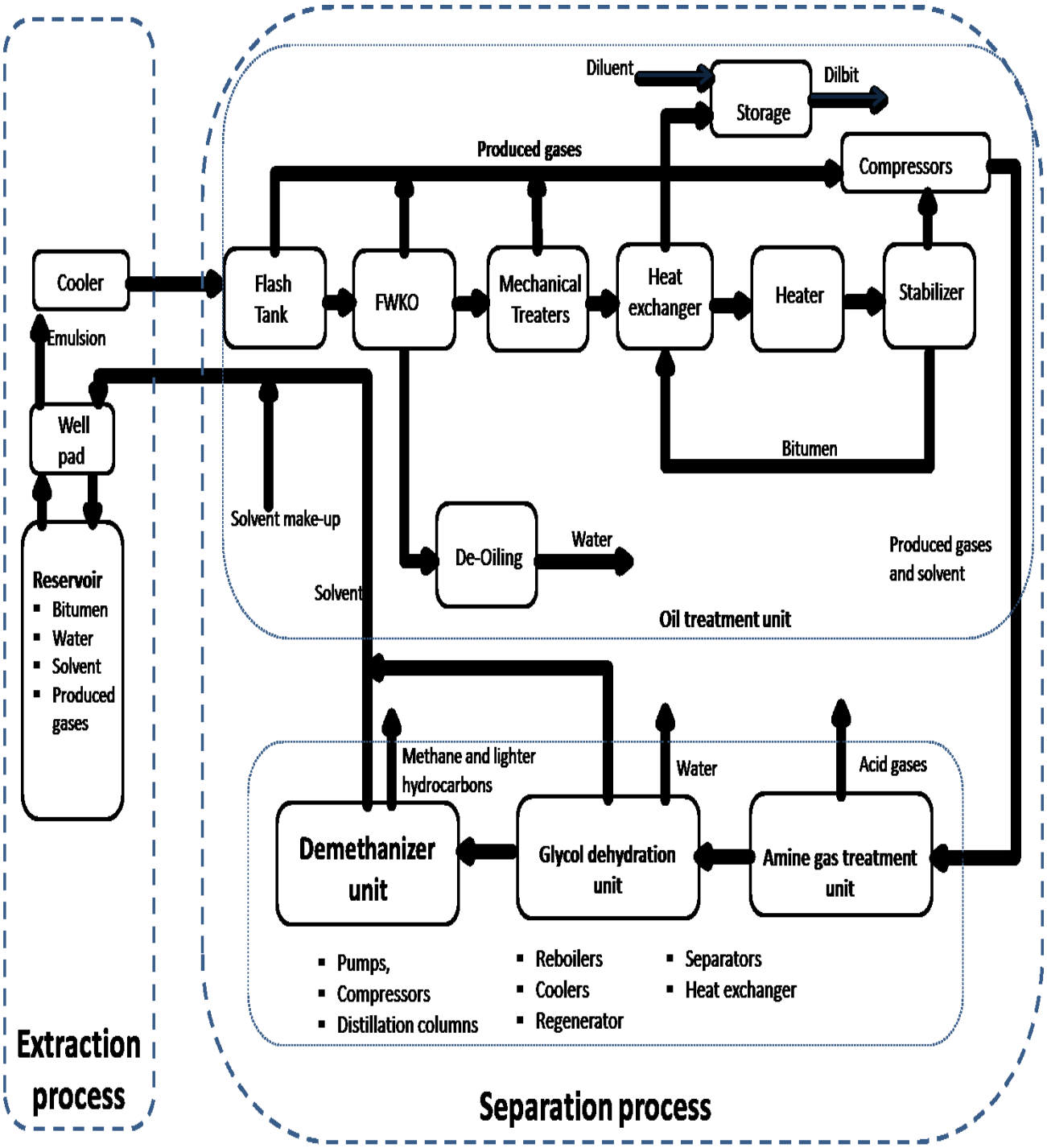

Fig. 2.3. Schematic diagram of the ESEIEH extraction and separation process.

Extraction process

The reservoir configuration of the extraction process is similar to SAGD [20] and uses standard oilfield handling equipment. It has a horizontal or vertical well pair with an injector and a production well that produces a mixture of bitumen, gas, solvent, and water as emulsion from the reservoir. A dipole antenna is installed in the injection well to transmit radio frequency waves into the reservoir [20]. The radio frequency wave heats the reservoir, making the bitumen less viscous. Solvent is injected into the reservoir to increase the mobility of the heated bitumen. The reservoir heating temperature and pressure are assumed to be 80^{o}C and 1.4 MPa, respectively, to produce emulsion in the production well [32, 63]. The reservoir pressure and temperature for effective operation of the ESEIEH process are lower than in the steam-based extraction process [45, 64]. Depending on the hydrocarbon solvent used, the well temperature ranges from 40^{o}C – 80^{o}C and the well pressure is operated such that it favors solvent condensation [20]. It is important that the conditions of the well are favorable to ensure that the solvent condenses. In this study, butane is used as solvent and reservoir operating conditions suitable for condensation are assumed [65].

Separation process

The separation process can be divided into four main processes: oil treatment, amine gas treating, glycol dehydration, and demethanizer. The use of steam reboiler and water coolers are more economical than other sources such as glycol mixtures and cooling fans, respectively. Therefore, in this study, it is assumed that regenerators use a steam reboiler and water cooler to boil and cool the top product, respectively. The pumps and

compressors are used to recirculate liquid and gases, respectively, to where they are required.

Oil treatment unit

Emulsion from the production well is pumped into the surface facility through a cooler that reduces its temperature. The coolers outlet temperature and pressure are regulated to control the amount of produced gases at the pre-flash tank where components in the gaseous phase are separated from the liquid phase (a mixture of bitumen, solvent, and water). The components in the liquid phase enter the free water knockout drum (FWKO) and mechanical treaters for water separation and further recovery of gases. In order to recover the liquid solvent remaining in the bitumen, the bitumen leaving the FKWO for the stabilizer unit is preheated to about 195^{o}C [66], thus vaporizing the solvent. The bitumen from the stabilizer unit is then sent to the storage tank where it is mixed with diluent to further improve its viscosity. The separated water is sent to the water treatment unit for treatment. Produced gases, along with separated solvent vapor from the flash tank, mechanical treaters, and stabilizer unit, are compressed and sent to the amine gas treatment unit as shown in Fig. 2.3.

Amine gas treatment unit

The amine gas treatment unit is considered for the removal of acid gases such as carbon dioxide (CO_2) and hydrogen sulfide (H_2S) from the produced gases using diethanolamine (DEA) solution. The amine gas treating process consists of an absorber tower, regenerator unit, pumps, and compressors. In the absorber tower, DEA solution flowing

down the tower absorbs CO_2, H_2S, and other contaminants from the produced gases entering at the bottom [67]. Sweet gas (gas free of acid gases and contaminants) is produced as distillate and sent to the dehydration process for water removal. DEAs rich in absorbed acid gases and contaminants are removed as a bottom product in the absorber tower. The rich DEA is sent to the regenerator to produce lean DEA for reuse and CO_2, H_2S, and other contaminants are removed as the distillate in the regenerator [67]. The details are shown in Fig. 2.3.

Glycol dehydration unit

The glycol dehydration unit consists of an absorber, regenerator, pumps, and compressors. In the absorber unit, triethylene glycol (TEG) flows down from the top of the tower and absorbs wet gas entering at the bottom as they contact each other. Dry gases are produced as distillate while the bottom product, the TEG/water mixture, is sent to the regenerator unit to produce lean TEG for reuse [67]. Depending on the purity of solvent, the recovered solvent is either recycled through the injection well or sent to the demethanizer unit.

Demethanizer unit

The main purpose of the demethanizer unit is to purify the solvent and separate methane from other lighter hydrocarbon components. The unit has a distillation tower and a refrigeration unit. The distillation tower, with a top cooler and bottom reboiler, is used to separate solvent (butane) from other lighter hydrocarbons. The refrigeration unit is required to condense the dry gases from the dehydration process, after which the dry

gases enter the distillation tower. The solvent leaves the tower at the bottom while the lighter gases leave as distillate [68]. Finally, the recovered and make-up solvent is re-injected into the reservoir.

2.2.2 Simulation of the ESEIEH process

2.2.2.1 Estimation of energy consumption

Table 2.1 lists all the values and assumptions that were used to estimate the energy use and associated GHG emissions for bitumen extraction in ESEIEH process.

Table 2.1: Input data in the model for evaluation of energy consumption and GHG emissions in bitumen extraction via ESEIEH

Parameter	Value
Solvent-to-oil ratio, m^3/m^3 [63]	1.33
Solvent hold-up in the reservoir, % [63, 69]	25.00
Solvent loss inside the reservoir, % [33, 63]	5.00
Make-up solvent temperature, °C [70]	10.00
Make-up solvent pressure, kPa [70]	200.00
Reservoir gas-to-oil ratio, (GOR)[*3], m^3/m^3 [8]	4.00
Reservoir depth, m [69]	153.00
Reservoir pressure, kPa [69]	1400.00
Wellhead pressure, kPa [45]	1800.00

[3] Amount of gas that is produced along with the bitumen at standard conditions.

Parameter	Value
Reservoir cumulative electricity-to oil-ratio (cEOR)[4], GJ/bbl [32, 63]	0.18
Antenna efficiency, %	72.00*
Furnace efficiency, % [71, 72]	80.00
Compressor efficiency, % [73]	80.00
Boiler efficiency, % [8]	85.00
Pump efficiency, % [74]	80.00
Pressure difference for pumping cooling water, kPa [75]	266.00
Energy intensity for water treatment, kwh/bbl of water [76]	0.16
Diluent-to-oil ratio, m^3/m^3 [64]	0.33
Dilbit storage tank temperature, °C [64]	50.00
Diluent storage tank temperature, °C [64]	5.80
Upstream emissions of solvent, kg CO_2eq/bbl of butane [35]	17.95
Emission factor of natural gas, kg CO_2eq/GJ [35]	68.00
[5]Emission factor of combusted gas in Pathway I, kg CO_2eq/GJ	80.24
[5]Emission factor of combusted gas in Pathway II, kg CO_2eq/GJ	61.88
[5]Emission factor of Alberta grid electricity (2016 mix), kg CO_2eq/MWh	701.00
[5]Emission factor of Alberta grid electricity (2030 mix), kg CO_2eq/MWh	372.00
Emission factor of electricity from cogeneration, kg CO_2eq/MWh [35, 77, 78]	484.00

[4] Amount of electrical energy that is required to be delivered to the reservoir for bitumen recovery.
[5] Calculated by authors

Parameter	Value
Emission factor of electricity from biomass power plants, kg CO_2eq/MWh [79]	20.26**

*Proprietary data from the industry. This value also includes the efficiency during transmission of the electricity into the reservoir.
** This value corresponds to the emissions during chopping, cropping, and transportation of feedstock to the power plant.

The following equations were used for estimation of energy consumption in different unit operations.

Energy consumption of antenna, A_E:

$$A_E = cEOR/\eta_a \quad (1)$$

where *cEOR* is the cumulative delivered energy to the reservoir-to-oil ratio (GJ/bbl), and η_a is the overall efficiency of the antenna including transmission losses of electricity and conversion of electricity to radio frequency energy.

Energy consumption of pumps, P_E:

$$P_E = V * P/\eta_p \quad (2)$$

where *V* is the emulsion volume (m^3/bbl), *P* is pressure difference, and η_p is the efficiency of the pump.

Energy consumption in pumps for emulsion extraction, P_{EE}:

$$P_{EE} = M_m * g * h + (M_v) * (P_{wellhead} - P_{reservior}) \quad (3)$$

where M_m is mass of water, solvent, and bitumen mixture (kg/bbl), *h* is the vertical depth of the production well (m), *g* is the gravity (m/s^2), M_V is the mixture volume (m^3), $P_{wellhead}$ is the wellhead pressure (kPa), and $P_{reservoir}$ is the reservoir pressure (kPa).

Energy consumption in the water treatment unit, W_E:

$$W_E = E_i * W_c \quad (4)$$

where E_i is the energy intensity for water treatment (Kwh/bbl of water), and W_c is the amount of water that is extracted along with bitumen known as water cut (%).

Solvent upstream emissions for bitumen production, $S_{up\text{-}emission\text{-}bitumen}$:

$$S_{up\text{-}emission\text{-}bitumen} = S_{up\text{-}emission} * SOR * S_L \quad (5)$$

where $S_{up\text{-}emission}$ is the upstream emissions of solvent (kg CO_2 eq/bbl solvent), SOR is solvent-to-oil ratio (m^3/m^3), and S_L is solvent loss (%).

2.2.2.2 Process simulation

The process simulation of the separation processes was carried out using Aspen HYSYS Version 9.0 [80]. The unit operations involved in the process simulation models are distillation columns, reboilers, valves, mixers, splitters, pumps, compressors, heat exchangers, coolers, heaters, and separators. In this study, two simulation models were developed for the analysis of the ESEIEH process. The first was developed to investigate the effects on energy consumption and GHG emissions when solvent, together with produced gases, is considered for purification in the demethanizer unit. The second simulation model assumes the produced gases, particularly from the pre-flash and mechanical treaters, are used for combustion in a steam boiler. In this case, the demethanizer unit was not considered. This is because the purity of solvent in the stabilizer unit, where most of the butane is recovered, is relatively high. In this study, for the sake of clarity, the model with the demethanizer is referred to as Pathway I and the other as Pathway II.

The Peng-Robinson, acid gas-chemical solvent, and glycol fluid packages were the equations of state used to develop the simulation models to predict the thermodynamic conditions of the oil treatment process and demethanizer, amine gas treating process, and dehydration unit, respectively. These fluid packages were adequate to predict the process conditions. The operating conditions of unit operations were found by optimizing the operation parameters in Aspen HYSYS. Those values are presented in Table A.4.

Natural gas and the Alberta electricity grid mix are the two sources of energy for process units. The energy required by each process unit to extract 25,000 bbl of bitumen is evaluated to give a reasonable account of the impact on the environment. The total amount of emulsion from the production well is 2.16 bbl per bbl of bitumen. The emulsion is a mixture consisting of 25,000 bbl of bitumen, 23,294 bbl of solvent, 5,500 bbl of water, and 560 Thousand Standard Cubic Feet per Day (MSCFD) produced gas (containing acid gases, hydrogen, and light hydrocarbons. The compositions are shown in Table A.1). In typical SAGD operations, produced gases from the well are directly used with natural gas to fire steam boilers [64]. However, in a solvent extraction process such as ESEIEH, options are available to either directly use the produced gases (which are in this case mixed with solvent) with natural gas to fire steam boilers or treat them to recover more solvent. The concern in the former approach is continuous solvent loss through combustion in the steam boiler. On the other hand, treating the produced gases to recover solvent may require additional investment and energy consumption. In this study, the two options are examined in terms of energy consumption and associated GHG emissions.

2.2.3 Scenarios for assessment of GHG emissions

In this study, the initial ESEIEH (base case) assessment was carried out using Alberta's current electricity grid mix to examine its GHG emissions. To explore the impact of electricity sources on the overall GHG emission footprint of the ESEIEH process, the electricity grid mix in 2030, cogeneration, and using a 100% renewable energy source were evaluated.

Current Alberta grid mix scenario

As of 2016, Alberta's electricity grid mix is dominated by GHG-intensive coal power plants, making up 39% of the total share.

2030 Alberta grid mix scenario

Currently, renewable energy makes up only 14% of the mix [81]. The province plans to phase out coal-fired electricity generation power plants and replace this share with renewables and natural gas by 2030 [82], which will raise the renewables' share to 30% [81]. This shift in grid mix will lower the grid carbon intensity and therefore has been adopted as a scenario in our study.

Cogeneration

A common practice for electricity generation in existing oil sands extraction processes is cogeneration [77, 83]. Part of the steam produced for bitumen extraction is used to generate electricity, thus reducing natural gas consumption and GHG emissions. As steam-based extraction processes are likely to operate alongside the ESEIEH process, it is important to consider the benefits of cogeneration.

Renewable electricity (biomass)

In addition, the benefits of renewable resources such as biomass, which is plentiful in northern Alberta [5, 84] are examined here. The concept is to use biomass-based electricity for the ESEIEH process.

2.2.4 Sensitivity and uncertainty analyses

Since process simulation-based models are deterministic in nature, the uncertainty in their outcomes needs to be quantified before they are used for decision making. The uncertainty in model output is due to the variability and uncertainty in model inputs. Performing sensitivity and uncertainty analyses provides a means to evaluate the variability in the output of the process simulation-based estimates. In this study, sensitivity analysis was used to identify input parameters that are sensitive to the model output. Monte Carlo simulation runs were performed to evaluate the uncertainties in the output. Triangular and uniform distributions were considered for the input parameters since there are limited data available on input variables [85]. Uniform distribution needs minimum and maximum values to be generated and maintains constant probability over this range of values. Triangular distribution requires a minimum, mode, and a maximum to be generated [86]. The GOR and cEOR depend on the reservoir properties. Moreover, there are few simulations and little field-scale data on the cEOR in different reservoirs. Therefore, uniform distributions were used for these variables. Triangular distribution was considered for the other parameters because of the scarcity of the data. The input variables and their distributions are listed in Table 2.2.

Table 2.2: Input parameters and their distributions for uncertainty analysis for bitumen recovery using ESEIEH method

Input	Monte Carlo distribution
Antenna efficiency, %	Triangular (54.00, 72.00, 86.00) *
cEOR,(GJ/bbl) [32, 63]	Uniform (0.16, 0.20)
SOR, m^3/m^3 [63]	Triangle (1.04, 1.33, 1.60)**
Solvent loss,% [33, 63]	Triangle (2.00, 5.00, 10.00)
Compressor efficiency, % [57]	Triangle (75.00, 80.00, 85.00)
Furnace efficiency, % [71, 72]	Triangle (70.00, 80.00, 92.00)
Boiler efficiency, % [8, 87-89]	Triangle (70.00, 85.00, 90.00)
Pump efficiency, % [56]	Triangle (70.00, 80.00, 92.00)
GOR, m^3/m^3 [8]	Uniform(1.00, 12.00)

*Proprietary data from industry

**The literature only reports a SOR of 1.33. The author considered a range of ±20%.

2.3 Results

The energy and GHG emissions associated with each process unit in the two pathways of bitumen extraction through ESEIEH were examined. In Pathway I, the simulation model was designed such that the produced gases from the flash tank and mechanical treaters were treated alongside the gases from the stabilizer unit in the amine unit, glycol dehydration, and demethanizer unit (Fig. 2.3). In Pathway II, however, these gases were used for combustion in steam boilers, thus eliminating the use of a demethanizer unit. Relevant information on how these pathways interact with reservoir operations and surface facilities in terms of energy consumed and associated GHG emissions are discussed.

The energy consumption and corresponding GHG emissions for the Pathway I (with a demethanizer) and Pathway II (without a demethanizer) pathway are 487.2 and 375.5 MJ/bbl, and 77.7 and 59.8 kg CO_2 eq/bbl, respectively. The extraction and separation processes made up 51.5% and 48.5% of Pathway I and 66.8% and 33.2% of Pathway II, respectively. Of the total energy consumed in both pathways, electrical energy makes up the largest share (Pathway I: 77.2%, Pathway II: 78.1), while the rest of the energy is in form of heat generated by natural gas and/or produced gas combustion. Table 2.3 presents the energy consumption and GHG emissions associated with each process. The energy required and the associated GHG emissions in the extraction process are crucial to the overall production processes for the pathways considered. In Pathway I, the inclusion of the demethanizer unit contributed an additional 102.2 MJ/bbl and 16.1 kgCO_2eq/bbl to energy consumption and GHG emissions, respectively.

Earlier studies on SAGD and surface mining give emissions values in the range of 45 – 190 and 16-57 kgCO_2eq./bbl of produced bitumen, respectively [8, 45]. The emissions values from the ESEIEH process (Pathways I and II) are within the range of values reported for these processes. It should be noted that direct comparison cannot be made at this level of operation because the bitumen produced by these processes may differ in composition and properties, suggesting that their volume flow and/or energy content are not equivalent. Direct comparison is suitable after bitumen upgrading and/or refining, when final products have similar properties.

Table 2.3: Energy and GHG emissions of the ESEIEH process

	Pathway I		Pathway II	
Process	**Energy consumption (MJ/bbl)**	**GHG emissions ($kgCO_2eq/bbl$)**	**Energy consumption (MJ/bbl)**	**GHG emissions ($kgCO_2eq/bbl$)**
Extraction process				
Emulsion lifting	0.6	0.1	0.6	0.1
Solvent injection	0.3	0.1	0.3	0.1
Antenna	250.0	48.7	250.0	48.7
Separation process				
Oil treatment	95.4	8.9	95.0	8.0
Amine gas treating	20.9	1.5	20.7	1.5
Glycol dehydration	10.8	1.7	9.0	1.4
Demethanizer	109.3	16.7	-	-
Total	487.2	77.7	375.5	59.8

2.3.1 Extraction process

The total energy consumed in the extraction process for Pathways I and II is ~251.0 MJ per barrel of bitumen. The energy required for solvent injection and emulsion pumping is less than 0.1% of the total energy consumed in the extraction process for both pathways. The energy required for heating the reservoir through the antenna is intensive; for both pathways, about 250 MJ of electrical energy needs to be converted to radio frequency energy to produce 1 barrel of emulsion. The GHG emissions associated with the extraction process were estimated to be ~49.0 $kgCO_2eq./bbl$ for both pathways.

2.3.2 Separation process

The energy consumed in the separation process and the corresponding GHG emissions are 236.4 and 124.7 MJ/bbl, and 28.8 and 10.9 kgCO_2eq./bbl for Pathways I and II, respectively. The oil treating process and the demethanizer process are the most emission-intensive units for Pathway I; they contributed about 31.0% and 57.9%, respectively, to the overall emissions of the separation process. In Pathway II, the oil treating process is also the most emission-intensive unit; it contributed 74.0%, while the amine process and glycol dehydration process contributed 13.5% and 12.5%, respectively. The overall solvent losses in the separation unit are 2.4% and 3.8% of the total solvent input for Pathway I and II, respectively. For both pathways, most of the solvent losses are from the stabilizer unit, amounting to 2.4%. In Pathway II, the use of produced gases from the flash tank and mechanical treaters for combustion were about 1.0% and 0.3%, respectively. There are no significant solvent losses in the free water knock out vessel and other units of the process.

The oil treating process for the both pathways is similar in configuration, operating conditions, and amount of produced gas. However, the differences are that the compression of the produced gases from the flash tank and mechanical treaters to the amine gas treatment unit is not required in Pathway II. In Pathway II, the produced gases are assumed to be used for heating purposes, while higher compression power and cooling are required to meet the operating conditions of the amine treating unit for Pathway I. The combusted produced gases (from the flash tank and mechanical treaters in Pathway II) contain some solvent, which is lost as a result of its use in the boiler. The

produced gases that are sent to the amine unit are predominately butane (96.9% for pathway I and 97.7 for pathway II), and their overall volume flow (standard cubic feet) per barrel of bitumen is 1,252.6. When the produced gases from the flash tank and mechanical treaters are not considered for treatment, the value is 1,214.0 SCF/bbl of bitumen (Pathway II). The reduction in the volume flow of the produced gases lowers the energy consumption and GHG emissions by 0.41 MJ/bbl and 0.89 kgCO_2eq./bbl, respectively, in the oil treatment unit. In the stabilizer unit, where most of the solvent in the emulsion is recovered, about 40% of the energy supplied by the fired heater is recovered through heat integration. However, the overall energy consumed by the stabilizer unit is over 80% of the total energy consumed in the oil treatment unit for both pathways. In the amine treatment unit, the steam reboiler, cooling water pump, and booster pump for the circulation of DEA are the main energy consumers. The steam reboiler is the most energy-intensive unit; it is responsible for over 97.0% of the total energy consumed by the amine treatment unit in both pathways. Although the amount of acid gases in Pathway I is higher than in Pathway II, the relative difference, 9.34 x 10^{-3} kg/bbl of bitumen for CO_2 and 1.29 x 10^{-5} kg/bbl of bitumen for H_2S, does not significantly contribute to the GHG emissions or the energy consumed. The reason is that the additional DEA required to sufficiently remove the increased acid gases has little impact on the energy consumed in the regenerator and booster pumps. The increase in energy consumed and emissions is 0.21 MJ/bbl of bitumen and 0.04 kgCO_2eq./bbl of bitumen, respectively, in the amine treatment unit. Similarly, the additional water removed from the glycol dehydration unit for Pathway I does not significantly influence energy consumption

and emissions. The increase in energy consumed and GHG emissions in Pathway I is 1.79 MJ/bbl and 0.35 kgCO_2eq./bbl of bitumen, respectively.

The drying of solvent (water removal) in the glycol dehydration unit is essential. Solvent purities are 98.6% and 99.3% for Pathway I and II, respectively, after drying. However, in Pathway I, because it is important to improve the purity of solvent beyond its present level and recover the light hydrocarbons (which are predominately methane), the dehydrated product was sent to the demethanizer. The purity of solvent increased to 99.8% after the light hydrocarbons, containing 95.5% methane, were removed. In this study, it is assumed that light hydrocarbons removed from the demethanizer are used for combustion in the steam boilers. The energy required to increase the purity of solvent by 1.2% in the demethanizer is ~109.3 MJ/bbl of solvent. In Pathway I, about 46.2% of the overall energy consumed in the separation process is by the demethanizer unit. Furthermore, the most energy-intensive units in the demethanizer are the compressors, which are responsible for 68.0% of the energy consumption, followed by the steam boiler (29.4%) and pumps (2.6%). The compressors provide external refrigeration in order to condense the feed composition to the demethanizer distillation column. Since the feed is predominately butane, more energy is required than in a typical demethanizer, in which the feed is composed of lighter hydrocarbons such as methane [68].

2.4 Discussion

2.4.1 Extraction and separation process

The antenna and demethanizer contribute significant amounts of energy and GHG emissions to the overall extraction and separation processes. The GHG emissions for

each pathway are comparable except for the relatively high amount of electrical energy required for refrigeration in the demethanizer unit in Pathway I.

In the reservoir, the GHG emissions in Pathway II are slightly higher because more make-up solvent and additional power for the injection of solvent into the reservoir are required. It is also important to mention that depending on the nature of the reservoir, SOR, type of solvent used, electromagnetic generator and the efficiency of antenna, GHG emissions and energy consumption estimates vary. Reservoirs with more water are more likely to show lower energy consumption because the radio frequency waves tend to generate more heat energy when it penetrates or travels through water [60]. This, on the other hand, is an opportunity to reduce the amount of solvent used. Reservoirs with high heavy metal content are more likely to increase energy demand because a strong frequency is required [90]. Reducing the SOR can lower energy consumption; however, this may involve a trade-off between bitumen recovery yield and energy consumption. Energy consumption can also be reduced by improving the efficiency of the antenna and using highly conductive electrical transmission lines that produce and transfer electromagnetic energy, respectively, to the antenna. Improved antenna design can also reduce energy use and GHG emissions [60].

During the separation process, capturing the produced gases from the production well increases unit operations and energy consumption because the composition of the produced gases from the well reduces the purity of solvent in the process before solvent re-injection into the well. Although reducing the solvent purity percentage does not

significantly consume energy in the amine and dehydration units, an additional unit (the demethanizer) is required to avoid solvent poisoning, which can lead to poor heat transfer in the reservoir. That said, lighter hydrocarbons such as methane and ethane are more likely to pose a serious threat to bitumen extraction because the operating conditions (temperature and pressure) of the reservoir do not favour methane and ethane condensation. Methane, which makes up about 63.6 mol% of the produced gases in the well, is the component most likely to impede heat and mass transfer. Its accumulation and increased concentration in the reservoir will increase the GOR , thus lowering the length of time bitumen is exposed directly to radio frequency energy from the antenna. These conditions can also result in the convective flow of light hydrocarbon gases in the production and injection well, thus raising their pressure and preventing the inflow of solvent through the injection well. Heavier hydrocarbons, however, are a low threat to bitumen extraction. They are more likely to condense at the operating conditions of the reservoir. That said, the increased concentration of heavier hydrocarbons in the solvent may lead to the expense of additional separation columns and increased energy consumption and emissions. The increase in energy is more likely to be from the refrigeration of the demethanizer feed streams and the column reboilers. For these reasons, it important to keep solvent purity as high as possible before the solvent is injected into the production well. In Pathway II, solvent loss to combustion through produced gases helps avoid both the energy consumption and emissions of additional units but at the expense of increased make-up solvent. It is important to mention that solvent loss depends on gas composition and flow rates in the reservoir. In situations where the flow rates of produced gases or methane in the reservoir are significantly high,

the overall required make-up solvent increases. In pathways where make-up solvent may have a significant impact on cost, an economic and environmental assessment is useful to identify the key trade-offs for a sustainable operation.

2.4.2 The impact of electricity sources on the ESEIEH process

The analyses of the ESEIEH process showed that electrical energy takes the largest share of the overall energy consumption and GHG emissions. Energy-related emissions can be significantly reduced by lowering the electrical emissions footprints. This can be done by lowering the electricity emissions factor by improving the electrical energy mix or utilizing a cleaner electrical source.

In this study, the impacts of Alberta's future grid mix, current electricity grid mix, renewable electricity, and cogeneration on the ESEIEH process were explored. Pathway II (without demethanizer) was analyzed. Because the results in both pathways are similar, for brevity, Pathway I (with demethanizer) is not shown or discussed.

With respect to the base case simulation model presented in Fig. 2.3 (Pathway I), Fig. 2.4 shows the current Alberta electricity grid mix, the proposed Alberta electricity grid mix by 2030, cogeneration, and 100% renewable energy, along with the corresponding contributions from the unit operations. The figure shows that ESEIEH process can be significantly improved by adopting the future grid mix, cogeneration, or 100% biomass. A 100% electricity supply from biomass, the Alberta electricity grid mix in 2030, and cogeneration show 83.4%, 39.3%, and 25.2% reductions in GHG emissions, respectively.

Furthermore, unlike the Alberta electricity grid mix in 2030 and cogeneration, where associated GHG emissions from the antenna contributed over 66% of the overall GHG emissions, the use of 100% biomass lowers antenna emissions share to 16.2%. A similar result is found in the uncertainty analyses of the four sources of electricity using a Monte Carlo simulation (see Fig. 2.5). The resulting life cycle emissions distributions show that biomass electricity sources have the lowest emissions intensity and the current Alberta grid mix has the highest. However, the error bars of the cogeneration and Alberta electricity grid mix by 2030 overlap, so it is not possible to confidently conclude which scenario has lower emissions. The results of uncertainty analyses indicate that the probability ranges in uncertainty in emissions vary from 10.0 – 87.7 $kgCO_2eq./bbl$, depending on the source of electrical energy and solvent recovery pathway. GHG emissions fall to their lowest values (10.0 – 13.1 kgCO2eq/bbl) when the source of electrical energy is biomass. The tornado plots in Fig. 2.6 show the input parameters with the highest impact on the output uncertainty for each electricity source considered. In the biomass power plant scenario, solvent loss is the main source of uncertainty mainly due to its relatively wide range (2-10%), emission intensive process for producing solvent, and insignificance contribution of electricity consuming units to the overall GHG emissions because of low emission factor assumed for the biomass. Antenna efficiency and cEOR are the main sources of uncertainty in the other scenarios because they have a significant impact on electricity consumption.

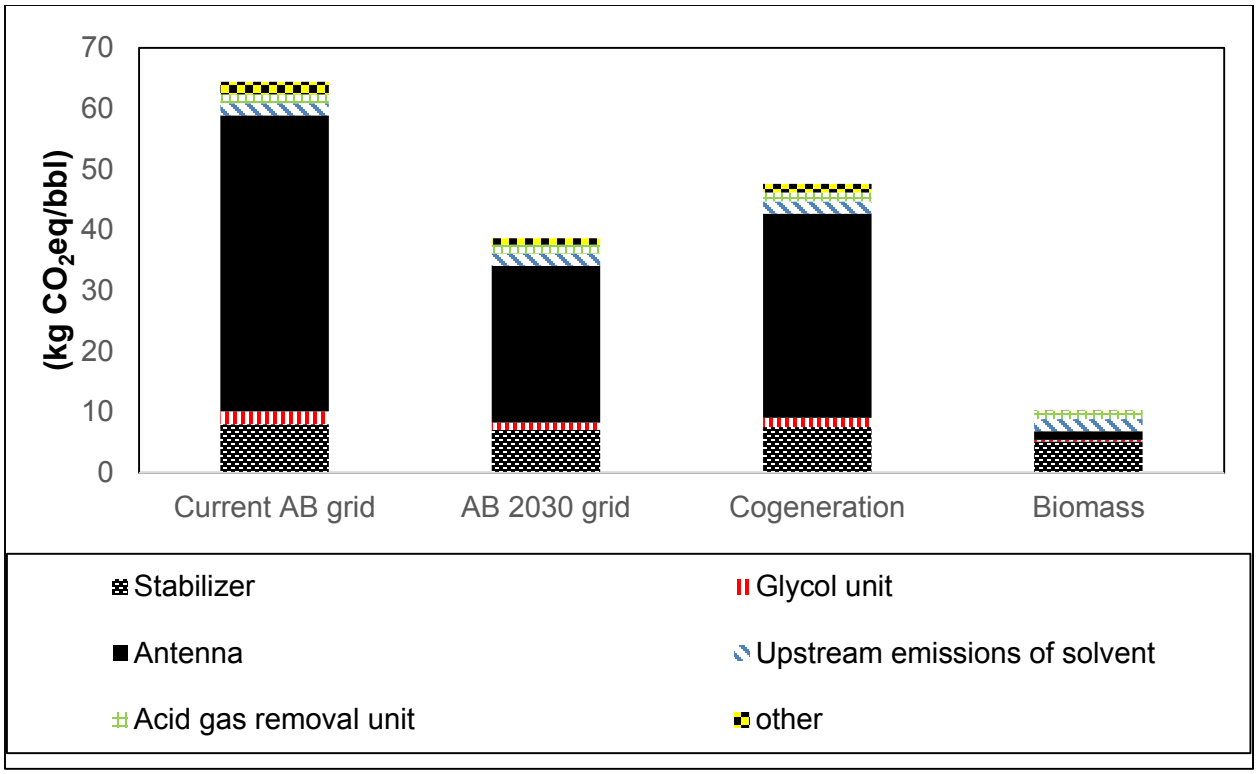

Fig. 2.4. The impact of electricity sources on the ESEIEH process (Pathway II)

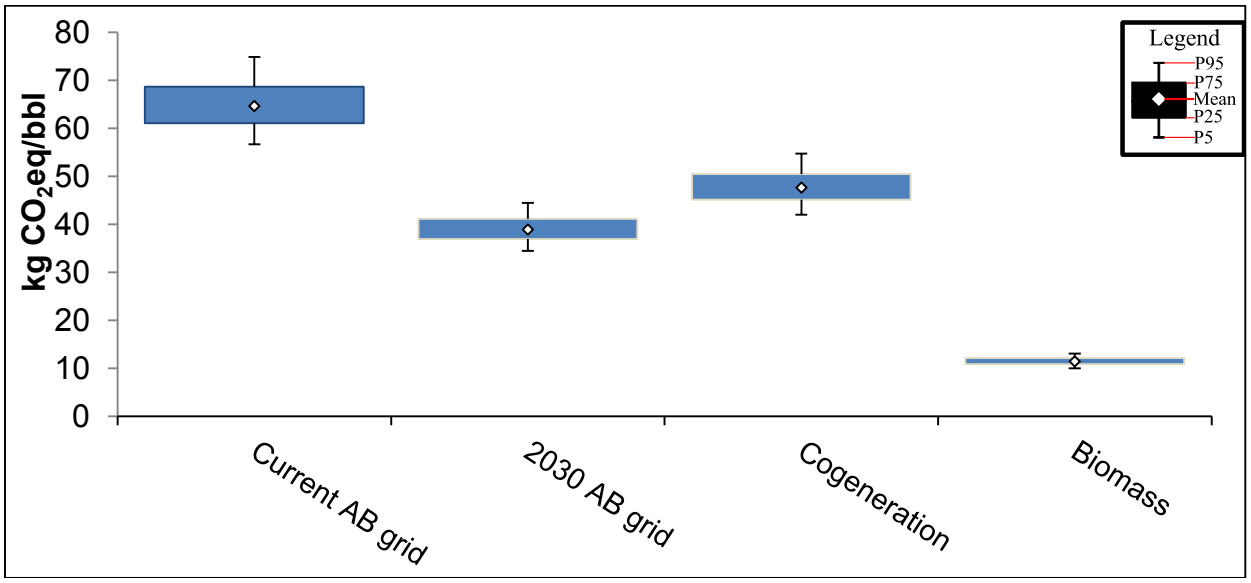

Fig. 2.5. Uncertainty analyses of the difference sources of electricity on the ESEIEH process (Pathway II)

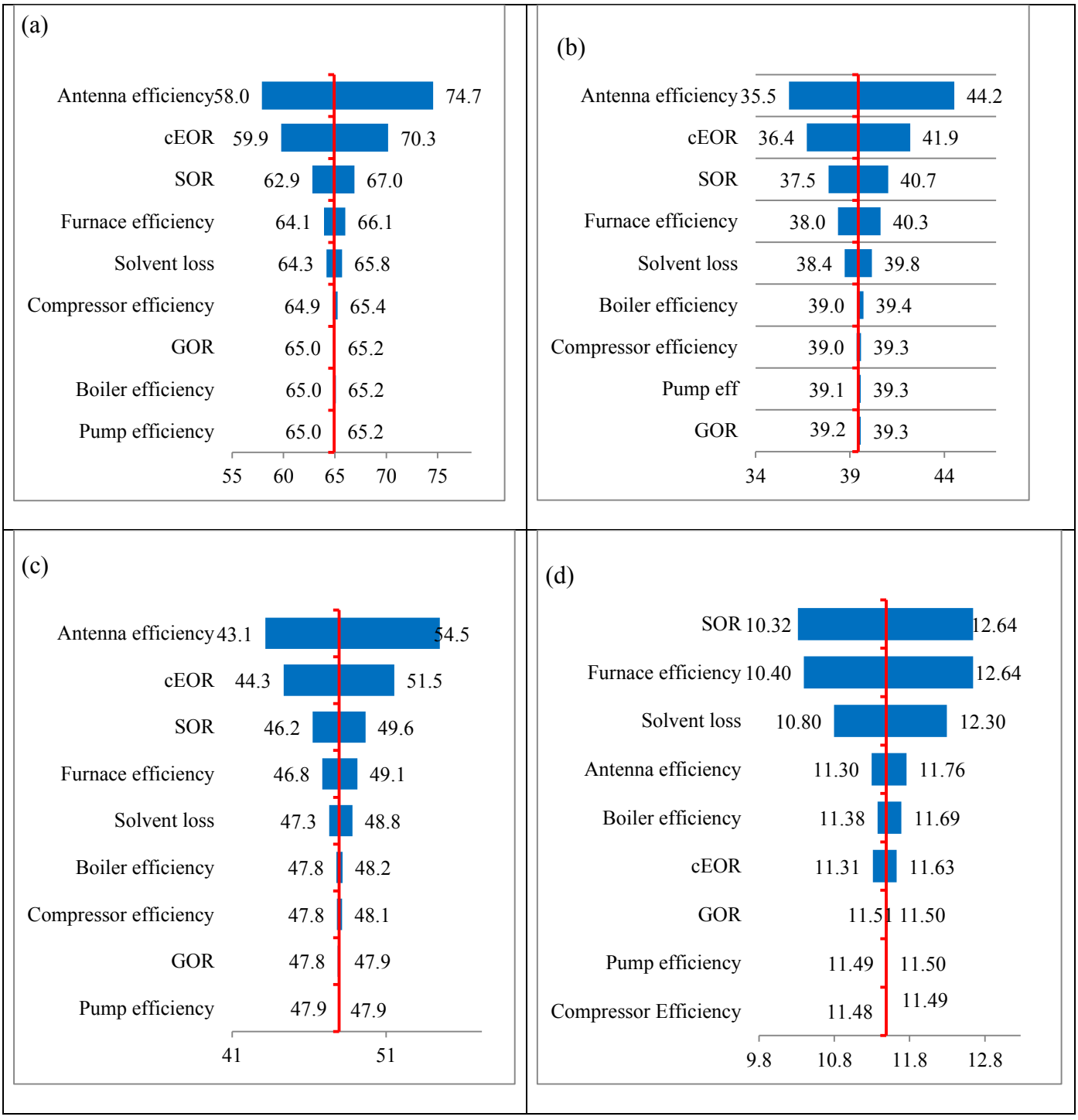

Fig. 2.6. Tornado plots. (a) Current Alberta electricity mix, (b) 2030 Alberta electricity mix, (c) Cogeneration, (d) Biomass

2.5 Conclusion

In this study, a process simulation model was developed to evaluate the energy and GHG emissions associated with the ESEIEH extraction process. In this study the recovery process was divided into two sections, extraction in the reservoir and separation at the surface, in order to identify the main areas of energy consumption and GHG emissions. For surface separation, two pathways were developed. In the first, the produced gases from the well are captured to minimize solvent losses and the second considers their use as fuel in steam boilers. The first pathway requires an additional unit to ensure the purification of solvent. Energy consumption in Pathway I and II is 487.2 and 375.5 MJ/bbl, respectively, with corresponding GHG emissions of 77.7 and 59.8 kg CO_2 eq/bbl, respectively. The first pathway is more emissions and energy intensive. In both pathways, electrical energy consumed by the antenna is responsible for the largest share of the overall energy consumption and GHG emissions. Any performance improvement in the antenna would considerably reduce the overall environmental impacts. Considering other sources of electricity, such as the proposed Alberta electricity grid mix by 2030, cogeneration, and 100% renewable energy, showed significantly reduced GHG emissions. Since process simulation-based models are deterministic in nature, the uncertainty in their outcomes needs to be quantified for reliable decision making. An examination of uncertainty results shows that probability ranges in uncertainty in GHG emissions from 9.96 – 87.7 kgCO_2eq./bbl, depending on the source of electrical energy and the pathway considered. The uncertainty results show that biomass electricity sources have the lowest emissions while the current Alberta grid mix has the highest. In the biomass scenario, solvent loss is the main source of uncertainty while antenna

efficiency and the cumulative energy-to-oil ratio of the reservoir are the main sources of uncertainty in Alberta's current electricity grid mix, Alberta's electricity grid mix by 2030, and cogeneration.

Chapter 3: Life cycle assessment of bitumen-derived transportation fuels from toe-to-heel air injection extraction technology

3.1 Introduction

Petroleum fuels make up one-third of global energy use. This use is expected to increase by 19% by 2030 [39]. Efforts to meet the demand have led to the exploitation of unconventional crude resources such as the oil sands in Alberta, a western province in Canada [2]. Alberta is the largest hydrocarbon base in North America. This is due to the large amounts of oil sands in Alberta, most of which are deep underground with large bitumen deposits [5]. Bitumen can be recovered from the oil sands and converted into useful petroleum fuels through extraction of bitumen using in situ or surface mining methods followed by upgrading and refining, respectively [5]. The recovery and conversion processes are energy and greenhouse gas emissions (GHG) intensive [8, 37, 38].

With increasing concerns about climate change impacts, global, national, and local governments are developing GHG emissions reductions initiatives. The California Low Carbon Fuel Standard (LCFS) [17], the European Fuel Quality Directive [16], the pan-Canadian carbon pollution price [91] and Clean Fuel Standard (CFS) initiative [19] are just a few examples. These initiatives and regulations call for appropriate assessment and quantification of the life cycle GHG emissions of various transportation fuels through life cycle assessment (LCA).

Given the need to reduce GHG emissions, means of lowering GHG emissions and energy consumption associated with bitumen extraction processes are sought.

About 80% of the bitumen deposits in Alberta, Canada can be recovered through in situ methods such as cyclic steam stimulation (CSS) and steam-assisted gravity drainage (SAGD) [92]. Currently, the amount of bitumen produced from in situ recovery in Alberta is about 1.6 million barrels per day (mbpd) (57% of total production) and is projected to reach 2.22 mbpd by 2030 [2]. Commercialized in situ recovery methods such as CSS and SAGD use large amounts of natural gas to produce steam in the recovery of bitumen [5]. The large energy requirements result in GHG emissions of 45-190 kg CO_2eq in the extraction of one barrel of bitumen [8, 45]. The produced bitumen is also viscous ; thus it requires diluent to meet pipeline transportation specifications and upgrading to meet refinery specifications [8, 56]. In addition, the level of upgrading (partial or full[6]) influences how much of the resource (i.e., hydrogen for hydrotreating and hydrocracking) is used in the refinery [9, 93]. Therefore, several new bitumen recovery technologies that could improve the environmental performance of petroleum fuels through their entire life cycle stages are being considered.

In order to reduce the environmental footprint of oil sands-derived fuels, bitumen in situ recovery methods such as solvent-based recovery (SBR) [20, 62, 94], in situ combustion

[6] Partial upgrading are the actions taken to mainly improve the API of bitumen to reduce or eliminate the need for diluent addition. While in full upgrading, in addition to API improvement, the bitumen impurities such as sulfur, metal, and asphaltene are drastically reduced.

(ISC) [95], toe-to-heel air injection (THAI) [21], and many others have been proposed [60, 96-98]. In SBR, a light vapor solvent is injected into the reservoir to heat, reduce bitumen viscosity and precipitate its heavy components to partially upgrade its physical and chemical properties [62]. In ISC, pressurized or enriched air is injected into the reservoir to initiate combustion. The combustion heat reduces bitumen viscosity and burns its heavy components while improving bitumen quality [28]. However, these extraction technologies face major challenges due to high solvent consumption and associated costs for solvent recycling and purification which negatively affects the economics of SBR processes [20, 33]. ISC has a low sweep efficiency[7] due to uneven propagation along the combustion front in the vertical producer well, which leads to low extraction rates [99, 100]. In order to improve ISC, THAI is proposed.

An overview of THAI is shown in Fig. 3.1. In THAI, a horizontal producer well is used in the ISC configuration; this improves both reservoir combustion and sweep efficiency [99]. Although THAI technology is not yet commercialized, there are three ongoing research and development (R&D) projects, one each in Canada, China, and India [29]. The THAI recovery technique is expected to have a high oil recovery factor (up to 85%), significantly reduces bitumen viscosity, and increases bitumen API [30]. In addition, the aromatics, resins, and asphaltene contents of bitumen are also expected to be lower using THAI recovery technique [31].

[7] Volume of the reservoir that is contacted by the injected fluid.

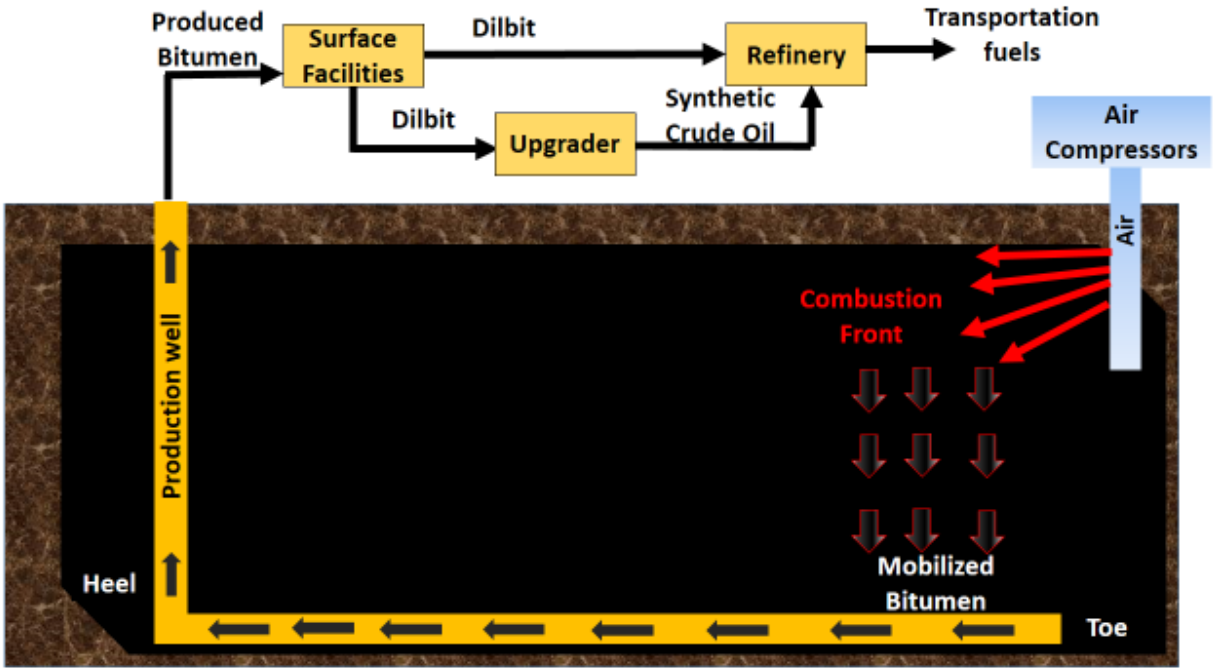

Fig. 3.1. High level diagram of the THAI process

Although THAI is considered to require less water, cost less, and have a higher oil recovery factor than CSS and SAGD [100, 101], there is no study on the assessment of the life cycle energy and GHG emission footprint of THAI process for extraction, upgrading and refining of bitumen from oil sands. Earlier studies are largely focused on understanding and improving the performance of THAI operations. Greaves and colleagues [102] developed a numerical simulation using 3-D cell experimental results to accurately predict the degree of bitumen upgrading and peak temperature of combustion inside the reservoir from the THAI process. Ado et al. [103] developed a detailed dynamic simulation model to predict oil production rate, oil recovery, the amount of oxygen in the produced gas, and the optimum air-to-oil ratio[8] (AOR) for stable combustion in the extraction stage of the THAI process. Boone and colleagues [33] estimated the GHG

[8] The amount of air at the standard conditions that is required to extract one barrel of bitumen.

emissions of THAI based on its pilot performance for the extraction stage only. The impacts of partially upgraded bitumen on downstream processes such as the transportation, upgrading, and refining stages in terms of energy consumption and GHG emissions including the associated uncertainties were not addressed. There is a need to estimate the life cycle energy consumption and GHG footprints of THAI process-based transportation fuel production.

The overall objective of the study is to conduct a comprehensive LCA of THAI process based on engineering principles. The specific objectives are:

- To develop a process model to quantify the energy consumption requirements at each stage of the fuel production from bitumen for THAI process including extraction, transportation, upgrading, and refining.
- To compare the energy and GHG emissions performance of three alternative fuel production pathways based on THAI process: direct refining, delayed coking, and hydroconversion upgrading.
- To conduct sensitivity and uncertainty analysis to understand the impact of various input parameters on the life cycle energy consumption and GHG emissions of petroleum fuels derived through the recovery of bitumen by THAI.

3.2 Method

LCA is a widely used tool that uses systems thinking to evaluate the impact of a product or technology over its whole life cycle. LCA can be used to assess both emerging and commercialized technologies and helps to identify key areas of improvement [24]. Performing an LCA of THAI can help to provide insights into its environmental footprints

during different life cycle stages. This could help both industry and government representatives determine whether this recovery method complies with environmental policies and regulations. An LCA could also facilitate climate policy developments and formulations. A detailed bottom-up LCA model was developed to estimate energy use and GHG emissions. The LCA framework is based on International Organization for Standardization (ISO) [25, 27] recommendations. All the inputs and outputs of the system in the form of material and energy are accounted.

3.2.1 Goal and scope definition

We conducted an LCA of transportation fuel production through the THAI extraction process. This study seeks to answer the following questions: What are the environmental impacts of bitumen extraction through the THAI process? What are the energy- and GHG emissions-intensive units in each life cycle stage of this technology? What parameters are sensitive to the overall life cycle GHG emissions? What are the uncertainties in the input data and results? Which THAI-based fuel production pathway would have lower GHG emissions? How does THAI compare with SAGD and surface mining in terms of well-to-combustion (WTC) GHG emissions?

The metrics used for the GHG emissions are $gCO_2eq./MJ$ of gasoline, $gCO_2eq./MJ$ of diesel and $gCO_2eq./MJ$ of jet fuel. The energy and material inputs are aligned with the functional units. The model does not include construction, land use change, or site reclamation as they are out of the scope of the study.

3.2.1.1 System boundary

Fig. 3.2 depicts the WTC life cycle stages of transportation fuel production from oil sands. After the bitumen is extracted from the reservoir, it is processed in surface facilities to remove produced gases, water, and other impurities. The separated bitumen is then mixed with lighter hydrocarbons, such as diluent, to decrease its viscosity and density so that it can be transported by pipeline. The mixture of diluent and bitumen, known as dilbit, can be sent to an upgrader to produce a higher quality crude (synthetic crude oil [SCO]) or blended with lighter crude before being refined. The transportation fuels produced in the refinery are later combusted in vehicle engines [37, 45]. In this study, we considered three pathways for the production of transportation fuels from THAI. In pathway I, four stages over the life cycle, bitumen extraction, crude transportation, refining, and fuel combustion, are considered. In pathways II and III, five stages over the life cycle, bitumen extraction, upgrading, crude transportation, refining, and fuel combustion, are considered. In pathway II, a delayed coker is used and in pathway III, a hydroconversion upgrader is used (see Fig. 3.2). In all three pathways, all life cycle stages from bitumen extraction to transportation fuel combustion are considered.

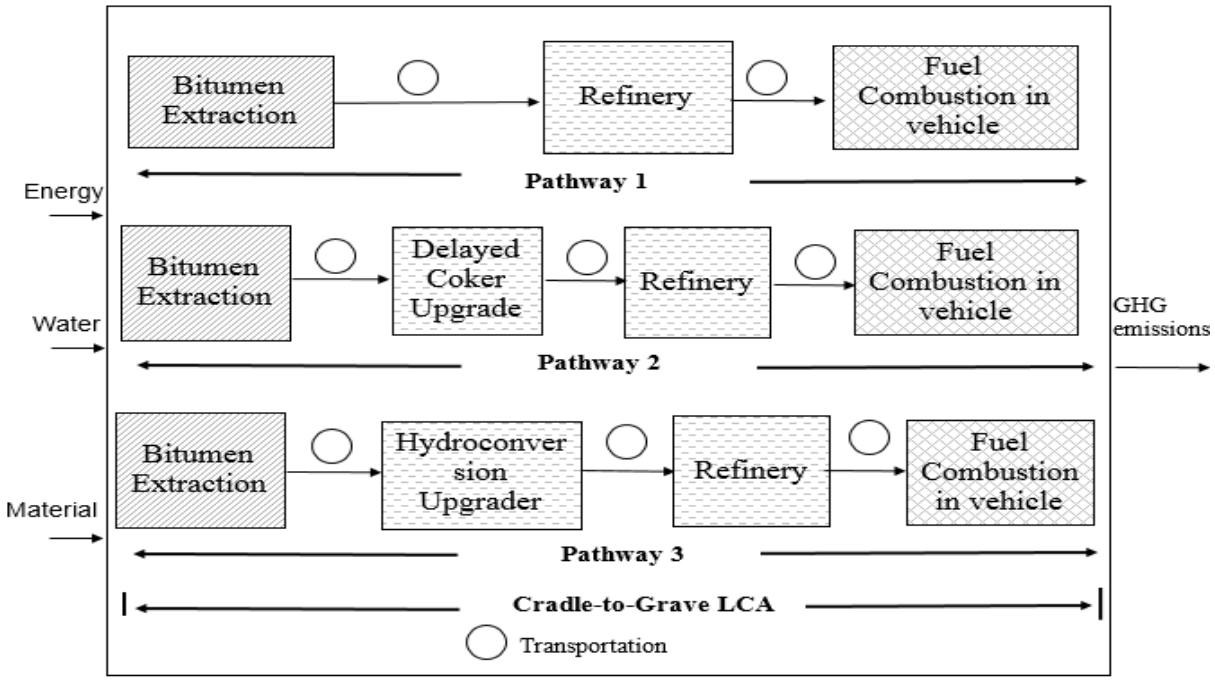

Fig. 3.2. Cradle-to-grave schematic of transportation fuel production from bitumen

3.2.2 Process description and data acquisition

This section describes each life cycle stages in the defined system boundary.

3.2.2.1 Extraction and surface facility

The detailed process schematic for the extraction stage is shown in Fig. 3.3. Initially, there is a long preheating period last several months in the reservoir where pressurized, high temperature steam is circulated through the injector well [104]. Compressed air is then injected into the formation to serve as the oxygen for the combustion in the reservoir [33]. The combustion is either initiated spontaneously or from an electrical igniter [105]. Due to the high heat of combustion, the pressure inside the reservoir increases to 4,000 kPa [104, 106]. The emulsion produced in the production well is comprised of bitumen, water, and the combustion gases. The emulsion is brought to the surface through a flash tank

where gaseous components are separated from the liquid. The liquid is sent to the free water knock out vessel (FWKO), which uses gravity to separate the water from the emulsion [107]. The separated water from the FWKO unit is then sent to water treatment unit before being disposed [104]. Bitumen from the FWKO is treated and blended with diluent in a storage tank [64]. The produced gases from the reservoir are sent to the flaring unit where they are combusted by electrical igniters in tall stacks [105].

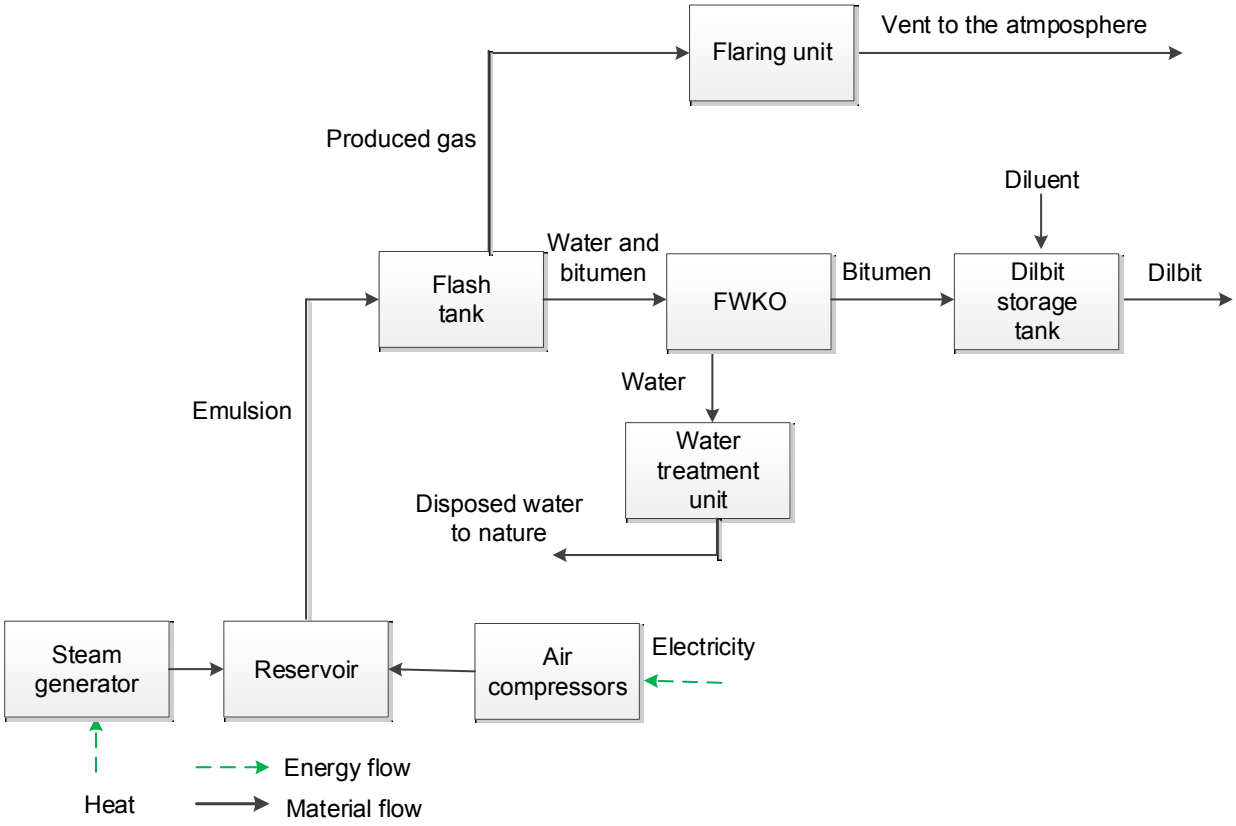

Fig. 3.3. Unit operations involved in extraction units for bitumen extraction in the THAI process.

3.2.2.2 Upgrading

There are different upgrading technologies for processing dilbit [108]. Fig. 3.4 presents a schematic of delayed coker and hydroconversion upgraders, the most common upgrading

technologies in Canada [109, 110]. The dilbit is fed to the atmospheric distillation unit (ADU), where diluent, naphtha, diesel, and the atmospheric residue (AR) are separated. The AR is sent to the vacuum distillation unit (VDU), where gasoil and the vacuum residue (VR) are separated. The VR is then sent to the conversion unit, either a coker or hydroconversion unit, to reduce its sulfur, nitrogen, and aromatic content [45]. In delayed coking, the VR is thermally cracked into lighter fractions while producing coke, a solid residue rich in carbon, nitrogen, and sulfur [111]. In the hydroconversion unit, the VR is converted into lighter products in the presence of catalysts and pressurized hydrogen [112]. Liquid products of the conversion unit are mixed with matching liquid streams produced in the ADU and the VDU and are directed to the corresponding hydrotreater units where hydrogen is added to the streams to further reduce the impurities [113]. Hydrotreater liquid products are combined and form SCO. The purged gases in the plant are routed to the amine treater unit where aqueous alkylamine solutions are used to remove the H_2S and CO_2 from the feed. The H_2S stream is then converted to elemental sulfur in the Claus sulfur recovery unit. However, this unit is not capable of converting all the H_2S. The unconverted hydrogen sulfide is sent to the tail gas treatment unit to be converted to elemental sulfur [112]. The treated gas in the amine treatment unit is routed to the plant fuel system (PFS).

The hydrogen requirements of the upgraders are met through the steam methane reforming (SMR) process, wherein steam and methane are reacted at high temperature and pressure conditions to produce hydrogen [114].

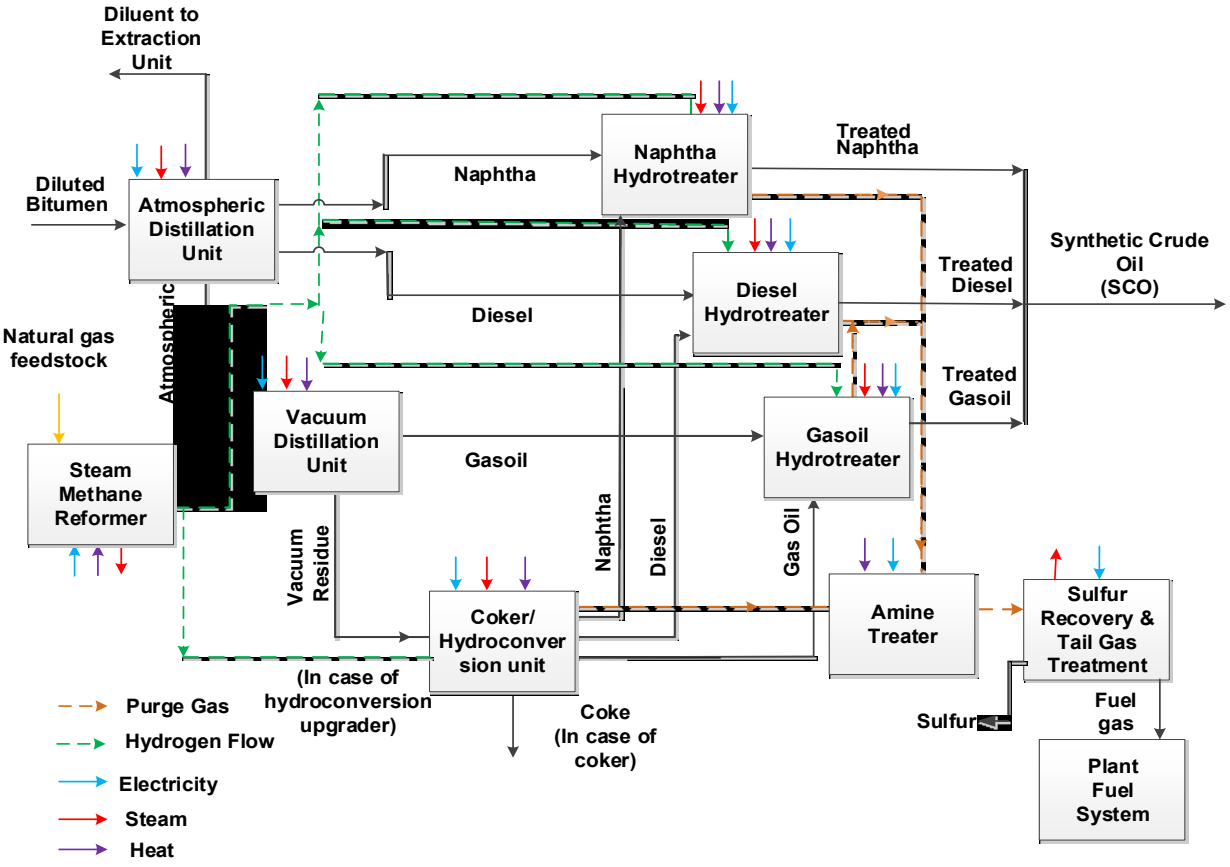

Fig. 3.4. Process flow diagram of the upgraders for processing THAI-based bitumen

3.2.2.3 Refinery

Fig. 3.5 shows the configuration of the deep conversion refinery considered in this study. Refineries use various chemical and physical processes to maximize product yield and produce diesel, jet fuel, fuel oil, gasoline, liquefied petroleum gas (LPG), fuel gas, and coke. A deep conversion refinery has three more processes than an upgrader: cracking, reforming, and alkylation. In the cracking units (fluid catalytic cracking [FCC] and hydrocracking), large hydrocarbons are broken down into smaller molecules in the presence of catalysts, hydrogen, and steam. The reforming unit involves a catalytic

process that rearranges, restructures, and breaks down the low octane naphtha into higher octane reformates in the presence of a catalyst to produce gasoline. Alkylation converts iso-butane, propene, and butene into high-octane gasoline products using catalysts [115-117].

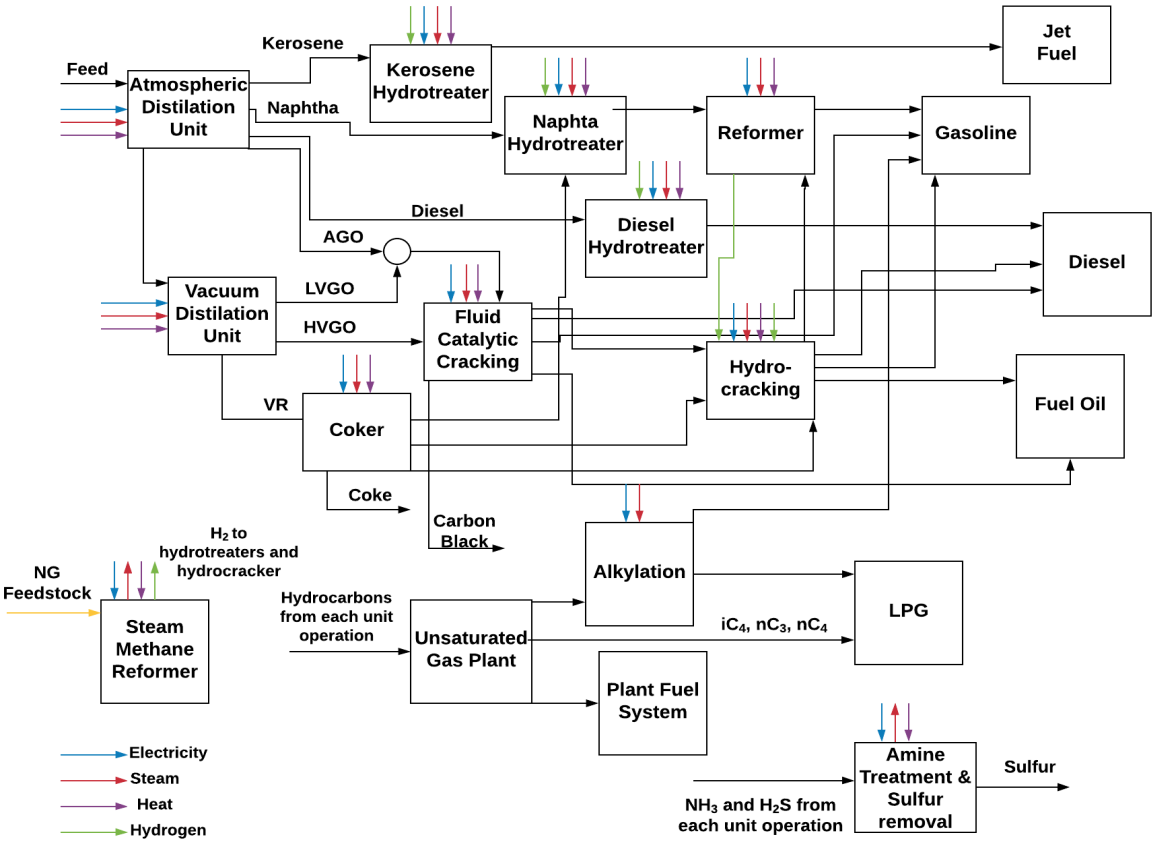

Fig. 3.5. Deep conversion refinery configuration for processing of THAI-based bitumen

3.2.2.4 Fuel delivery, distribution, and combustion in vehicles

Transportation fuels are delivered from refineries to bulk terminals by barge, ocean tanker, rail, and pipeline. Trucks are then used to distribute the fuels from bulk terminals to vehicle fueling stations.

3.2.3 Model development

3.2.3.1 Extraction stage

The pump work for emulsion extraction was calculated using Equation B.1. In order to calculate the energy use and associated GHG emissions during the preheating period, the total amount of steam used for preheating was divided by the total amount of bitumen produced during the lifetime of the well. The compressor work was calculated using Equations B.2-B.5. Air is compressed in several stages. At each stage, the outlet is cooled and compressed again. Since the injection pressure is high, it is assumed that the maximum compression ratio in each stage is 5. A higher compression ratio results in an excessive outlet air temperature, which increases energy consumption and decreases efficiency [118]. The GHG emissions from reservoir combustion and flaring of produced gases are calculated using Equations B.6-B.7. Further details on the calculation of energy and GHG emissions for the extraction stage is provided in the sections B.1-B.4.

It is assumed that natural gas is used to heat the reboiler. The combustion emissions, as well as the upstream emissions associated with recovery, production, and distribution, are considered in the GHG emissions assessment.

It is assumed that Alberta's electricity grid is used to supply electricity in the extraction stage; all the GHG emissions associated with its production and transmissions are considered in the model.

The default values used in the model for the simulation of the extraction stage are presented in Table 3.1.

Table 3.1: Input values for the calculation of energy use and GHG emissions in the extraction stage

Parameter	Value
Preheating stage	
Quality of steam, % [104]	80.00
Steam-to-oil ratio, m^3/m^3 [104]	0.25
Steam pressure, MPa [104]	8.00
Boiler efficiency,% [8]	85.00
Natural gas EF, kg CO_2eq/Gj [35]	68.00
Compression stage	
Air-to-oil ratio, m^3/m^3 [29]	1500.00
Compressed air pressure, MPa [104, 106]	6.00
Specific heat ratio of air [118]	1.31
Compressor efficiency, % [118]	80.00
Interstage cooling, % [118]	80.00
Alberta grid emission factor, gCO_2eq./kwh [9, 83]	712.00
Produced gas composition (vol%) [119]	
CH_4	5.15
C_2H_6	0.73
C_3H_8	0.47
C_4H_{10}	0.10
CO	1.46
CO_2	15.00
N_2	73.60
O_2	0.30

H_2S	0.39
Combustion EF (kg CO_2eq/m^3) [120]	
CH_4	1.92
C_2H_6	3.46
C_3H_8	5.11
C_4H_{10}	7.15
Emulsion extraction	
Density of bitumen, kg/m^3 [121]	984.00
Extraction temperature, °C [104]	250.00
Wellhead pressure, MPa [104]	4.00
Formation water cut, % [104]	23.00
Vertical well depth, m [29]	750.00
Pump efficiency, % [56]	80.00
Water treatment	
Electricity requirements, Kwh/bbl of water [76]	0.16

3.2.3.2 Upgraders

Rigorous upgrader models were developed in Aspen HYSYS Version 9 [80] to obtain mass balance and utility consumption in each unit operation. A typical upgrading capacity of 150 kbpd was considered [122]. The Peng-Robinson equation of state was the fluid package selected in Aspen HYSYS. An ebullated-bed reactor was used to simulate the hydrocracking unit. The operating conditions of the conversion and hydrotreater units were taken from the literature [111, 123, 124]. The correlations suggested by Edgar [125, 126] and the properties of the hydrotreated liquid products [113] (as shown in Table 3.3) were used to estimate the hydrogen requirements in the hydrotreater units. The hydrogen consumption in the hydroconversion unit is assumed to be 1.5% of the weight of the VR,

as suggested by several authors [112-114, 127]. Energy and feedstock requirements for H_2 production in the steam methane reformer (SMR) unit were taken from literature [128]. The utility consumption in the amine treater, sulfur recovery, and tail gas treatment units were calculated based on values suggested by Pacheco et al. [9].

Steam produced in the Claus sulfur recovery unit is used to fulfil a portion of the plant's steam demand. Natural gas is assumed to be the main source of heat and steam production. It is also assumed that the combustion of the produced gas in the plant fuel system (PFS) unit supplies a portion of the plant's heat demand, and its energy content and GHG emissions factor were calculated based on its composition. Using coke for heat and steam production is GHG-emissions intensive [129]. Currently, coke is mostly stockpiled in Canada because of low natural gas prices and strict environmental regulations [9, 130]. Thus, coke is assumed to be a by-product and is stockpiled. Finally, it is assumed that the electricity demands of the upgraders are satisfied by the Alberta grid.

Table 3.2: Input values for the calculation of energy use and GHG emissions in the upgrading stage

Parameter	Value
Electricity consumption in the ADU, kWh/bbl[a,b] [38]	0.90
Electricity consumption in the VDU, kWh/bbl[a,b] [38]	0.30
Steam consumption in the ADU, MJ/bbl[a,b] [38, 111]	10.75

Steam consumption in the VDU, MJ/bbl[a,b] [38, 111]	9.60
Heater efficiency, % [71, 72]	80.00
Boiler efficiency, % [8]	85.00
NHT H_2 consumption in the DCU, m^3/bbl[a] (calculated)	21.18
DHT H_2 consumption in DCU, m^3/bbl[a] (calculated)	23.95
GHT H_2 consumption in DCU, m^3/bbl[a] (calculated)	27.18
NHT H_2 consumption in HCU, m^3/bbl[a] (calculated)	18.97
DHT H_2 consumption in HCU, m^3/bbl[a] (calculated)	20.78
GHT H_2 consumption in HCU, m^3/bbl[a] (calculated)	23.59
H_2 consumption in the HCU hydrocracker, m^3/bbl[a] (calculated)	27.36
Heat consumption in the amine treater unit[b], MJ/tonne feed [9]	500.00
Amine treater unit electricity use[b], kWh/tonne feed [9]	13.12
Sulfur recovery unit electricity use[b], kWh/tonne feed [9]	64.87
SMR unit electricity use[b], kWh/m^3 of H_2 [38]	0.028
SMR unit steam use[b], kg/ m^3 of H_2 [38]	0.86
SMR unit fuel requirement[b], m^3 NG/m^3 H_2 [38]	0.04
SMR unit feedstock requirement[b], m^3 NG/m^3 of H_2 [38]	0.36
Produced gas EF in the DCU, g CO_2eq./kg (calculated)	2756.45
Produced gas EF in the HCU, g CO_2eq./kg (calculated)	2776.74
Electricity EF for the upgraders, kg CO_2eq/MWh [9, 83]	712.00

[a]: bbl and feed refers to the inlet to that unit operation, not to the whole refinery or upgrader

[b]: These values are the same for upgraders and refineries

Table 3.3: Upgrader product specifications [113]

Properties	Naphtha	Diesel	Gasoil
Aromatic content, wt%	15.8	36.5	50.9
Nitrogen content, wppm	21	264	455
Sulfur, wt%	0.014	0.044	0.15

The same methods, assumptions, and values were used for H_2 production, the source of heat, and the calculation of energy consumption in the amine treater, the Claus sulfur recovery unit, and the tail gas treatment unit in the refinery section.

3.2.3.3 Refinery stage

The built-in deep conversion refinery model in Aspen HYSYS [80] was used to simulate the refinery process for dilbit and SCO produced in upgraders at a refining capacity of 150 kbpd. Aspen HYSYS obtained the yields from the separation units (ADU and VDU) and the associated energy consumption based on the crude's distillation curve and physical and chemical properties, such as the API and the sulfur content [131]. The crude assays for SCO and dilbit are presented in Tables B.2 and B.3. Other processing units in the refinery are simulated with petroleum shift reactors. These reactors are empirical models that calculate the product yields and utility consumption of each unit operation based on feed flow rate, feed properties, and a set of linear equations [132].

It is assumed that the refineries are located in the USA as 94% of non-upgraded bitumen produced in Alberta and 56% of the upgraded bitumen is exported to US refineries [3]. Refinery electricity emissions factors were calculated by taking the weighted average of each state's electricity emission factor and the corresponding refinery capacity of each state [45]. However, we have also conduced the sensitivity analysis for processing of bitumen in Alberta's refinery and hence used the associated electricity emission factors.

Since refinery processes result in several products, and products do not undergo the same processes, proper allocation of the refinery products is required [133]. The energy consumption and associated GHG emissions were allocated at the sub-process level in

this study, as suggested by ISO 14041 [26]. The energy consumption and associated GHG emissions in each unit operation were distributed among the product streams based on the product's mass. The quantity and type of energy use were traced through the refinery from the ADU to the refinery products. Fuel oil, coke, LPG, and produced gas are considered as by-products. The energy consumption and associated GHG emissions were distributed to gasoline, diesel, and jet fuel in proportion to their mass yields and per MJ of product (MJ of gasoline/diesel/jet fuel). The lower heating value (LHV) of transportation fuels was taken from literature [35].

Table 3.4: Input values for the calculation of energy use and GHG emissions in the refining stage

[a]: bbl and feed refers to the inlet to that unit operation, not to the whole refinery or upgrader

Parameter	Value
H_2 consumption in the HC unit in the bitumen refinery, wt% of the feed[a] [80]	2.83
H_2 consumption in the HC unit for the SCO refinery, wt% of the feed[a] [80]	2.52
H_2 consumption in the NHT unit for the bitumen refinery, m^3/bbl[a] [80]	19.22
H_2 consumption in the KHT unit for the bitumen refinery, m^3/bbl[a] [80]	13.84
H_2 consumption in the DHT unit for the bitumen refinery, m^3/bbl[a] [80]	35.99
H_2 consumption in the NHT unit for the DC SCO refinery, m^3/bbl[a] [80]	1.33
H_2 consumption in the KHT unit for the DC SCO refinery, m^3/bbl[a] [80]	2.33
H_2 consumption in the DHT unit for the DC SCO refinery, m^3/bbl[a] [80]	2.30
H_2 consumption in the NHT unit for the HC SCO refinery, m^3 /bbl[a] [80]	0.73
H_2 consumption in the KHT unit for the HC SCO refinery, m^3/bbl[a] [80]	2.39
H_2 consumption in the DHT unit for the HC SCO refinery, m^3/bbl[a] [80]	2.28
H_2 production in the reformer unit for the bitumen refinery, wt% of the feed[a] [80]	2.22
H_2 production in the reformer unit for the SCO's refinery, wt% of the feed[a] [80]	2.01
Produced gas EF in the bitumen refinery, g CO_2eq./kg (calculated)	2730.10
Produced gas EF in the DC SCO refinery, g CO_2eq./kg (calculated)	2736.30
Produced gas EF in the HC SCO refinery, g CO_2eq./kg (calculated)	2741.29
Electricity EF for the refinery, kg CO_2eq./MWh [134]	581.00
LHV of gasoline, MJ/kg [35]	41.74
LHV of diesel, MJ/kg [35]	42.61
LHV of jet fuel, MJ/kg [35]	43.2

3.2.3.4 Crude transportation and transportation and distribution of transportation fuels stages

Adapting the pipeline model for the transportation of 750,000 bpd of bitumen or SCO (as developed by Nimana et al. [56]), we estimated the energy consumption and associated GHG emissions at the crude transportation stage. In order to account for the diluent amount, the shipped volume was increased to 855,288 bpd in the dilbit case and diluent was calculated using Equation B.10. It is assumed that 100% of the diluent is recycled and sent back to the extraction site after being processed in the upgrader or refinery [135].

The detailed calculations and formulas are presented in Equations B.10-B.18. The emissions factor of the electricity used for transportation to the upgrader is taken from Alberta's grid mix, and for transportation to the refinery, the distance weighted average for the electricity emissions factor across the Alberta-Gulf Coast pipeline path was used [56]. It is assumed that the bitumen extraction site, upgrader units, and refineries are located in Fort McMurray, Fort Saskatchewan, and the Gulf Coast, respectively [37, 56].

The GHG emissions attributed to the transportation fuels' transportation and distribution (T&D) to bulk terminals and fueling stations were imported from literature [35].

Table 3.5: Input values for the calculation of energy use and GHG emissions in the transportation, delivery, and distribution stages

Parameter	Value
Pipeline target velocity, m/s [56]	1.40
Dilbit API [136]	21.40
Diluent API [136]	66.00
Diluent kinematic viscosity, cSt [136]	1.30
Dilbit kinematic viscosity, cSt [136]	268.00
Extraction site distance to the upgrader, km [37]	500.00
Distance from the extraction site to the refinery, km [56]	3000.00
Elevation change from the extraction site to the upgrader, m [137]	-350.00
Elevation change from the extraction site to the refinery, m [137, 138]	+632.00
Electricity EF for crude transportation to the refinery, kgCO_2eq./MWh [139]	725.30
T&D emissions of gasoline, g CO_2eq./MJ of gasoline [35]	0.49
T&D emissions of diesel, g CO_2eq./MJ of diesel [35]	0.43
T&D emissions of jet fuel, g CO_2eq./MJ of jet fuel [35]	0.42

3.2.3.5 Combustion of transportation fuels

The literature values [35] were used to estimate the GHG emissions in the transportation fuels' combustion stage. GHG emissions at each life cycle stage are aggregated and normalized to the functional unit in order to estimate the total emissions per MJ refinery output, as shown in Equations B.26 and B.27. The GHG emissions were allocated to gasoline, diesel and jet fuel based on their mass yields in the refinery.

3.2.4 Sensitivity and uncertainty analyses

The Morris global sensitivity analysis method was used to screen and determine the sensitive input parameters [140]. The method is based on a partial derivative calculation in randomized locations of the whole range of inputs and is more robust than a local sensitivity analysis that only analyzes the variations in a limited range of input variables [141]. Table 3.6 lists the ranges of input variables considered for the sensitivity analysis.

Uncertainty analysis was used to determine the most probable ranges of GHG emissions in each transportation fuel production pathway. The uncertainty analysis was performed only on the sensitive inputs using a Monte Carlo simulation [142].

Triangular and PERT distributions, which require minimum, mode, and maximum values, were considered in this study in performing a Monte Carlo simulation that resulted in conservative outputs [86, 143]. Triangular distribution is used when limited data are available on the input variable and the mode is known. PERT puts more weight on the mode and less on the minimum and maximum. However, large amounts of historical data or expert opinion are required in order to use it [85].

The mode considered for the AOR is based on the performance of the Kerrobert pilot plant in Canada [29]. The AOR range is wide because of different reservoir properties worldwide [29, 105, 144, 145], thus the PERT distribution is used in order to put more weight on the technology's performance in Canadian reservoirs.

PERT is also used to put more weight on the Aspen HYSYS values determined for hydrotreaters (HTs), hydrocracking units (HCs), and reformer H_2 consumption/production. The range of H_2 consumption in the refinery HT units given in the literature is wide because of differences in the feedstock (heavy, light, medium, sweet, sour, etc.) [38]. Since the objective of this study is to analyze the THAI bitumen and produced SCO, considering the wide range from the literature is not appropriate. Therefore, a range of ±25% of the base case value is considered in sensitivity and uncertainty analyses. Specifications of transportation fuels and desired refinery product yield determine the H_2 consumption in the HC unit [146]. H_2 production in the reformer unit is affected by the reaction pressure, desired octane number of the gasoline, and the level of reduction in the aromatics and benzene required to meet environmental regulations [116, 147-149]. Values reported in the literature for H_2 in the reformer and the HC unit were used to conduct sensitivity and uncertainty analyses. Given limited availability of data, a triangular distribution was used for the other parameters.

The modes are the default values in the model (shown in Tables 3.1, 3.2, 4 and 3.8). The range of input variables and their corresponding distributions are listed in Table 3.7.

Table 3.6: Range of variables considered for the sensitivity analysis

Input	Range
Extraction	
Air-to-oil ratio, m^3/m^3 [105, 145]	1000 – 2700
Injected air pressure, MPa [106, 145]	3.5 – 8
Compressor efficiency, % [118]	75 – 85
Interstage cooling, % [118, 143]	60 – 100
Steam-to-oil ratio, m^3/m^3 [104]	0.18 – 0.30
NG boiler efficiency, % [8, 87-89]	70 – 90
Vertical well depth, m [29, 99]	380 – 780
Water cut, % [99, 104]	22 – 70
CO_2 in the produced gas, vol% [22, 105]	12 – 17
Hydrocarbon content of the produced gas, vol% [119]	5.8 – 7.1
Electricity EF[a], g CO_2eq/kWh [35, 77, 150, 151]	484 – 845
Upgrading	
DCU NHT H_2 use, scf /bbl	561 – 935
DCU DHT H_2 use, scf /bbl	634 – 1057
DCU GHT H_2 use, scf /bbl	720 – 1200
HCU NHT H_2 use, scf /bbl	502 – 837
HCU DHT H_2 use, scf /bbl	550 – 917
HCU GHT H_2 use, scf /bbl	625 – 1041
HCU HC H_2 use, scf /bbl	725 – 1208
Heater efficiency [b], % [71, 118, 143, 152]	70 – 90
ADU steam consumption [b], lb/bbl [9, 38]	6.6 – 10
ADU electricity use [b], kWh/bbl [9, 38]	0.7 – 0.9
VDU steam consumption [b], lb/bbl [9, 38]	5.8 – 6.5
SMR electricity use [b], MWh/m^3 of H_2 [38]	0.0215 – 0.0294
SMR steam use [b], kg/ m^3 of H_2 [38]	0.6465 – 1.0775
SMR fuel requirement [b], m^3 NG/m^3 H_2 [38]	0.02985 – 0.04975
SMR feedstock requirement [b], m^3 NG/m^3 of H_2 [38, 111, 116, 128, 153, 154]	0.22 – 0.362
Heat consumption in the amine treater unit [b], MJ/tonne feed [9]	375 – 625
Amine treater electricity use [b], kWh/tonne feed [9]	10 – 16
Sulfur recovery unit electricity use [b], kWh/tonne feed [9]	49 – 81

Refinery	
HC H_2 use, wt% of feed [114]	1.5 – 4.0
Reformer H_2 production, wt% of feed [116]	1.6 – 2.6
H_2 use in HTs in the bitumen refinery, scf/bbl	656.1 – 1093.5
H_2 use in HTs in the DCU SCO refinery, scf/bbl	43.6 – 72.7
H_2 use in HTs in the HCU SCO refinery, scf/bbl	40.3 – 67.2
H_2 use in the NHT in the bitumen refinery, scf/bbl	514.6 – 857.7
H_2 use in the KHT in the bitumen refinery, scf/bbl	370.5 – 617.6
H_2 use in the DHT in the bitumen refinery, scf/bbl	962.7 – 1604.5
H_2 use in the NHT in the DCU SCO refinery, scf/bbl	35.5 – 59.2
H_2 use in the KHT in the DCU SCO refinery, scf/bbl	62.3 – 103.8
H_2 use in the DHT in the DCU SCO refinery, scf/bbl	70.9 – 118.2
H_2 use in the NHT in the DCU SCO refinery, scf/bbl	19.6 – 32.7
H_2 use in the KHT in the DCU SCO refinery, scf/bbl	64.1 – 106.7
H_2 use in the DHT in the DCU SCO refinery, scf/bbl	61.1 – 101.9
Electricity EF, g CO_2eq/kWh [c] [35]	484 – 1048
Transportation	
Pipeline target velocity, m/s [56]	0.7 – 2.0
Pump efficiency, % [56]	75 – 92
Electricity EF, g CO_2eq/kWh [56]	701 – 990
Diluent API [136]	57.2 – 72.1

Table 3.7: Input parameter ranges and distribution for the Monte Carlo simulation

Input	**Range**
Extraction	
Air-to-oil ratio, m^3/m^3 [29, 33, 105, 144, 145]	PERT (1000, 1500, 2700)
Injected air pressure, MPa [104, 106, 145]	Triangular (3.5, 6, 8)
Compressor efficiency, % [118]	Triangular (75, 80, 85)
Interstage cooling, % [118, 143]	Triangular (60, 80, 100)
NG boiler efficiency, % [8, 87-89]	Triangular (70, 80, 90)
CO_2 in produced gas, vol % [22, 119]	Triangular (12, 15, 17)
Hydrocarbon content of the produced gas, vol% [119]	Triangular (5.8, 6.45, 7.1)
Electricity EF[a], g CO_2eq/kWh [9, 35, 77, 78, 83, 150]	Triangular (484, 712, 845)

Upgrading	
DCU NHT H_2 use, scf /bbl	PERT (561, 748, 935)
DCU DHT H_2 use, scf /bbl	PERT (634, 845.5, 1057)
DCU GHT H_2 use, scf /bbl	PERT (720, 960, 1200)
HCU NHT H_2 use, scf /bbl	PERT (502, 669.5, 837)
HCU DHT H_2 use, scf /bbl	PERT (550, 733.5, 917)
HCU GHT H_2 use, scf /bbl	PERT (625, 833, 1041)
HCU HC H_2 use, scf /bbl	PERT (725, 966.5, 1208)
Heater efficiency [b], % [71, 118, 143, 152]	Triangular (70 ,80, 90)
SMR electricity use [b], kWh/m^3 of H_2 [38]	Triangular (0.0215, 0.02545, 0.0294)
SMR steam use [b], kg/ m^3 of H_2 [38]	Triangular (0.6465, 0.862, 1.0775)
SMR fuel requirement [b], m^3 NG/m^3 H_2 [38]	Triangular (0.02985, 0.0398, 0.04975)
SMR feedstock requirement [b], m^3 NG/m^3 of H_2 [38, 111, 116, 128, 154]	Triangular (0.22, 0.291, 0.362)
Refinery	
Bitumen refinery HC H_2 use, wt% of feed [114]	PERT (1.50, 2.83, 4.00)
DCU SCO refinery HC H_2 use, wt% of feed [114]	PERT (1.50, 2.52, 4.00)
HCU refinery HC H_2 use, wt% of feed [114]	PERT (1.50, 2.52, 4.00)
Bitumen refinery reformer H_2 production, wt% of feed [116]	PERT (1.60, 2.22, 2.60)
DCU SCO refinery reformer H_2 production, wt% of feed [116]	PERT (1.60, 2.01, 2.60)
HCU SCO refinery reformer H_2 production, wt% of feed [116]	PERT (1.60, 2.01, 2.60)
H_2 use in HT's in bitumen refinery, scf/bbl	PERT (656.1, 874.8, 1093.5)
H_2 use in HT's in DCU SCO refinery, scf/bbl	PERT (43.60, 58.15, 72.70)
H_2 use in HT's in HCU SCO refinery, scf/bbl	PERT (40.30, 53.75, 67.20)
Electricity EF for refinery, g CO_2eq/kWh [35, 134]	Triangular (484, 581, 1048)[c]
Transportation	
Pipeline target velocity, m/s [56]	Triangular (0.7,1.4, 2.0)
Pump efficiency, % [56]	Triangular (75, 85, 92)

[a]: The same value was used for upgrader electricity EF. The minimum value refers to getting the electricity from a nearby SAGD cogeneration plant and the maximum value represents the higher estimate of the current Alberta grid mix.

[b]: These values are the same for the refinery section.

[c]: Mean refers to the weighted average of the electricity emissions factors in each state with refinery in the United States and the lower and maximum values refer to getting the electricity from the cogeneration and coal power plant, respectively.

3.3 Results and discussion

This section provides the key findings of the study. First, the detailed analysis and associated results of the important life cycle stages that significantly contribute to the overall GHG emissions of the transportation fuel are presented. This is followed by the overall life cycle GHG emissions results.

3.3.1 Extraction and surface facilities

The overall energy consumption of the THAI extraction process is 273.2 MJ per barrel of bitumen. As shown in Fig. 3.6, the compressors are the main energy-intensive units and consume 57% of the overall energy, followed by the natural gas boiler, which makes up 42% of the total. The water treatment unit and pumps consume only 1% of energy.

The GHG emissions associated with each unit operation in the extraction stage are also presented in Fig. 3.6. The combustion in the reservoir is the main contributor to the overall GHG emissions in this stage. Next to reservoir combustion are the flaring of the produced gases and the compressors. The GHG emissions associated with the combustion in the reservoir were estimated to be in the range of 14.5-16.8 $gCO_2eq./MJ$ of transportation fuels. A high amount of energy is required to mobilize the bitumen from the reservoir. In

the THAI operation, the energy to move the bitumen can be met through the combustion of the reservoir. The AOR in this case is relatively high. To produce one m^3 of oil requires, about 1,500 m^3 of air, thus releasing a large amount of GHG emissions through the reaction between air and light hydrocarbons in the reservoir. The GHG emissions associated with the flaring of produced gases and compressors were estimated to be 7.3-8.4 $gCO_2eq./MJ$ and 5.5-6.3 $gCO_2eq./MJ$ of transportation fuels. These values are a function of the AOR. An increase in the AOR increases the amount of produced gas from the reservoir and the compressor power. Preheating the reservoir contributes only 5% to the overall GHG emissions; this figure is low mainly because of the short preheating period. The pumps and water treatment unit have a negligible impact on the GHG emissions.

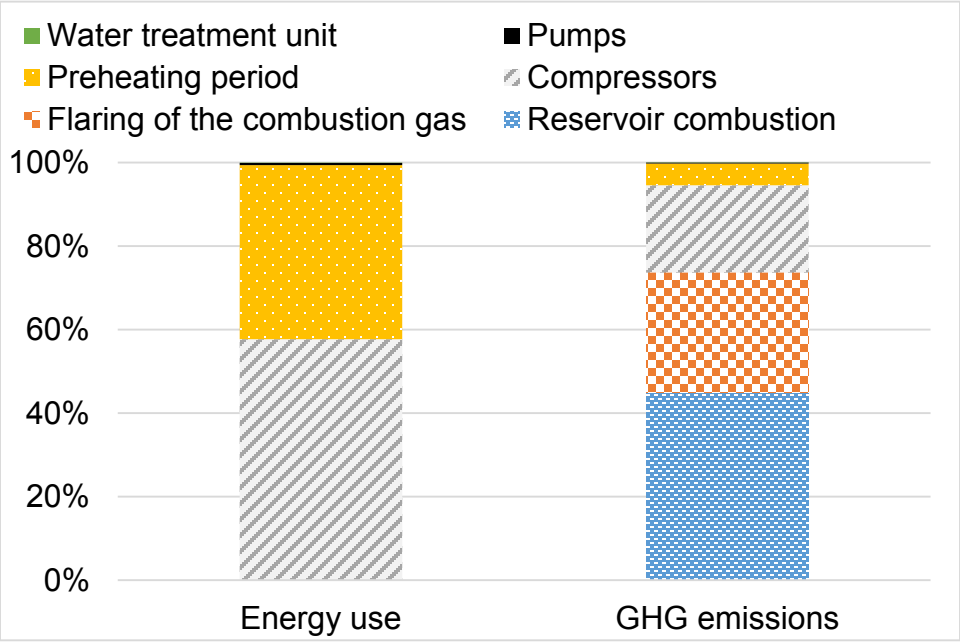

Fig. 3.6. Shares of energy use and GHG emissions in different unit operations in crude extraction in the THAI process

3.3.2 Upgrading

The base case energy consumption for the delayed coking upgrader (DCU) and the hydroconversion upgrader (HCU) are 0.73 and 0.9 GJ/bbl of bitumen, respectively. The fuel required for heat and steam generation, along with the natural gas used as feedstock for hydrogen production, is the largest source of energy consumption. Electricity comprises only 2% and 2.8% of the overall energy consumption in the DCU and the HCU, respectively. A significant portion of the heat requirement in both upgraders is met using the gas produced in the plant (48% in the DCU and 34% in the HCU). The hydroconversion upgrader consumes more energy because it requires more hydrogen, which results in higher fuel, feedstock, and electricity consumption. Furthermore, the hydrocracking unit consumes more electricity than the delayed coker unit. This is because of the high compression energy required by hydrogen for the optimal hydrotreating reaction and the pump energy required for increased product yield [113, 135]. The utility consumption in each upgrader unit operation is presented in Table 3.8.

Table 3.8: Upgrader yields and utility consumption

Upgrader yields			
	Unit	Delayed coking	Hydroconversion
SCO	m^3/m^3 bitumen	0.96	1.09
SCO	kg/kg bitumen	0.84	0.96
Coke	kg/bbl bitumen	13.62	--
H2S	kg/bbl bitumen	2.88	4.42
Utility consumption			
	Delayed coking	Hydroconversion	Units
Fuel gas	5.12	4.07	kg/bbl bitumen
NG[a]	12.1	16.7	m^3/bbl bitumen
Steam[a,b]	8.59	11.06	kg/bbl bitumen
Electricity	4.24	7.33	kwh/bbl bitumen
H_2[a]	1.93	2.55	kg/bbl bitumen

[a]: Emissions from hydrogen and steam production are included in natural gas, fuel gas, and electricity emissions.
[b]:2.79 MJ/kg is considered for the LHV of the steam [111].

The SCO produced in the DCU is different than that obtained from the HCU in quality, mass, and volume yield. The simulation results show the DCU and the HCU mass yields of 84% and 96%, respectively. The increased yield in the hydroconversion unit is because of the improved conversion of the vacuum residue to lighter hydrocarbons, leaving little or no by-product coke. That said, 8.8 wt% of the bitumen is converted to coke in the DCU. Furthermore, higher hydrogen consumption and lower gas production in the HCU results in a higher mass yield than in the delayed coker. Detailed information on upgrader yields can be found in Table 3.8.

GHG emissions from the upgraders range from 8.11-8.39 g CO_2eq/MJ in the DCU and from 9.06-9.37 gCO_2eq./MJ in the HCU for the three products. There are two main reasons for the relatively higher GHG emissions from the HCU. First, the HCU uses the hydrogen- and emission-intensive hydrocracker to convert the vacuum residue (VR), while coker unit does not consume hydrogen. Second, higher yield of vacuum residue in hydrocracker compared to the coker means more products are treated in hydrotreaters [113, 155].

Fig. 3.7 presents the GHG emissions percentage contributions of different unit operations involved in both upgraders. Hydrogen production appears to be the main contributor, with 43.70% and 47.20% from the DCU and the HCU. This is mainly because of the large steam requirement and of natural gas both as fuel and as feedstock in the SMR process [128]. The ADU is the second largest contributor to GHG emissions with shares of 32.50%

and 26.2%, from the DCU and the HCU, respectively. The consumption of natural gas and fuel gas are the key sources of GHG emissions, with more than 90% contribution. Electricity forms only 7% and 9% of total emissions in the DCU and the HCU, respectively.

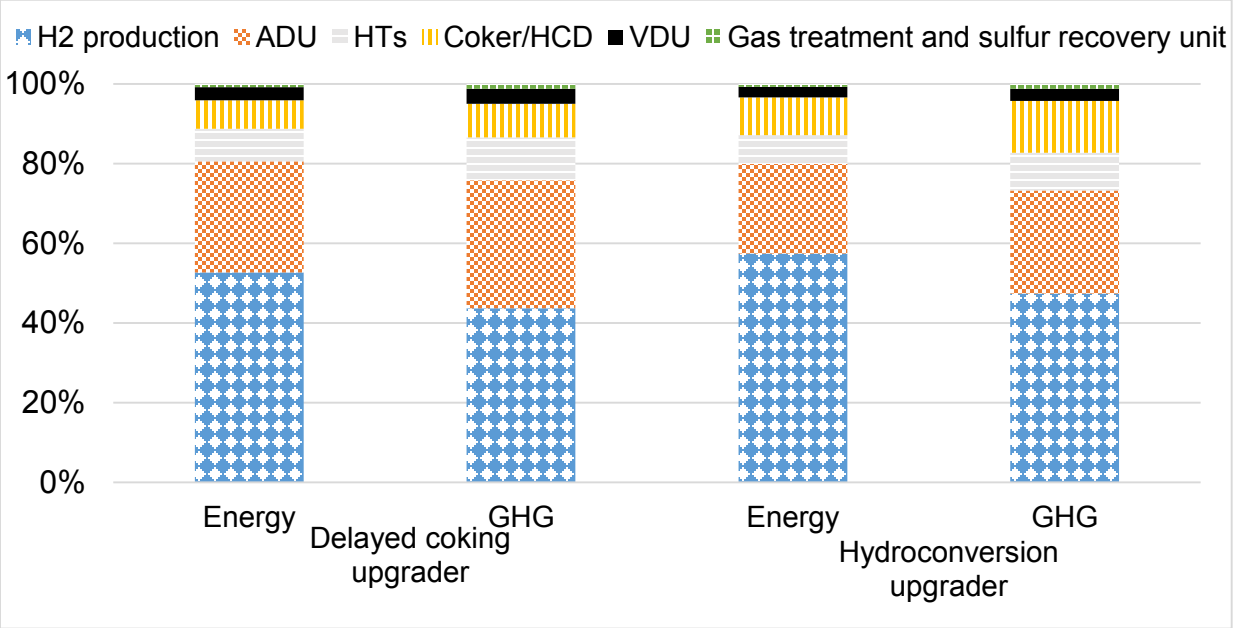

Fig. 3.7. GHG emissions contribution from different unit operations in delayed coking (DCU) and hydroconversion (HCU) upgraders

3.3.3 Refinery

The deep conversion refinery model described in section 3.2.2.3 was used to determine product yield, energy use, and associated GHG emissions for bitumen both directly sent for and undergoing upgrading. Bitumen is rich in heavier fractions such as vacuum residue and gasoil while SCO is a lighter crude rich in naphtha, kerosene, and diesel (see Table B.3). Refining of SCO yields more diesel and jet fuel than bitumen does, while more gasoline is produced in the bitumen pathway. Moreover, 8.80 wt% of bitumen is converted into coke during the refining process, as stated in section 3.3.2. On the other hand, SCO

produces little or no coke (bottomless) in the refinery. More fuel oil is produced in the bitumen refinery than the SCO refinery because bitumen has more heavier fractions than SCO [37]. Because of the pre-processing of bitumen into SCO, H_2S production is considerably lower for SCO in the refinery. Additional information on refinery yields is provided in Table 3.9.

Table 3.9: Refinery yields and utility consumption

		Refinery yields		
	Unit	Bitumen	DC SCO	HC SCO
Gasoline	bbl/bbl crude	0.58	0.43	0.43
Diesel	bbl/bbl crude	0.23	0.33	0.31
Jet fuel	bbl/bbl crude	0.20	0.26	0.26
Fuel oil	bbl/bbl crude	0.08	0.05	0.04
LPG	bbl/bbl crude	0.02	0.01	0.01
Fuel gas	kg/bbl crude	6.81	3.29	2.67
H2S	kg/bbl crude	2.20	0.07	0.04
Coke	kg/bbl crude	13.06	0.00	0.02
		Utility consumption		
NG	m3/bbl crude	13.13	7.40	7.87
Steam[a]	kg/bbl crude	28.90	15.10	15.60
Electricity	kwh/bbl bitumen	12.60	8.54	8.04
H2[b]	kg/bbl bitumen	0.97	-0.26	-0.40

[a]:2.79 MJ/kg is considered for the LHV of the steam [111].

[b]:The produced H_2 in the reformer unit exceeds the H_2 consumption in the hydrotreaters and the hydrocracker unit for both SCOs.

The energy consumed to refine bitumen is 0.65 GJ/bbl while it is 0.35 and 0.36 GJ/bbl for DC and HC SCO. Fig. 3.8 gives the breakdown of energy use shares for refining bitumen, delayed coker SCO, and hydroconversion SCO. Refining bitumen requires up to 87.5% more heat and 56.0% more electricity than does SCO. There are two main reasons for these differences. First, bitumen is much richer in heavy ends that require more heat for vaporization and separation in distillation units. Secondly, because of the low H/C ratio

and the high sulfur, metal, and nitrogen content of bitumen compared to SCO, more H_2 and a more severe treatment are required to convert the bitumen into final products and meet desired specifications. The produced gases in different unit operations are directed to the PFS unit and used to satisfy a portion of the heat requirement in the refinery. They supply 54.2%, 46.8%, and 45.1% of the heat demand for bitumen refining, DC SCO, and HC SCO, respectively.

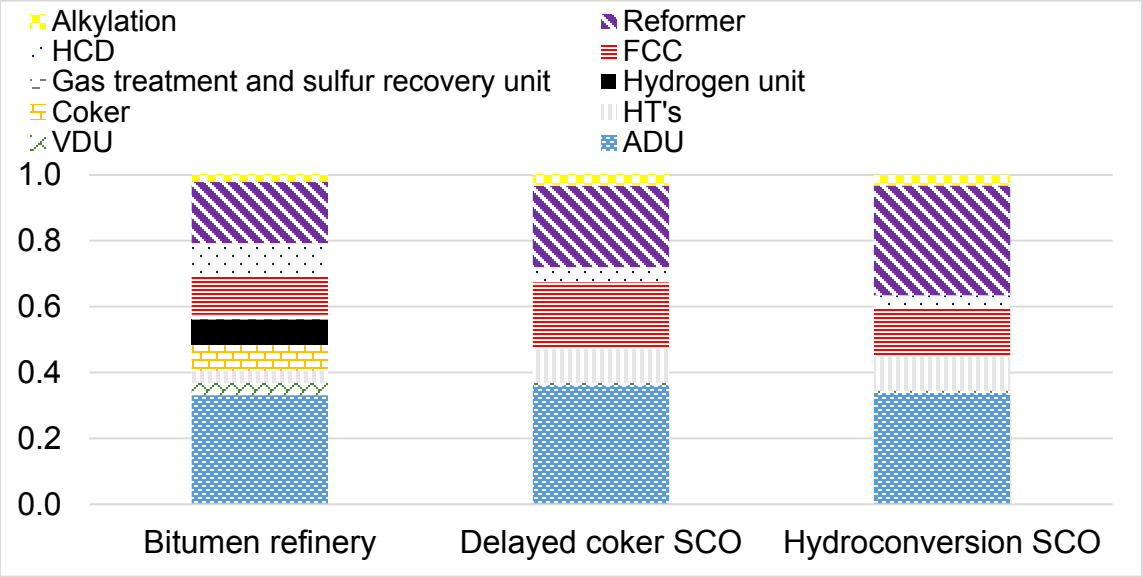

Fig. 3.8. Share of energy use in refining of bitumen, delayed coker SCO, and hydroconversion SCO

As shown in Fig. 3.8, the ADU is the major contributor to the overall heat consumption, followed by the reformer and the FCC unit. Heat consumption in the reformer is relatively high and almost equal to that of the ADU in the hydroconversion SCO refinery. This is because of the large fraction of naphtha distillate in the HC SCO that undergoes an energy-intensive reforming process [156] (see Table B.3). The FCC and alkylation units are the most electricity-intensive units. The energy consumption of the coker unit for refining the DC and the HC SCO is not significant, unlike in bitumen refining. This is

because the coker and hydroconversion SCO have little or no vacuum residue, while bitumen has 30 wt% (see Table B.3). As illustrated in Table 3.9, the H_2 produced in the reformer unit exceeds the H_2 requirements of the DC SCO and HC SCO refinery. Hence, zero energy consumption is assigned to the H_2 production unit for the SCO refinery. However, this unit makes up 8.20% of the overall heat and 2.60% of the total electricity use in refining the bitumen. It is assumed that the excess H_2 is exported to the nearby chemical and petrochemical facilities and an emissions credit equal to what is emitted to produce this amount of H_2 is assigned to it.

The GHG emissions associated with refining bitumen and SCO are presented in Fig. 3.9. Refining SCO emits fewer GHGs than bitumen because of the lower processing energy requirements. However, it should be noted that SCO has undergone the emission intensive upgrading process. Hence, life cycle assessment approach is needed to compare the environmental performance of these products. The allocated refinery emissions for jet fuel are considerably lower than for other products. This is because only three unit operations are used in the production of jet fuel (ADU, VDU, and kerosene hydrotreating unit (KHT). Diesel produced from bitumen is the most emissions intensive because of the high H_2 requirement in the DHT and the HC units. The GHG emissions associated with producing transportation fuels are slightly lower for processing HC SCO than DC SCO. This is because of the higher H/C ratio and lower sulfur content of HC SCO compared to DC SCO, which is a result of severe hydrotreating and hydrocracking during the upgrading stage.

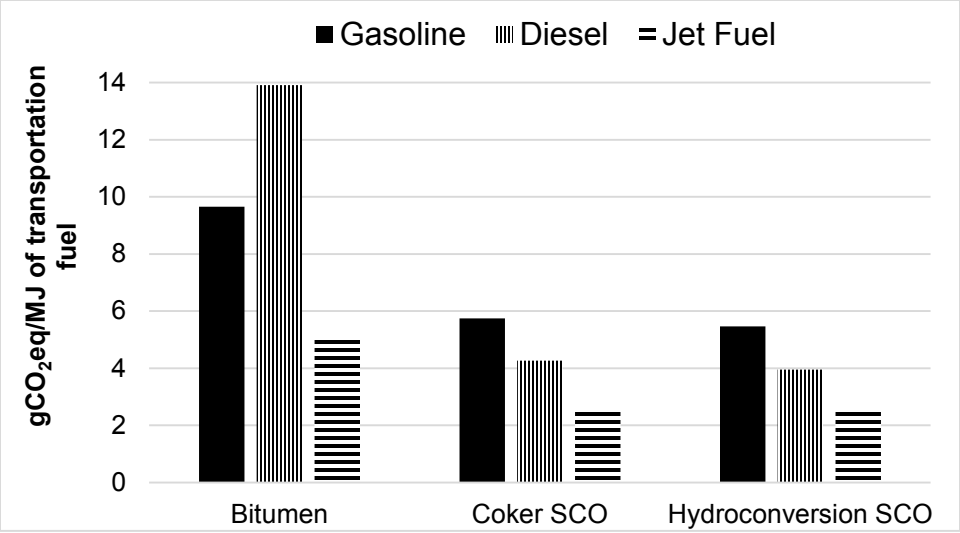

Fig. 3.9. GHG emissions associated with refining bitumen and SCO

3.3.4 Crude transportation

The model predicts the crude transportation GHG emissions of 0.46 gCO_2eq./MJ in pathway 1, 0.38 gCO_2eq./MJ in pathway 2, and 0.32 gCO_2eq./MJ in pathway 3 under the base case assumptions.

The reason behind higher GHG emissions in pathway 1 is that diluent is transported for 3,000 km along with the bitumen and returns back to the production facility while in SCO pathways the diluent is transported only for 500 km to the upgrader unit and recycle back to the extraction site. Furthermore, SCOs are lighter and less viscous compared to dilbit that require lower pumping energy.

GHG emissions due to transportation of bitumen to hydroconversion upgrader is lower than the coker upgrader. The reason is that lower volume flow of dilbit is required to be transported to the HCU to produce the same amount SCO by the DCU (Table 3.8). This is because the HCU produces higher yield of SCO processing the same volume of dilbit

by the DCU. As earlier discussed, unlike the DCU, more hydrogen is required by the HCU to converts vacuum residue that would have been discarded as coke.

3.3.5 The WTC comparative assessment results

Table 3.10 presents the global WTC GHG emissions of THAI-based transportation fuels. Gasoline, diesel, and jet fuel are the main output products considered. For each product, three alternative energy conversion pathways were analyzed. In each pathway, the combustion stage has the highest share of global GHG emissions, more than 63%. Next to combustion is the extraction stage with a significant contribution (22%). The refinery and upgrading stages make up 4.8-13.0% of total WTC GHG emissions. The GHG emissions from transportation of crude and transportation fuels are minimal in all cases.

Table 3.10: Breakdown of WTC emissions in the production of transportation fuels through different pathways ($gCO_2eq./MJ$)

Life cycle stages	Gasoline			Diesel			Jet fuel		
	P1	P2	P3	P1	P2	P3	P1	P2	P3
Extraction	29.0	29.5	26.4	28.4	28.9	25.8	28.0	28.5	25.5
Upgrading	0.0	8.4	9.4	0.0	8.2	9.2	0.0	8.1	9.1
Crude transportation	0.5	0.4	0.3	0.5	0.4	0.3	0.5	0.4	0.3
Refinery	9.6	5.8	5.6	13.9	4.3	4.0	5.1	2.6	2.5
T&D	0.5	0.5	0.5	0.4	0.4	0.4	0.4	0.4	0.4
Combustion	72.7	72.7	72.7	74.9	74.9	74.9	72.8	72.8	72.8
Total	112.3	117.3	114.9	118.2	117.2	114.7	106.8	112.8	110.6

P1: Pathway 1, P2: Pathway 2, P3: Pathway 3

3.3.6 Uncertainty analysis

The results presented and discussed thus far are based on default inputs and a number of modelling and parameter assumptions. However, each input has uncertainty associated with its base values and hence has a range that needs to be considered when assessing the variation in the results. Sensitivity analysis was performed to identify the key parameters and areas in which to reduce overall GHG emissions. Uncertainty analysis was carried out on the sensitive inputs to obtain the most likely ranges of GHG emissions. This section describes the WTC uncertainty analysis.

The tornado plots in Fig. 3.10 are used to identify the inputs with the largest influence on the output uncertainty. The AOR appears to be the main source of uncertainty in all pathways, as seen in its wide range and its effect on compressor work, reservoir combustion, and the amount of produced fuel gas. The amount of CO_2 in the produced gas is the second main source of uncertainty based on its impact on the reservoir's combustion emissions.

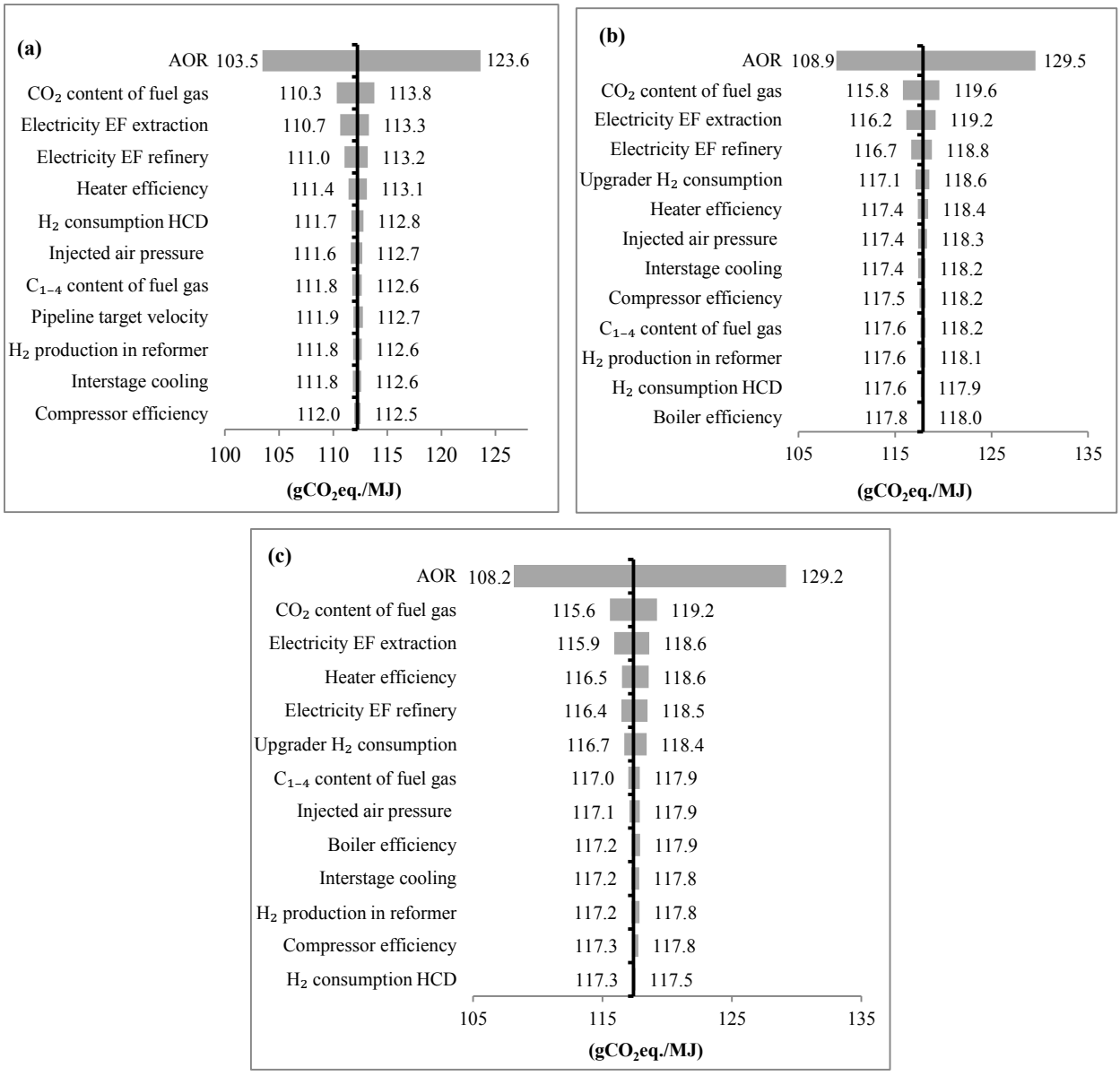

Fig. 3.10. Tornado plots for the WTC emissions in the production of gasoline in different pathways. (a): Pathway 1; (b): Pathway 2; (c): Pathway 3.

Tornado plots for diesel and jet fuel production are presented in Figs B. 10-B. 15. The uncertainty results are shown in Fig. 3.11 using the 5th and 95th percentiles (P5, P95).

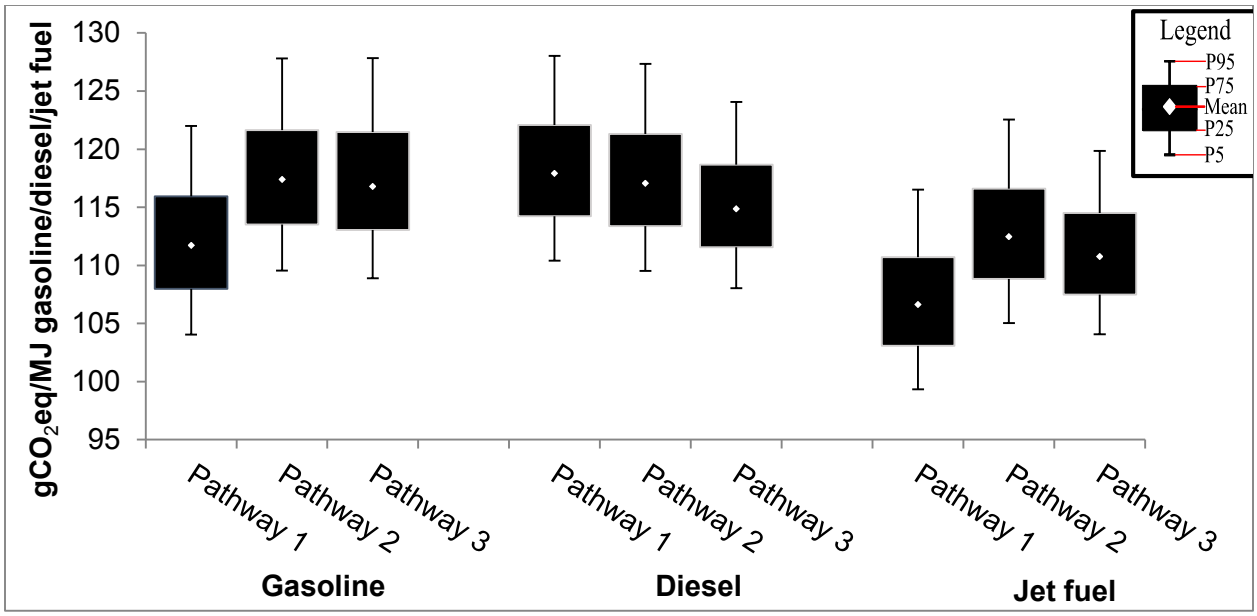

Fig. 3.11. Uncertainty in WTC GHG emissions in the production of transportation fuels from THAI

The uncertainty results show WTC GHG emissions for gasoline production in the range of 104.10-121.98, 109.56-127.80, and 108.90-127.85 $gCO_2eq./MJ$ gasoline in pathways 1-3, respectively. Diesel WTC emissions were found to be 110.40-128.02, 109.51-127.34, and 108.04-124.07 $gCO_2eq./MJ$ diesel in pathways 1-3, respectively. The production of jet fuel results in WTC GHG emissions of 99.34-106.63, 105.04-122.56, and 104.06-122.56 in pathways 1-3, respectively. The mean of its WTC GHG emissions is lower than gasoline's or diesel's because there are fewer unit operations in the jet fuel refinery, as discussed in 3.3.3.

Since all the error bars overlap, it is difficult to say which pathway is the better option. The bars overlap because of the conservative approach used to define the input distributions and range of variables. The results can be improved with more accurate data from industry. However, the emissions means for gasoline and jet fuel production in pathway

1 are lower than in the other two pathways, largely because neither goes through the GHG emissions-intensive upgrading stage. Furthermore, the gasoline yield is higher from bitumen than SCO, as discussed in section 3.3.3. The diesel production WTC GHG emissions mean in pathway 3 is lower than in pathways 1 and 2, mainly because HCU yields more diesel than the DCU and the refining HC SCO yields more diesel than bitumen does.

3.3.7 Comparison of life cycle GHG emission of THAI with SAGD and Surface Mining

A comparison of this study's results and the surface mining and SAGD WTC emissions found in the literature [10-12, 34, 36, 157] was carried in order to determine which technology has lower GHG emissions. The literature report the range of GHG emissions in surface mining and SAGD to be 86.2-115.6 and 98.1-131.8 $gCO_2eq./MJ$, respectively. Our model results for transportation fuel production pathways are within the range of all reported values for SAGD except TIAX's [11]. TIAX uses a simple approach to estimate pre-refinery emissions and assumes a medium conversion refinery that is less GHG emission intensive than the deep conversion one.

Although THAI has an emission-intensive extraction stage, the higher quality of the produced bitumen results in lower emissions in the upgrading and refining stages, a higher yield of SCO during the upgrading stage and transportation fuels production in the refinery unit [8, 37, 38] makes its WTC emissions in the range of those of SAGD.

3.4 Conclusion

This study developed a bottom-up WTC LCA model as FUNNEL-GHG-OS-THAI to assess the energy consumption and associated GHG emissions of transportation fuels produced through the THAI extraction method. Different pathways for transportation fuel production were considered to determine the least emission-intensive pathway.

The results indicate that the WTC GHG emissions are in the range of 104-128, 108-128, and 99-123 g CO_2eq/MJ for the production of gasoline, diesel, and jet fuel, respectively. The combustion emissions dominate the well-to-combustion emissions at 63-67%. The extraction stage is the second most emission-intensive stage and constitutes 21-25% of well-to-combustion emissions. The well-to-combustion emission results show that the air-to-oil ratio is the most significant variable affecting the environmental performance of the toe-to-heel-air injection (THAI) extraction process. Any improvement in the air-to-oil ratio could significantly lower the environmental impact of the recovery method. We compared this study's results with the steam assisted gravity drainage (SAGD) well-to-combustion emissions results found in the literature and found that the well-to-combustion emissions of SAGD and THAI are within the same range. The uncertainty results provide the most likely ranges of the GHG emissions for each product and alternative pathway considered but also highlight the need to further refine key input parameters to have a better interpretation. The results of this study provide a framework for oil sands producers and policy makers to make more informed decisions for GHG emission reduction strategies for THAI-based bitumen products.

Chapter 4: Conclusion and Recommendations for Future Work

4.1 Conclusion

Detailed, transparent, and comprehensive process-based LCA models were developed to evaluate energy use and GHG emissions of Enhanced Solvent Extraction Incorporating Electromagnetic Heating (ESEIEH) and Toe-to-Heel Air Injection (THAI) bitumen recovery methods. For the ESEIEH method, all of the extraction activities were separated into two groups, activities taking place below ground and those taking place above the ground. The extraction of bitumen from the ground was modeled using fundamental science-based theoretical equations, while the energy and GHG emissions from surface facilities were modeled using two rigorous Aspen HYSYS models. The effects of four different electricity sources on the overall GHG emissions were analyzed. For the THAI process, extraction, surface facilities, and crude transportation were simulated based on fundamental science-based theoretical equations while upgrading and refinery stages were simulated on Aspen HYSYS.

4.2 Greenhouse Gas Footprint of ESEIEH Method for Bitumen Extraction

Two alternative pathways were considered for solvent recovery in the ESEIEH process, one with and one without a demethanizer. With a demethanizer, ESEIEH extraction resulted in higher energy use, 487.2 MJ per barrel of bitumen produced. Avoiding the use of a demethanizer resulted in 23% less energy use, although it could lead to 44% more solvent loss from the surface facilities. The base case GHG emissions were estimated to be 77.2 and 59.8 kg CO_2eq/bbl with and without a demethanizer, respectively. In both cases, electricity comprises around 78% of the total energy use. Therefore, four different

scenarios for the source of electricity were considered to assess their impacts on the overall GHG emissions. Supplying the electricity from a renewable source could reduce overall GHG emissions to as low as 10.6 kg CO_2eq/bbl in both pathways.

A Monte Carlo simulation was also performed to arrive at the most likely range of GHG emissions and also to provide a realistic representation of the environmental footprint of these technologies. The uncertainty analysis on the model results show GHG emissions of 10.0-87.7 kg CO_2eq/bbl of bitumen, depending on use of a demethanizer and the source of electricity. Results from the tornado plots highlight that solvent-to-oil ratio (SOR), Cumulative electricity-to-oil ratio of the reservoir (cEOR), and antenna efficiency are the most sensitive inputs.

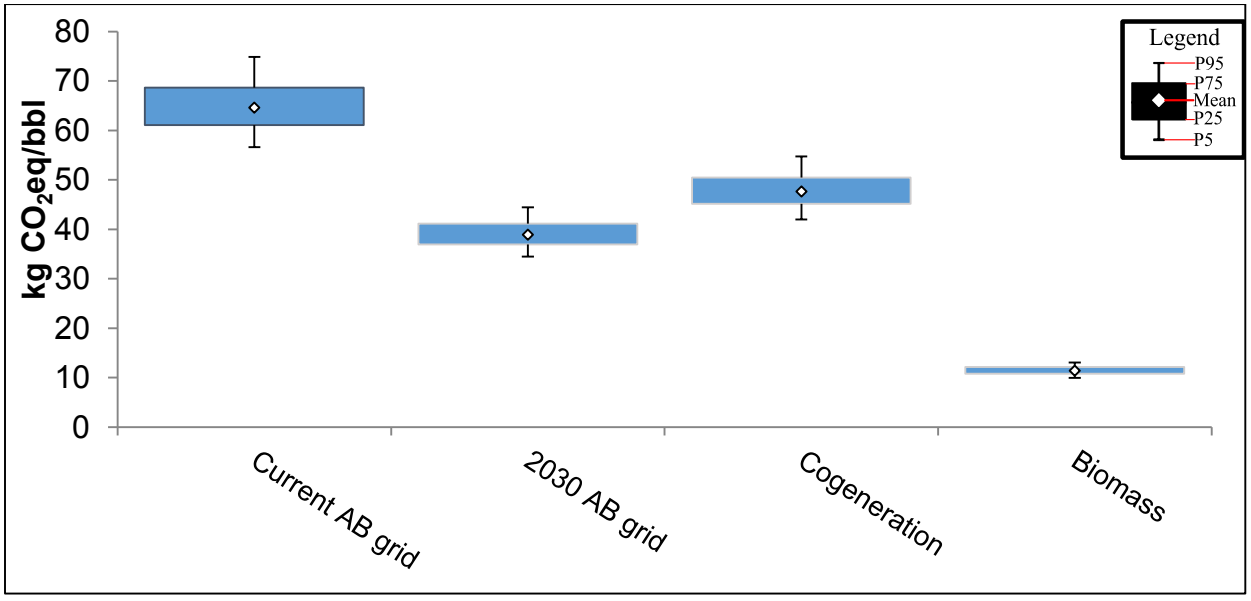

Fig. 4.1. Uncertainty analyses of the difference sources of electricity on the ESEIEH process (In the case of no demethanizer)

4.3 Comparison of ESEIEH GHG emissions in extraction stage with Steam Assisted Gravity Drainage (SAGD) and surface mining

Earlier studies on SAGD and surface mining give emissions values in the range of 45 – 190 and 16-57 kgCO_2eq./bbl of produced bitumen, respectively [8, 45]. The emissions values from the ESEIEH process (Fig. 4.1) are within the range of values reported for the SAGD and surface mining processes. It should be noted that direct comparison cannot be made at this level of operation because the bitumen produced by these processes may differ in composition and properties, suggesting that their volume flow and/or energy content are not equivalent. Direct comparison is suitable after bitumen upgrading and/or refining, when final products have similar properties.

4.4 Greenhouse Gas Footprint of (THAI) for Bitumen Extraction

For THAI process-based transportation fuel production, comparative environmental assessments of three alternative pathways were conducted. The three pathways were: directly sending bitumen to the refinery unit (Pathway 1), upgrading bitumen using a delayed coker (Pathway 2), and upgrading bitumen through hydroconversion (Pathway 3) before sending it to a refinery. Similar to the ESEIEH method, the belowground activities were modeled using fundamental science-based theoretical equations based on technical parameters, while the upgraders and refinery processes were modelled using Aspen HYSYS. Aspen HYSYS allows the user to predict mass yield as well as the physical and chemical properties of the produced SCOs and refinery products. The transportation stage was modeled using engineering equations based on technical parameters such as pipeline velocity, distance, diameter, and friction coefficient.

Sensitivity and uncertainty analyses were also performed to identify the key parameters and the range of values, respectively. A detailed sensitivity analysis based on the Morris method was performed to pinpoint the significant variables and identify areas for further improvement of the technologies. The well-to-combustion (WTC) GHG emissions results for gasoline and diesel production were found to be 111.2-116.1 and 113.8-117.0 gCO_2eq/MJ, respectively. Direct refining of bitumen results in the lowest GHG emissions for gasoline and jet fuel production, while the hydroconversion upgrading pathway resulted in the lowest GHG emissions for jet fuel production. The combustion of fuels in vehicle engines was the main contributor to overall GHG emissions with a share of 63-67%. GHG emissions during the extraction stage were the second contributors to the total GHG emissions with a share of 21-25%. The sensitivity analysis showed that the air-to-oil (AOR) and amount of CO_2 in the produced gas from the reservoir were the most sensitive parameters. The uncertainty analysis showed a GHG emissions range of 104.1-122.0 and 109.6-127.8 g CO_2eq/MJ in the production of gasoline and diesel, respectively. Getting more detailed information about the sensitive inputs could decrease the uncertainty in the overall results.

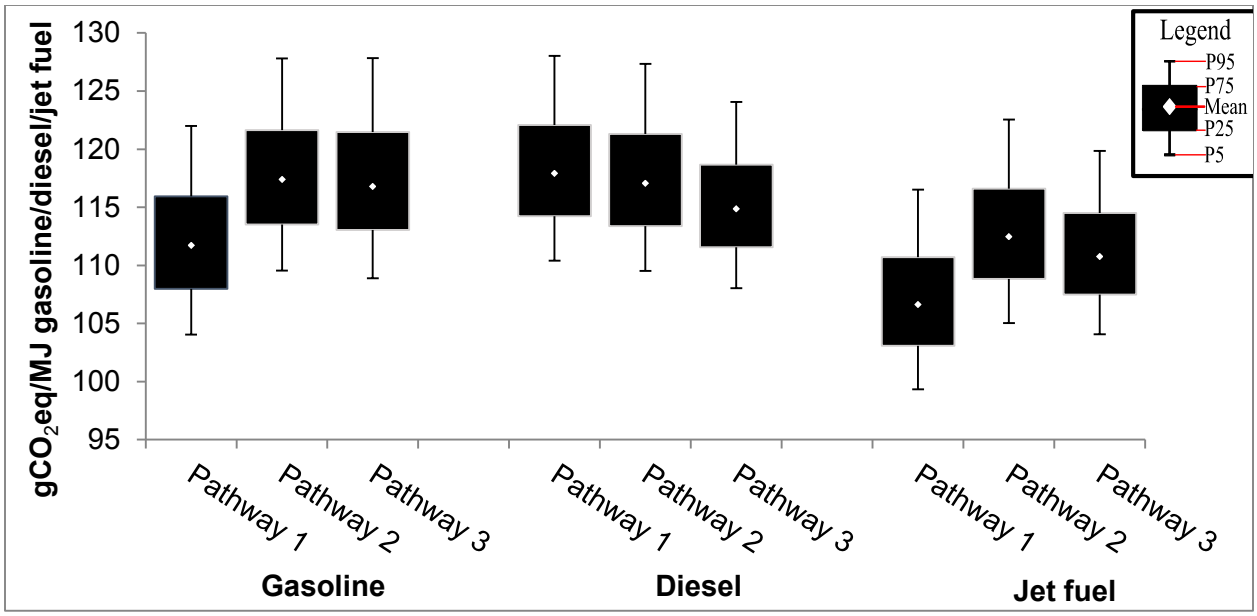

Fig. 4.2. Uncertainty in WTC GHG emissions in the production of transportation fuels from THAI

4.5 Comparison of WTC GHG emissions of transportation fuel production from THAI process with SAGD and surface mining

The WTC GHG emissions of SAGD and surface mining from various literature were found to be between 98.1-131.8 and 86.2-115.6 g CO_2eq/MJ, respectively. The range of WTC GHG emissions of the THAI process (shown in Fig 4.2) are in the same range of the SAGD and surface mining.

4.6 Recommendations for Future Work

Further research is required in the following areas in order to improve the current models:

- Extending the process simulation of the upgrader, refinery, and transportation stages in the ESEIEH process is required to complete the WTC life cycle assessment of this process.

- A detailed techno-economic study is needed to determine the cost of the solvent and antenna, and its electricity usage to provide more insights about the two pathways of ESEIEH.
- Further research is required to assess the impacts of using different solvents and refrigerants on energy use and emissions during the extraction stage in ESEIEH.
- A detailed techno-economic study is required to assess the feasibility of implementing carbon capture and storage technology on the gases produced during the combustion of the reservoir during THAI. Since the combustion of the reservoir contributes significantly to the overall results, capturing its emissions could drastically reduce the environmental footprint of THAI.
- The effects of renewable hydrogen production on overall GHG emission results should be analyzed.
- The recent focus and investment in partial upgrading technologies make it necessary to analyze their energy use and associated GHG emissions. These methods have the potential to lower the carbon footprint of the oil sands industry when coupled with emerging recovery methods.
- Other refinery configurations such as hydroskimming and medium conversion need to be analyzed as they may result in lower WTC GHG emissions.

An attempt should be made to quantify the emissions attributed to the production of specific equipment used in each technology and also the land-use emissions.

Bibliography

1. Alberta Energy. Energy resources: Facts and statistics. 2017 [cited 2018 July 7]; Available from: https://open.alberta.ca/dataset/c600fe79-0fd3-4793-82af-5391bb937204/resource/f69855b7-4cb5-4c58-8b05fbd1ca0f6719/download/fsenergyresources.pdf.

2. Canadian Association of Petroleum Producer. 2017 Crude oil forecast, markets and transportation. 2017 [cited 2018 January 17]; Available from: https://www.capp.ca/publications-and-statistics/crude-oil-forecast.

3. Oil Sands Magazine. Products from the oil sands: Dilbit, synbit & synthetic crude explained. 2018 [cited 2018 April 9]; Available from: https://www.oilsandsmagazine.com/technical/product-streams.

4. Liu, J., Z. Xu, and J. Masliyah, Processability of oil sand ores in Alberta. Energy & Fuels, 2005. 19(5): p. 2056-2063.

5. Gosselin, P., et al. Environmental and health impacts of Canada's oil sands industry. Royal Society of Canada Expert Panel Report, Ottawa, ON 2010 [cited 2017 September 12]; Available from: https://rscsrc.ca/sites/default/files/pdf/RSC%20Oil%20Sands%20Panel%20Main%20Report%20Oct%202012.pdf.

6. Walker, S., et al., Implementing power-to-gas to provide green hydrogen to a bitumen upgrader. International Journal of Energy Research, 2016. 40(14): p. 1925-1934.

7. Puttagunata, V., B. Singh, and A. Miadonye, Correlation of bitumen viscosity with temperature and pressure. The Canadian Journal of Chemical Engineering, 1993. 71(3): p. 447-450.

8. Charpentier, A.D., et al., Life cycle greenhouse gas emissions of current oil sands technologies: GHOST model development and illustrative application. Environmental Science & Technology, 2011. 45(21): p. 9393-9404.

9. Pacheco, D.M., et al., Development and application of a life cycle-based model to evaluate greenhouse gas emissions of oil sands upgrading technologies. Environmental Science & Technology, 2016. 50(24): p. 13574-13584.

10. Keesom, W., S. Unnasch, and J. Moretta. Life cycle assessment comparison of North American and imported crudes, Alberta Energy Research Institute. 2009 [cited 2017 March 23]; Available from: https://seeds4green.net/sites/default/files/life%20cycle%20analysis%20jacobs%20final%20report.pdf.

11. Rosenfeld, J., et al. Comparison of North American and imported crude oil life cycle GHG emissions. Final Report Prepared for Alberta Energy Research Institute, TIAX LLC. 2009 [cited 2018 January 13]; Available from: https://www.assembly.ab.ca/lao/library/egovdocs/2009/aleri/173913.pdf.

12. Di Lullo, G., H. Zhang, and A. Kumar, Uncertainty in well-to-tank with combustion greenhouse gas emissions of transportation fuels derived from North American crudes. Energy, 2017. 128: p. 475-486.

13. IHS CERA, Oil sands, greenhouse gases, and US oil supply getting the numbers right. 2010 [cited 2017 March 17]; Available from: https://thehill.com/images/whitepapers/oil_sands_energy_dialogue_0810.pdf.

14. Natural Resources Canada. Crude oil facts. 2018 [cited 2018 April 9]; Available from: https://www.nrcan.gc.ca/energy/facts/crude-oil/20064.

15. Government of Alberta. Carbon Competitiveness Incentive Regulation. 2018 [cited 2018 July 8]; Available from: http://www.qp.alberta.ca/1266.cfm?page=2017_255.cfm&leg_type=Regs&isbncln=9780779800193.

16. European Commission. Fuel quality. 2015 [cited 2018 January 20]; Available from: https://ec.europa.eu/clima/policies/transport/fuel_en.

17. California Energy Commission. Low Carbon Fuel Standard. 2007 [cited 2018 April 16]; Available from: https://www.energy.ca.gov/low_carbon_fuel_standard/UC_LCFS_study_Part_1-FINAL.pdf.

18. Government of Canada. Progress towards Canada's greenhouse gas emissions reduction target. 2018 [cited 2018 Decemebr 1]; Available from:

https://www.canada.ca/en/environment-climate-change/services/environmental-indicators/progress-towards-canada-greenhouse-gas-emissions-reduction-target.html.

19. Government of Canada. Clean Fuel Standard. 2018 [cited 2018 July 24]; Available from: https://www.canada.ca/en/environment-climate-change/services/managing-pollution/energy-production/fuel-regulations/clean-fuel-standard.html.

20. Trautman, M., et al. Effective solvent extraction system incorporating electromagnetic heating. Google Patents, 2013; Available from: https://www.google.ca/patents/US8776877.

21. Greaves, M., et al., THAI-new air injection technology for heavy oil recovery and in situ upgrading. Journal of Canadian Petroleum Technology, 2001. 40(03): p. 38-47.

22. Burger, J., et al., Thermal methods of oil recovery. 1985: Gulf Publishing Company, Book Division.

23. Xia, T. and M. Greaves, Upgrading Athabasca tar sand using toe-to-heel air injection. Journal of Canadian Petroleum Technology, 2002. 41(08): p. 51-57.

24. Matthews, H., C. Hendrickson, and D. Matthews. Life cycle assessment: Quantitative approaches for decisions that matter. 2015 [cited 2017 November 12]; Available from: https://app.boxcn.net/s/5mnzyq1y3gcyjrveubf4/folder/2952576445.

25. International Organization for Standardization. ISO 14040: International standard. Environmental management—Life cycle assessment—Principles and framework 2006 [cited 2018 March 27]; Available from: https://web.stanford.edu/class/cee214/Readings/ISOLCA.pdf.

26. International Organization for Standardization. ISO 14041: Environmental management—life cycle assessment—goal and scope definition—inventory analysis. 1998 [cited 2018 September 11]; Available from: https://www.sis.se/api/document/preview/611594/.

27. International Organization for Standardization. ISO 14044: Environmental management-Life cycle assessment-Requirements and guidelines. 2006 [cited 2018 March 16]; Available from: https://wap.sciencenet.cn/home.php?mod=attachment&id=4637.

28. Turta, A. and A. Singhal, Overview of short-distance oil displacement processes. Journal of Canadian Petroleum Technology, 2004. 43(02): p. 29-38.

29. Alex Turta, M.G., Toe-to-heel air injection (THAI) – The first oil recovery process producing underground upgraded oil. 2017, Presented at the Canadian Prairies Group of Chartered Engineers (CPGCE), Calgary, Alberta, Canada.

30. Xia, T., et al., THAI process-effect of oil layer thickness on heavy oil recovery, in Canadian International Petroleum Conference. 2002, Petroleum Society of Canada: Calgary, Alberta, Canada. p. 1-11.

31. Xia, T. and M. Greaves, In situ upgrading of Athabasca tar sand bitumen using THAI. Chemical Engineering Research and Design, 2006. 84(9): p. 856-864.

32. Patterson, C. An overview of oil recovery using radio frequency heating technology: The tools, techniques and processes behind the ESEIEH hydrocarbon extraction process. Presented at the World Heavy Oil Conference, Calagry, Alberta, Canada, 2016.

33. Boone, T., Sampath, Kelly, Assessment of GHG emissions associated with in-situ heavy oil recovery processes, in World Heavy Oil Congress. 2012: Aberdeen, Scotland. p. 1-8.

34. Englander, J. and A. Brandt. Oil sands energy intensity analysis for GREET model update. Department of Energy Resources Engineering, Stanford University, Stanford, USA. 2014 [cited 2018 May 24]; Available from: https://greet.es.anl.gov/files/lca-update-oil-sands.

35. Argonne National Laboratory. GREET_1_2017. 2017 [cited 2017 March 10]; Available from: https://greet.es.anl.gov.

36. Natural Resources Canada. GHGenius model version 4.01a. 2012 [cited 2017 March 10]; Available from: https://ghgenius.ca/.

37. Nimana, B., C. Canter, and A. Kumar, Life cycle assessment of greenhouse gas emissions from Canada's oil sands-derived transportation fuels. Energy, 2015. 88: p. 544-554.

38. Abella, J.P., K. Motazedi, and J.A. Bergerson. Petroleum Refinery Life Cycle Inventory Model (PRELIM) PRELIM v1. 2. 2017 [cited 2017 March 10]; Available from: https://ucalgary.ca/lcaost/files/lcaost/prelim-v1.2_1.xlsm.

39. Finley, M., The oil market to 2030—Implications for investment and policy. Economics of Energy & Environmental Policy, 2012. 1(1): p. 25-36.

40. Energy Information Administration. International energy outlook 2016. 2016 [cited 2017 June 2017]; Available from: https://www.eia.gov/outlooks/ieo/pdf/0484(2016).pdf.

41. British Petroleum. BP Statistical Review Of World Energy June 2016. 2016 [cited 2018 November 29]; Available from: https://oilproduction.net/files/especial-BP/bp-statistical-review-of-world-energy-2016-full-report.pdf.

42. Jaffe, A.M., K.B. Medlock III, and R. Soligo, The status of world oil reserves: conventional and unconventional resources in the future supply mix. 2011 [cited 2018 November 29]; Available from: https://www.bakerinstitute.org/files/540/.

43. Alberta Energy. Facts and Statistics. 2016 [cited 2018 2/5]; Available from: https://www.energy.alberta.ca/OilSands/791.asp.

44. International Energy Agency. Oil. 2018 [cited 2018 January 20]; Available from: https://www.iea.org/about/faqs/oil/.

45. Nimana, B., C. Canter, and A. Kumar, Energy consumption and greenhouse gas emissions in the recovery and extraction of crude bitumen from Canada's oil sands. Applied Energy, 2015. 143: p. 189-199.

46. Walden, Z. Emission abatement potential for the Alberta oil sands industry and carbon capture and storage (CCS) applicability to coal-fired electricity generation and oil sands. 2011 [cited 2015 October 14]; Available from: https://www.ceri.ca/studies/Emission-abatement-potential-for-the-Alberta-oil-sands-industry-and-carbon-capture-and-storage-(CCS)-applicability-to-coal-fired-electricity-generation-and-oil-sands.

47. Mukhametshina, A. and E. Martynova, Electromagnetic heating of heavy oil and bitumen: A review of experimental studies and field applications. Journal of Petroleum Engineering, 2013. 2013: p. 1-7.

48. Ordorica-Garcia, G., et al., Assessing the Potential of Power and Hydrogen Technologies with CO2 Capture to Optimize Future Energy Production in the Canadian Oil Sands Industry. International Journal of Energy and Environmental Engineering, 2014. 5:323–332

49. Bolea, I., A.A. Checa, and L.M. Romeo, Assessment of the integration of CO 2 capture technology into oil–sand extraction operations. International Journal of Energy and Environmental Engineering, 2014. 5(4): p. 323-332.

50. Betancourt-Torcat, A., A. Elkamel, and L. Ricardez-Sandoval, Optimal integration of nuclear energy and water management into the oil sands operations. AIChE, 2012. 58(11): p. 3433-3453.

51. Kraemer, D., et al., Solar assisted method for recovery of bitumen from oil sand. Applied Energy, 2009. 86(9): p. 1437-1441.

52. Ashrafi, O., et al., Heat recovery optimization in a steam-assisted gravity drainage (SAGD) plant. Energy, 2016. 111: p. 981-990.

53. Carreon, C.E., et al., Evaluation of energy efficiency options in steam assisted gravity drainage oil sands surface facilities via process integration. Applied Thermal Engineering, 2015. 87: p. 788-802.

54. Orellana, A., et al., Statistically enhanced model of in situ oil sands extraction operations: An evaluation of variability in greenhouse gas emissions. Environmental Science & Technology, 2017. 52 (3): p. 947–954

55. IHS Markit. Greenhouse gas intensity of oil sands production: Today and in the future. 2018 [cited 2018 September 16]; Available from: https://ihsmarkit.com/forms/contactinformation.html?efid=tFSzO+2aeGqpKuUQPMWZ3Q==.

56. Nimana, B., et al., Life cycle analysis of bitumen transportation to refineries by rail and pipeline. Environmental Science & Technology, 2016. 51(1): p. 680-691.

57. El-Houjeiri, H., et al. Oil production greenhouse gas emissions estimator–OPGEE version 2 draft D: User guide & technical documentation. Department of Energy Resources Engineering. Stanford University, Stanford, USA. 2017 [cited 2017 March 13]; Available from: https://pangea.stanford.edu/departments/ere/dropbox/EAO/OPGEE/OPGEE_documentation_v2.0b.pdf.

58. Jha, A.K., N. Joshi, and A. Singh, Applicability and assessment of micro-wave assisted gravity drainage (mwagd) applications in mehsana heavy oil field, India, in SPE Heavy Oil Conference and Exhibition. 2011, Society of Petroleum Engineers: Kuwait City, Kuwait. p. 1-9.

59. Nenniger, J. and S. Dunn, How fast is solvent based gravity drainage?, in Canadian International Petroleum Conference. 2008, Petroleum Society of Canada: Calgary, Alberta, Canada. p. 1-7.

60. Kasevich, R.S. Method and apparatus for in-situ radiofrequency assisted gravity drainage of oil (RAGD). Google Patents, 2008; Available from: https://www.google.com/patents/US20090050318.

61. Pedro Vaca, D.P., Michal Okoniewski. The application of radio frequency heating technology for heavy oil and oil sands production. 2014 [cited 2017 November 14]; Available from:

https://www.acceleware.com/sites/all/pdf/20140604_RF_HEATING_WHITEPAPER.pdf.

62. Nenniger, J. and E. Nenniger. Method and apparatus for stimulating heavy oil production. Google Patents, 2005; Available from: https://google.com/patents/CA2351148C?cl=no.

63. Wise, S. and C. Patterson, Reducing supply cost with Eseieh™ pronounced easy, in SPE Canada Heavy Oil Technical Conference. 2016, Society of Petroleum Engineers: Calgary, Alberta, Canada. p. 1-12.

64. Canada's Oil Sands Innovation Alliance. Water and energy recovery from flue gas. 2014 [cited 2017 June 14]; Available from: https://www.cosia.ca/uploads/files/challenges/ghg/COSIA%20Challenge%20GHG%20-%20Water%20and%20Energy%20Recovery%2016-10-14.pdf.

65. National Institute of Standards and Technology. Thermophysical properties of fluid systems. Standard Reference Database. 2017 [cited 2017 April 17]; Available from: https://webbook.nist.gov/chemistry/fluid/.

66. Manning, F.S. and R.E. Thompson, Oilfield processing of petroleum: Crude oil. Vol. 2. 1995: Pennwell Books.

67. Manning, F.S. and R.E. Thompson, Oilfield processing of petroleum: Natural gas. Vol. 1. 1995: Pennwell Books.

68. Nawaz, M. and M. Jobson, Synthesis and optimization of demethanizer flowsheets for low temperature separation processes. Distillation Absorption, 2010: p. 79-84.

69. Bogdanov, I., et al. Heavy oil recovery via combination of radio-frequency heating with solvent injection. SPE Canada Heavy Oil Technical Conference. 2016. Society of Petroleum Engineers.

70. Soiket, M.I.H., Life Cycle Assessment (LCA) of Oil Sands-Derived Transportation Fuels Produced from the Vapor Solvent-Based Extraction Process. 2017, University of Alberta.

71. Titan Air. Direct fired vs. indirect fired heaters. 2016 [cited 2017 July 19]; Available from: https://blog.titan-air.com/blog/direct-fired-vs.-indirect-fired-heaters.

72. Shah, R.K. and D.P. Sekulic, Fundamentals of heat exchanger design. 2003: John Wiley & Sons.

73. El-Houjeiri, H., et al. Oil Production Greenhouse Gas Emissions Estimator–OPGEE v1. 1 Draft D: User guide & Technical documentation. Department of Energy Resources Engineering. 2014; Available from: https://pangea.stanford.edu/departments/ere/dropbox/EAO/OPGEE/OPGEE_documentation_v2.0b.pdf.

74. Nesbitt, B., Handbook of pumps and pumping: Pumping manual international. 2006: Elsevier.

75. Turton, R., et al., Analysis, synthesis and design of chemical processes. 2008: Pearson Education.

76. Vlasopoulos, N., et al., Life cycle assessment of wastewater treatment technologies treating petroleum process waters. Science of the Total Environment, 2006. 367(1): p. 58-70.

77. David B. Layzell, et al. Cogeneration options for a 33,000 bpd SAGD facility: Greenhouse gas and economic implications. 2016 [cited 2017 November 16]; Available from: https://www.cesarnet.ca/sites/default/files/CESAR-Scenarios-Cogeneration-Options-for-SAGD-Facility.pdf.

78. Government of Alberta. Technical guidance for completing specified gas compliance reports. 2014 [cited 2017 October 12]; Available from: https://aep.alberta.ca/climate-change/guidelines-legislation/specified-gas-emitters-regulation/documents/TechGuidanceCompletingSpecGasComplianceRpts-Feb2014.pdf.

79. Thakur, A., C.E. Canter, and A. Kumar, Life-cycle energy and emission analysis of power generation from forest biomass. Applied Energy, 2014. 128: p. 246-253.

80. Aspen HYSYS, Version 9.0. Aspen Technology Inc, 2016.

81. Alberta Electric System Operator. AESO 2016 long-term outlook. 2016 [cited 2018 December 1]; Available from: https://www.aeso.ca/download/listedfiles/AESO-2016-Long-term-Outlook-WEB.pdf.

82. Government of Alberta. Capping oil sands emissions: Transitioning to an output-based allocation approach and a legislated limit to oil sands emissions under the Climate Leadership Plan. 2017 [cited 2017 September 7]; Available from: https://www.alberta.ca/climate-oilsands-emissions.aspx.

83. Doluweera, G., et al., Evaluating the role of cogeneration for carbon management in Alberta. Energy Policy, 2011. 39(12): p. 7963-7974.

84. Alberta Wilderness Association. Boreal-forest. 2018 [cited 2018 March 15]; Available from: https://albertawilderness.ca/issues/wildlands/forests/boreal-forest/.

85. Prakash, V. 3 point estimate: Triangular distribution vs. beta distribution (PERT). 2017 [cited 2017 June 27]; Available from: https://www.pmchamp.com/3-point-estimate-triangular-distribution-vs-beta-distribution-pert/.

86. Law, A.M., W.D. Kelton, and W.D. Kelton, Simulation modeling and analysis. Vol. 2. 1991, New York: McGraw-Hill.

87. Brooks, C. Facts about firetube boilers and boiler efficiency. 2010 [cited 2017 July 27]; Available from: https://cleaverbrooks.com/referencecenter/insights/Boiler%20Efficiency%20Guide.pdf

88. Stark, C. Reducing energy cost through boiler efficiency. Department of Poultry Science North Carolina State University, Raleigh, USA 2015 [cited 2016 March

16]; Available from: https://www.ncsu.edu/project/feedmill/pdf/E_Reducing%20Energy%20Cost%20Through%20Boiler%20Efficiency.pdf

89. International Energy Agency. Industrial combustion boilers. 2010 [cited 2017 June 27]; Available from: https://iea-etsap.org/E-TechDS/PDF/I01-ind_boilers-GS-AD-gct.pdf.

90. Wheeler, T.J., W.R. Dreher Jr, and D.K. Banerjee, Accelerating the start-up phase for a steam assisted gravity drainage operation using radio frequency or microwave radiation, Google Patents; Available from: https://patents.google.com/patent/US8607866

91. Government of Canada. Guidance on the pan-Canadian carbon pollution pricing benchmark. 2018 [cited 2018 July 28]; Available from: https://www.canada.ca/en/services/environment/weather/climatechange/pan-canadian-framework/guidance-carbon-pollution-pricing-benchmark.html.

92. Canadian Association of Petroleum Producers. Canada's oil sands. 2018 [cited 2018 July 28]; Available from: https://www.capp.ca/~/media/capp/customerportal/publications/316441.pdf?modified=20180726084112.

93. Abella, J.P. and J.A. Bergerson, Model to investigate energy and greenhouse gas emissions implications of refining petroleum: Impacts of crude quality and refinery configuration. Environmental Science & Technology, 2012. 46(24): p. 13037-13047.

94. Léauté, R.P., K.E. Corry, and B.K. Pustanyk. Liquid addition to steam for enhancing recovery of cyclic steam stimulation or LASER-CSS. Google Patents, 2004; Available from: https://patents.google.com/patent/US6708759B2/en.

95. Martin, W.L., J.D. Alexander, and J.N. Dew, Process variables of in situ combustion. Society of Petroleum Engineers, 1958. 213: p. 28-35.

96. Pfefferle, W.C. Method for CAGD recovery of heavy oil. Google Patents, 2007; Available from: https://patents.google.com/patent/US20070187094A1/en.

97. Chen, B. and Q. Chen, Solvents and non-condensable gas coinjection. Google Patents, 2016; Available from: https://patents.google.com/patent/US20160153270

98. Chen, B., Q. Chen, and T.J. Wheeler, Non-condensable gas coinjection with fishbone lateral wells. Google Patents, 2014; Available from: https://patents.google.com/patent/CA2913765A1/en

99. Alex Turta. Toe-to-heel air injection (THAI) process. 2018 [cited 2018 April 20]; Available from: https://www.insitucombustion.ca/docs/Advanced_THAI_Brochure.pdf.

100. Kulkarni, M. and D. Rao, Analysis of the novel toe-to-heel air injection (THAI) process using simple analytical models, AIChE Annual Meeting. 2004: Austin, Texas, USA. p. 1-22.

101. University of Bath. Toe-to-heel air injection maximizing heavy oil recovery & in-situ upgrading. 2002 [cited 2017 Febraury 18]; Available from: https://www.infomine.com/library/publications/docs/THAI2002.pdf..

102. Greaves, M., L. Dong, and S. Rigby, Simulation study of the toe-to-heel air injection three-dimensional combustion cell experiment and effects in the mobile oil zone. Energy & Fuels, 2012. 26(3): p. 1656-1669.

103. Rabiu Ado, M., M. Greaves, and S.P. Rigby, Dynamic simulation of the toe-to-heel air injection heavy oil recovery process. Energy & Fuels, 2017. 31(2): p. 1276-1284.

104. Norwest Corporation. Whitesands experimental pilot project design basis memorandum. 2004 [cited 2017 September 9]; Available from: https://www.energy.alberta.ca/xdata/IETP/IETP%202007/01-019%20Whitesands%20Experimental%20Project/Formatted%20DBM%20%20Feb%2027.pdf.

105. Turta, A., et al., Current status of commercial in situ combustion projects worldwide. Journal of Canadian Petroleum Technology, 2007. 46(11): p. 8-14.

106. Rahnema, H., Combustion assisted gravity drainage (CAGD): An in-situ combustion method to recover heavy oil and bitumen from geologic formations using a horizontal injector/producer pair. 2012, Texas A&M University.

107. Abdel-Aal, H.K., M.A. Aggour, and M.A. Fahim, Petroleum and gas field processing. 2015: CRC Press.

108. Gray, M.R. Tutorial on upgrading of oil sands bitumen. 2003 [cited 2018 July 12]; Available from: https://www.ualberta.ca/~gray/Links%20&%20Docs/Web%20Upgrading%20Tutorial.pdf.

109. Rana, M.S., et al., A review of recent advances on process technologies for upgrading of heavy oils and residua. Fuel, 2007. 86(9): p. 1216-1231.

110. Chrones, J. and R. Germain, Bitumen and heavy oil upgrading in Canada. Fuel Science & Technology International, 1989. 7(5-6): p. 783-821.

111. Parkash, S., Refining processes handbook. 2003: Elsevier.

112. Gray, M.R., Upgrading oil sands bitumen and heavy oil. 2015: University of Alberta Press.

113. Alvarez-Majmutov, A., C. Jinwen, and M. Munteanu, Simulation of bitumen upgrading processes. Petroleum Technology Quarterly, 2013. 18(3): p. 39-43.

114. Fahim, M.A., T.A. Al-Sahhaf, and A. Elkilani, Fundamentals of petroleum refining. 2009: Elsevier.

115. Speight, J.G., The chemistry and technology of petroleum. 2014: CRC press.

116. Maples, R.E., Petroleum refinery process economics. 2000: Pennwell Books.

117. Leprince, P., Petroleum refining. Vol. 3. Conversion processes. 2001: Editions Technip.

118. El-Houjeiri, H., et al. Oil production greenhouse gas emissions estimator–OPGEE version 2 draft D: User guide & technical documentation. Department of Energy Resources Engineering. Stanford University, Stanford, USA. 2014 [cited 2017 March 13]; Available from: https://pangea.stanford.edu/departments/ere/dropbox/EAO/OPGEE/OPGEE_documentation_v2.0b.pdf.

119. Petrobank Energy and Resources Ltd. IETP 01-019 Whitesands experimental project – final/annual (2009) report. 2009 [cited 2017 March 17]; Available from: https://www.energy.alberta.ca/xdata/IETP/IETP%202009/01-019%20Whitesands%20Experimental%20Project/IETP%20approval%2001_019%20final%20and%202009%20report.pdf.

120. United States Environmental Protection Agency. Greenhouse gas inventory guidance direct emissions from stationary combustion sources. 2016 [cited 2018 March 12]; Available from: https://www.epa.gov/sites/production/files/201603/documents/stationaryemissions_3_2016.pdf.

121. Hart, A., et al., Down-hole heavy crude oil upgrading by CAPRI: Effect of hydrogen and methane gases upon upgrading and coke formation. Fuel, 2014. 119: p. 226-235.

122. Colt Engineering Corporation. Greater Edmonton area bitumen upgrader supply chain study. 2007 [cited 2018 April 12]; Available from:

https://industrialheartland.com/wp-content/uploads/2016/07/bitumen-upgrader-supply-chain-study-2007.pdf.

123. Robinson, P.R. and G.E. Dolbear. Hydrotreating and hydrocracking: Fundamentals. Practical Advances in Petroleum Processing. Springer 2006.

124. Martínez, J., et al., A review of process aspects and modeling of ebullated bed reactors for hydrocracking of heavy oils. Catalysis Reviews, 2010. 52(1): p. 60-105.

125. Edgar, M. Hydrotreating Q&A. in NPRA Annual Meeting. 1993. San Antonio, Texas,USA.

126. Ancheyta, J., Modeling of processes and reactors for upgrading of heavy petroleum. 2013: CRC Press.

127. Bishop, W. LC-Finer operating experience at Syncrude. Proceedings of Symposium on Heavy Oil: Upgrading to Refining, CSChE, Calgary, Alberta, Canada. 2007.

128. Spath, P.L. and M.K. Mann. Life cycle assessment of hydrogen production via natural gas steam reforming. National Renewable Energy Laboratory. 2001 [cited 2018 March 28]; Available from: https://www1.eere.energy.gov/hydrogenandfuelcells/pdfs/27637.pdf.

129. Tao, W. Managing China's petcoke problem. Beijing: Carnegie-Tsinghua Center for Global Policy. 2015 [cited 2018 June 16]; Available from: https://carnegieendowment.org/files/petcoke.pdf.

130. Government of Canada. Coal-fired electricity generation regulations - overview. 2013 [cited 2018 March 16]; Available from: https://www.canada.ca/en/environment-climate-change/services/climate-change/greenhouse-gas-emissions/regulations/coal-fired-electricity-generation.html.

131. Chang, A.-F., K. Pashikanti, and Y.A. Liu, Refinery engineering: Integrated process modeling and optimization. 2013: John Wiley & Sons.

132. Aspen HYSYS. Aspen HYSYS petroleum refining unit operations & reactor models reference guide. 2015 [cited 2018 March 14]; Available from: https://edoc.site/download/hysys-petroleum-refining-ops-v8-8-4-pdf-free.html.

133. Wang, M., H. Lee, and J. Molburg, Allocation of energy use in petroleum refineries to petroleum products. The International Journal of Life Cycle Assessment, 2004. 9(1): p. 34-44.

134. Nimana, B., C. Canter, and A. Kumar, Energy consumption and greenhouse gas emissions in upgrading and refining of Canada's oil sands products. Energy, 2015. 83: p. 65-79.

135. Netzer, D. Alberta bitumen processing integration study. 2006 [cited 2018 September 16]; Available from: https://www.assembly.ab.ca/lao/library/egovdocs/2006/alet/158261.pdf.

136. Crude Monitor. Crude quality data summary. 2018 [cited 2018 March 18]; Available from: https://www.crudemonitor.ca/condensates/index.php?acr=CHN.

137. Safety Codes Council. Alberta private sewage systems 2009 standard of practice handbook. 2009 [cited 2018 April 16]; Available from: https://www.safetycodes.ab.ca/Public/Documents/PSSSOP_Handbook_Version_12_Online_Feb_21_2012b.pdf.

138. Texas Department of Transportation Planning and Programming Division Data Analysis Mapping and Reporting Branch. Elevation map. 2008 [cited 2018 March 20]; Available from: ftp://ftp.txdot.gov/pub/txdot-info/tpp/gulf_coast_elevation_map.pdf.

139. Tarnoczi, T., Life cycle energy and greenhouse gas emissions from transportation of Canadian oil sands to future markets. Energy Policy, 2013. 62: p. 107-117.

140. Morris, M.D., Factorial sampling plans for preliminary computational experiments. Technometrics, 1991. 33(2): p. 161-174.

141. Brevault, L., et al., Comparison of different global sensitivity analysis methods for aerospace vehicle optimal design, in 10th World Congress on Structural and Multidisciplinary Optimization. 2013: Orlando, Florida, USA. p. 1-12.

142. Metropolis, N. and S. Ulam, The Monte Carlo method. Journal of the American Statistical Association, 1949. 44(247): p. 335-341.

143. Di Lullo, G., H. Zhang, and A. Kumar, Evaluation of uncertainty in the well-to-tank and combustion greenhouse gas emissions of various transportation fuels. Applied Energy, 2016. 184: p. 413-426.

144. Turta, A. Role of reservoir temperature as a favorable factor for application of in-situ combustion (focus on heavy oil reservoirs). Presented at the World Heavy Oil Congress, Calgary, Alberta, Canda, 2016.

145. Wenlong, G., et al., Field control technologies of combustion assisted gravity drainage (CAGD). Petroleum Exploration and Development, 2017. 44(5): p. 797-804.

146. Scherzer, J. and A.J. Gruia, Hydrocracking science and technology. 1996: CRC Press.

147. Webb, R.M. Increasing gasoline octane levels to reduce vehicle emissions: A review of federal and state authority, Sabin Center for Climate Change Law, Columbia Law School. 2017 [cited 2018 May 22]; Available from: https://columbiaclimatelaw.com/files/2017/01/Webb-2017-01-Regulating-Gasoline-Octane-Levels.pdf.

148. Row, J. and A. Doukas. Fuel quality in Canada: Impact on tailpipe emissions, Pembina Institute. 2008 [cited 2018 June 25]; Available from: https://www.globalautomakers.ca/files/pressreleases/Fuel%20Quality%20in%20Canada%20-%20Final%20Report%20NEW.pdf.

149. Martineau, R.J. and D.P. Novello. The Clean Air Act handbook. 2004. American Bar Association.

150. Environment and Climate Change Canada. National inventory report 1990-2014: Greenhouse gas sources and sinks in Canada, United Nations framework convention on climate change. 2016 [cited 2017 January 28]; Available from: https://unfccc.int/files/national_reports/annex_i_ghg_inventories/national_inventories_submissions/application/zip/can-2016-nir-14apr16.zip.

151. Government of Alberta. Climate Leadership Plan Progress report. 2017 [cited 2018 March 25]; Available from: https://www.alberta.ca/assets/documents/CLP-progress-report-2016-17.pdf.

152. Wildy, F. Fired heater optimization. AMETEK Process Instruments, Pittsburgh, USA. 2000 [cited 2018 March 25]; Available from: https://www.analitech.ru/files/Fired%20Heater%20Optimization.pdf.

153. Gary, J.H., G.E. Handwerk, and M.J. Kaiser, Petroleum refining: Technology and economics. 2007: CRC press.

154. Skone, T.J. and K. Gerdes. Development of baseline data and analysis of life cycle greenhouse gas emissions of petroleum-based fuels. National Energy Technology Laboratory 2008 [cited 2018 March 28]; Available from: https://www.netl.doe.gov/File%20Library/Research/Energy%20Analysis/Life%20Cycle%20Analysis/NETL-LCA-Petroleum-based-Fuels-Nov-2008.pdf.

155. Alvarez-Majmutov, A. and J. Chen, Analyzing the energy intensity and greenhouse gas emission of Canadian oil sands crude upgrading through process modeling and simulation. Frontiers of Chemical Science and Engineering, 2014. 8(2): p. 212-218.

156. Elgowainy, A., et al., Energy efficiency and greenhouse gas emission intensity of petroleum products at US refineries. Environmental Science & Technology, 2014. 48(13): p. 7612-7624.

157. Cai, H., et al., Well-to-wheels greenhouse gas emissions of Canadian oil sands products: Implications for US petroleum fuels. Environmental Science & Technology, 2015. 49(13): p. 8219-8227.

158. Myhre, G., et al., Anthropogenic and natural radiative forcing. Climate Change, 2013. 423: p. 658-740.

159. HATCH. Life cycle assessment literature review of nuclear, wind and natural gas power generation. 2014 [cited 2017 October 8]; Available from: https://cna.ca/wp-content/uploads/2014/05/Hatch-CNA-Report-RevE.pdf.

160. Gagnon, L. and J.F. Van de Vate, Greenhouse gas emissions from hydropower: The state of research in 1996. Energy policy, 1997. 25(1): p. 7-13.

161. Intrinsik Corporation. Greenhouse gas emissions associated with various methods of power generation in Ontario. 2016 [cited 2017 September 25]; Available from: https://www.opg.com/darlingtonrefurbishment/Documents/IntrinsikReport_GHG_OntarioPower.pdf.

162. Mallia, E. and G. Lewis, Life cycle greenhouse gas emissions of electricity generation in the province of Ontario, Canada. The International Journal of Life Cycle Assessment, 2013. 18(2): p. 377-391.

163. Jarrell, P.M., et al., Practical aspects of CO2 flooding. Vol. 22. 2002: Society of Petroleum Engineers, Richardson, TX.

164. UNEP Electrical Energy Equipment. Compressors and compressed air systems. 2006 [cited 2017 June 28]; Available from: https://www.energyefficiencyasia.org/.../Compressors%20and%20Compressed%20Air%20Sy...

165. Petrobank Energy. Whitesands pilot field study. 2008 [cited 2017 March 13]; Available from: https://www.petrobank.com/hea-whitesandsproject.html.

166. Mashuga, C.V. and D.A. Crowl, Derivation of Le Chatelier's mixing rule for flammable limits. Process safety progress, 2000. 19(2): p. 112-117.

167. Matheson Gas Products. Lower and upper explosive limits for flammable gases and vapors (LEL/UEL). 2013 [cited 2017 December 15]; Available from: https://www.mathesongas.com/pdfs/products/Lower-(LEL)-&-Upper-(UEL)-Explosive-Limits-.pdf.

168. American Petroleum Institute. 5L (2007) specifications for line pipe. 2007 [cited 2018 January 5]; Available from: https://law.resource.org/pub/us/cfr/ibr/002/api.5l.2004.pdf.

169. Kiijarvi, J. Darcy friction factor formulae in turbulent pipe flow. Lunowa Fluid Mechanics Paper. 2011 [cited 2018 March 22]; Available from: https://www.kolumbus.fi/jukka.kiijarvi/clunowa/fluid_mechanics/pdf_articles/darcy_friction_factor.pdf.

170. Colebrook, C.F., et al., Turbulent flow in pipes, with particular reference to the transition region between the smooth and rough pipe laws.(includes plates). Journal of the Institution of Civil Engineers, 1939. 12(8): p. 393-422.

Appendix A

Appendix A contains supplementary information for chapter 2.

A.1 Produced gas energy content and emission factor calculation

The energy content and GHG emissions from the combustion of produced gas from the reservoir are calculated using equations A.1 and A.2 and from the values presented in Tables A.1.

Table A.1: Composition of the combusted gases in Pathway I and II [64, 65, 80]

Component	Mass content in Pathway I (%)	Mass content in Pathway II (%)	Lower heating value (MJ/kg)	Combustion emission (gCO_2 eq/MJ)
CH_4	38.88	6.79	50	56.51
C_2H_6	1.86	0.17	47.62	56.81
C_3H_8	3.33	0.11	46.35	59.81
C_4H_{10}	0.66	87.20	45.75	60.20
C_5H_{12}	2.43	0.02	43.20	62.30
CO_2	50.44	4.61	-	-
N_2O	2.18	0.36	-	-
H_2S	0.169	0.01	-	-
H_2	0.02	0.01	119.96	-

Equation A.1: Heat generated by produced gas (MJ/kg) = $\sum_{i=1}^{n} \frac{(LHV)_i * m_i}{\eta_b}$

Equation A.2: Combustion emissions of the produced gas (gCO_2 eq./Mj)

$= \sum_{i=1}^{n} \frac{(LHV)_i * m_i * e_i}{\eta_b}$

where *i* is the individual gas component, *n* is the total number of gas components, *LHV* is lower heating value (MJ/kg), m_i is volume content of individual gas (%), e_i is combustion emissions of individual gas (gCO_2 eq/MJ), and η_b is burner efficiency.

A.2 Calculation of the Alberta grid emission factor in 2016 and 2030

The emission factor of Alberta's grid electricity mix in 2016 and 2030 is calculated based on values from Table A.2 and A.3 and Equation A.3. The emission factor of different electricity production technologies is calculated based on the global warming potential of CO_2, CH_4, and N_2O with a 100-year time horizon [158].

Table A.2: Share of technologies in Alberta's grid mix in 2016 and 2030 [81]

Technology	2016 share	2030 share
Coal-fired	39%	0%
Cogeneration	29%	25%
Combined-cycle	12%	37%
Simple-cycle	6%	10%
Hydroelectric	5%	4%
Wind	9%	24%

Table A.3: Emission factor of different technologies for electricity generation

Technology	Emission factor (g CO_2 eq/kwh)	Source
Coal-fired	1188	[35]
Cogeneration	484	[35, 77, 78]
Combined-cycle	484	[35]
Simple-cycle	782	[35]
Hydroelectric	15	[159, 160]
Wind	11	[159, 161, 162]

Equation A.3: Emission factor of grid electricity = $\sum_{i=1}^{n}(EF)_i * share_i$

where *i* is each technology, *n* is the total number of technologies, and *EF* is the emission factor.

The Alberta Climate Leadership Plan considers the emission factor of electricity from cogeneration to be the same as for combined cycle [78]. Thus, the same value is considered for combined cycle and cogeneration.

A.3 Operating conditions considered for unit operations in the surface facilities

Table A.4 lists the operating conditions and mass flow rates in each unit operation for production of 25000 barrels of bitumen per day by using ESEIEH method.

Table A.4: Process conditions of each unit operation in the ESEIEH process [80]

Stream description	Value
Temperature of emulsion from cooler (°C)	50
Pressure of emulsion from cooler (kPa)	1100
Flow rate of emulsion from cooler (kg/hr)	296000
Temperature of flash tank (°C)	48.8
Operating pressure of flash tank (kPa)	621
Flow rate of separated gas from flash tank (kg/hr)	1972
Flow rate of separated emulsion from flash tank (kg/hr)	294012
Temperature of FWKO (°C)	48.8
Operating pressure of FWKO (kPa)	621
Flow rate of separated water from FWKO (kg/hr)	36305
Flow rate of separated emulsion from FWKO (kg/hr)	257707
Temperature of mechanical treater (°C)	48.8
Operating pressure of mechanical treater (kPa)	596
Flow rate of separated gas from mechanical treater (kg/hr)	326
Flow rate of separated emulsion from mechanical treater (kg/hr)	257380
Temperature of bitumen returned to heat exchanger (°C)	195
Flow rate of bitumen returned to heat exchanger (kg/hr)	168466
Flow rate of diluent to dilbit storage tank (kg/hr)	40427
Temperature of stored dilbit in the tank (°C)	50
Operating tempreture of stabilizer (°C)	195
Operating pressure of stabilizer (kPa)	450
Flow rate of emulsion to the stabilizer (kg/hr)	257380
Flow rate of separated gas from the stabilizer (kg/hr)	88913
Temperature of gases after compression (°C)	163.6

Pressure of gases after compression (kPa)	6000
Flow rate of gases to the compressor in Pathway I (kg/hr)	88680
Flow rate of gases to the compressor in Pathway II (kg/hr)	86793
Top pressure of acid gas removal unit absorber (kPa)	3535
Bottom pressure of acid gas removal unit absorber (kPa)	3549
Top temperature of acid gas removal unit (°C)	43
bottom temperature of acid gas removal unit (°C)	31
Steam consumption in Pathway I (kg/hr)	8456
Steam consumption in Pathway II (kg/hr)	8455
Amine solution pressure before being pumped (kPa)	227.5
Amine solution pressure after being pumped (kPa)	3618
Separated acid gas in acid gas removal unit in Pathway I (kg/hr)	377
Separated acid gas in acid gas removal unit in Pathway II (kg/hr)	298
Sweet gas flow rate to glycol removal unit in Pathway I (kg/hr)	88271
Sweet gas flow rate to glycol removal unit in Pathway II (kg/hr)	85837
Top pressure of acid gas removal unit absorber (kPa)	200
Bottom pressure of acid gas removal unit absorber (kPa)	220
Top temperature of the glycol removal unit absorber (°C)	32
Bottom temperature of the glycol removal unit absorber (°C)	29
Steam consumption in the glycol removal unit in both pathways (kg/hr)	1403
TEG flow rate in the glycol removal unit in both pathways (kg/hr)	5640
TEG pressure before being pumped in the glycol removal unit (kPa)	103
TEG pressure after being pumped in the glycol removal unit (kPa)	6274
Water separated in glycol removal unit in pathway I (kg/hr)	90
Water separated in glycol removal unit in pathway II (kg/hr)	83
Purified butane pressure in Pathway II (kPa)	165
Purified butane temperature in Pathway II (°C)	46
Purified butane flow rate in Pathway II (kg/hr)	87358
Inlet stream pressure to the demethanizer unit (kPa)	1300
Inlet stream temperature to the demethanizer unit (°C)	123
Refrigerant (propene) flow rate in the demethanizer unit (kg/hr)	260000
Refrigerant temperature before compression (°C)	99

Refrigerant pressure before compression (kPa)	51
Refrigerant temperature after compression (°C)	93
Refrigerant pressure after compression (kPa)	2100
Purified butane temperature in Pathway I (°C)	86
Purified butane pressure in Pathway I (kPa)	1150
Purified butane flow rate in Pathway I (kg/hr)	88000

A.4 Equation for calculating sampling errors for the Monte Carlo simulation

The Monte Carlo sampling error is calculated using the following equation and illustrates the error between simulations [86].

Sampling error is calculated using equation below,

Equation A.4: $\bar{X}=\frac{Z*\sigma}{\sqrt{n}}$

where n is the number of samples, σ is the standard deviation of the mean, and Z is equal to 2.58 for 99% confidence interval [86].

The number of simulation runs in each scenario was determined in order to keep the simulation sampling error below 0.1 kg CO2/bbl.

Table A.5: Number of simulation runs in each scenario [86]

Scenario	Number of simulation runs
2016 Alberta grid mix	20,000
2030 Alberta grid mix	7,000
Biomass	1,000
Cogeneration	10,000

Appendix B

Appendix B contains supplementary information for chapter 3.

B.1 Equation for the estimation of pump work

Equation B.1: $W_p = M_m * g * h + (M_v) * (P_{wellhead} - P_{reservior})$

where W_p is the pump work (kJ/bbl.), M_m is the mass of water and bitumen mixture (kg/bbl.), g is the gravity (m/s^2), h is the depth of the production well (m), M_V is the mixture volume (m^3), $P_{wellhead}$ is the wellhead pressure (kPa), and $P_{reservior}$ is the reservoir pressure (kPa).

B.2 Equations for the estimation of compressor work

The number of required compression stages is calculated through Equation B.2 [118]:

Equation B.2: $$m = ROUNDUP\left[\frac{ln(\frac{Pout}{P\,in})}{ln(CR\ max)}\right]$$

where m is the number of compression stages required, P_{in} is the inlet pressure [MPa], P_{out} is the outlet pressure [MPa], and CR_{max} = 5.

The discharge temperature at each compression stage is calculated through Equation B.3 [163].

Equation B.3: $$\frac{T_d}{T_s} = \left(\frac{P_{out}}{P_{in}}\right)^{\left[\frac{Cp/Cv}{Cp/Cv-1}\right]}$$

where Td is the discharge temperature [°R], T_s is the suction temperature [°R], and C_p/C_v is the ratio of specific heat at standard conditions.

Assuming 80% interstage cooling, the suction temperature of the next compression stage is calculated as follows [164]:

Equation B.4: $T_{S2} = T_s + (0.2)*(T_d - T_s)$

Assuming reciprocating compressors, the ideal isentropic compressor work in each compression stage is calculated as follows [163]:

Equation B.5: $-W_N = \left(\frac{Cp/Cv}{Cp/Cv - 1}\right) * \left(3.027 * \frac{14.7}{520}\right) * (T_d - T_s)$

where W_N is the adiabatic work of compressor at N_{th} stage ([hp-d/MMscf].

B.3 Equations for the estimation of GHG emissions from reservoir combustion and produced gas flaring

Associated GHG emissions from reservoir combustion [33] and flaring the produced gas are calculated with Equations B.6-B.7; compositions of produced gas are presented in Table 3.1; and the assumption is that the volume of produced gas is equal to the amount of injected air in the reservoir [33, 165].

Equation B.6: $GHG_{\text{reservoir combustion}} = AOR * \%CO_2 * \rho_{CO2}$

Equation B.7: $GHG_{flaring} = AOR * \sum_{i=1}^{4}(\%C_i * CEF_i)$

where the GHG emissions of reservoir combustion and hydrocarbon flaring are in $kgCO_2eq/m^3$ of bitumen, *AOR* is the air-to-oil ratio (m^3/m^3), $\%CO_2$ is the volume percent of CO_2 in the produced gas, ρ_{CO2} is the carbon-dioxide density at standard conditions (1.87 kg/m^3 [65]), $\%C_i$ is the mole percent of hydrocarbon i in the produced gas, and CEF_i is the combustion emission factor of hydrocarbon i (kg CO_2eq/m^3).

B.4 Assessing the flammability of the gas mixture

In order to determine whether a gas mixture is combustible or not, Le Chatelier's mixing rule for flammable limits is used [166]. First, the concentration of combustibles should be determined using Equation B.8:

Equation B.8: $C_c = \sum_{i=1}^{n} y_i$

where C_c is the concentration of combustibles, y_i is the mole fraction of the i^{th} component and, *n* is the number of components in the mixture.

Then lower flammability limit of mixture is obtained using Equation B.9:

Equation B.9: $LFL_{mix} = \frac{1}{\sum_{i=1}^{n} \frac{y_i}{LFL_i}}$ if $C_c \geq LFL_{mix}$, the mixture is combustible

where LFL_{mix} is the lower flammability of the mixture and LFL_i is the lower flammability limit of the i^{th} component.

The LFL of each hydrocarbon is taken from mathesongas.com [167]. Using these

equations B.8 and B.9, the gas mixture produced in the THAI process through reservoir combustion is found to be combustible.

B.5 Equations for the calculation of energy use in the transportation stage

The diluent ratio (DR) is calculated using Equation B.10 and found to be 12.28 vol % [112].

Equation B.10: $$DR = \frac{\rho_{dilbit} - \rho_{bitumen}}{\rho_{diluent} - \rho_{bitumen}}$$

The shipped volume (m^3/day) is calculated using Equation B.11 [56]:

Equation B.11: *Shipped volume,* $$\dot{V}_{shipped} = \frac{\dot{V}_{actual}}{1-DR}$$

In order to calculate the pipe diameter (in inches), Equation B.12 is used [56]:

Equation B.12: $$D_{approximate} = \left[\left[\sqrt{\frac{\dot{V}_{Shipped} * 4}{24*3600*\pi*V_{target}}}\right]\right] * \frac{1}{0.0254}$$

where V_{target} is the target velocity of the crude (m/s).

The closest value in the API 5 L standard [168] is chosen as the actual diameter of the pipeline, and the actual velocity of crude (V_{fluid}, m/s) is calculated using the equation below.

Equation B.13: $$V_{actual} = \frac{\dot{V}_{shipped} * 4}{24*3600*\pi*(D*0.0254)^2}$$

The Reynolds number of the flow is calculated from Equation B.14 [56]:

Equation B.14: $Re = \frac{\rho * D * V_{actual}}{\mu}$

where ρ is the density of crude (kg/m^3) and μ is its dynamic viscosity (Pa.s).

The initial friction factor is calculated from the Haaland friction factor [169]:

Equation B.15: $\frac{1}{f_{in}} = \frac{6.9}{Re} - 1.8 \log_{10}\left[\frac{(e/D)}{3.7}\right]^{1.11}$

where e is the relative roughness of the pipeline.

The exact friction factor is calculated using the Colebrook friction factor [170]:

Equation B.16: $\frac{1}{\sqrt{f_{out}}} = \frac{2.51}{Re\sqrt{f_{in}}} - 2.01 \log_{10}\left[\frac{(e/D)}{3.7}\right]^{1.11}$

where f_{out} is the iterative friction factor. The iteration is completed when the difference between the input (f_{in}) and output (f_{out}) friction factors is negligible (< 10^{-5}).

The working power of the pump (W) is calculated from the pressure loss from pipe friction ($P_{friction}$) and the change in elevation ($P_{elevation}$) using Equation B.17 [56]:

Equation B.17: $W_{pump} = ((P_{friction} + P_{elevation}) * \dot{V}_{shipped} * \frac{1}{24*3600}) / (\eta_{pump})$

where η_{pump} represents the pump efficiency.

Pumping energy is calculated using Equation B.18 [56]:

Equation B.18: $E_{pump} = \frac{W_{pump}}{\dot{V}_{shipped}} * \frac{24}{1000}$

B.6 Products and diluent cut point temperatures

The cut point temperature range for crude fractions that are used in Aspen HYSYS are presented in Table B.1.

Table B.1: Distillation temperature range of crude fractions [113]

Name of fraction	Temperature range °C
Diluent	71-135
Naphtha	135-235
Diesel	235-343
Gasoil	343-524
Vacuum residue	+ 524

B.7 Bitumen, dilbit, and SCO assays

The physical properties and distillation curve of THAI bitumen, dilbit, and SCO obtained from delayed coking and hydroconversion upgraders are presented in Tables B.2 and B.3, respectively. THAI bitumen distillation curve and physical properties were obtained from the Whitesands Experimental Project Annual Report and Hart et al. [119, 121]. The dilbit distillation curve was found by mixing naphtha and THAI bitumen with a diluent-to-bitumen ratio of 12.28 vol% in Aspen HYSYS [80], as discussed in section 3.2.2.2. The properties of SCO's are obtained from the upgrader simulation in Aspen HYSYS [80].

Table B.2: Bitumen, dilbit, and SCOs physical and chemical properties [80, 119, 121, 136]

Properties	Bitumen	Dilbit	DC SCO	HC SCO
API	14.10	22.10	34.33	34.48
Sulfur content, wt%	3.52	3.12	0.11	0.08
Viscosity at 20°C , mPa s	1091.00	268.00	17.74	8.76
CCR, wt%	7.20	6.38	0.02	0.05

Table B.3: Distillation curve of bitumen, dilbit, and SCO [80, 119, 121, 136]

	Bitumen	Dilbit	DC SCO	HC SCO
Mass%		Temp (°C)		
5	148	98	150	152
10	184	108	165	167
15	211	117	186	193
20	234	130	215	221
25	257	155	236	244
30	282	199	256	260
35	307	228	270	273
40	333	257	280	285
45	360	288	290	296
50	389	320	300	306
55	421	353	310	315
60	457	389	320	325
65	497	430	331	335
70	542	476	342	347
75	594	530	354	372
80	654	593	367	403
85	720	670	382	424
90	780	751	402	444
95	838	824	430	472
99	887	884	467	520
100	900	900	482	626

B.8 Calculation of the H_2 requirements of hydrotreaters in upgraders

The amount of H_2 required in the upgrader hydrotreater units is calculated from Equation B.19-B.21 taken from Edgar and Ancheyta [125, 126].

Equation B.19: $HDS=97.5 \frac{scf}{bbl} * wt\%\ sulfur\ removed$

Equation B.20: $HDN=325 \frac{scf}{bbl} * wt\%\ nitrogen\ removed$

Equation B.21: $HDA= 27 \frac{scf}{bbl} * wt\%\ aromatic\ saturated$

where *HDS*, *HDN*, and *HDA* are hydrodesulphurization, hydrodenitrogenation and hydrodearomatization.

H_2 is added to the hydrotreater feed to meet the specifications of upgrader products (naphtha, diesel, and gasoil) as shown in Table 3.3.

B.9 Produced gas energy content and emission factor calculation

The energy content and GHG emissions from the combustion of gas produced in upgraders and refineries are calculated using Equations B.22 and B.23 and from the values presented in Table B.4. The compositions of produced gases are obtained from the Aspen HYSYS simulation.

Equation B.22: Heat generated by produced gas (MJ/kg) = $\sum_{i=1}^{n} \frac{(LHV)_i * m_i}{\eta_b}$

Equation B.23: Combustion emissions of the produced gas ($gCO_2eq./MJ$) = $\sum_{i=1}^{n} \frac{(LHV)_i * m_i * EF_i}{\eta_b}$

where *i is the* individual gas component, *n* is the total number of gas components, *LHV* is the lower heating value (MJ/kg), m_i is the mass content of individual gas (%), EF_i is the combustion emission of individual gas (gCO_2 eq./MJ), and η_b is the burner efficiency.

Table B.4: Composition of the produced gas in upgraders and refineries

Component	LHV (MJ/kg), [65]	CEF (gCO_2 eq./MJ), [120]	Mass content [80]				
			DCU	HCU	Bitumen refinery	DC SCO refinery	HC SCO refinery
Hydrogen	119.96	0.00	1.67	0.12	1.15	0.76	0.57
Methane	50.00	50.59	39.92	48.00	38.33	33.33	31.64
Ethylene	47.62	62.89	12.41	13.00	10.72	9.84	7.55
Ethane	47.62	56.83	18.29	16.00	35.29	39.15	40.61
Propene	46.35	59.94	11.49	8.00	0.00[a]	0.00[a]	0.00[a]
Propane	46.35	59.94	2.98	4.80	14.51	16.92	19.64
i-Butane	45.75	61.92	1.34	2.10	0.00[a]	0.00[a]	0.00[a]
1-Butene	45.75	61.76	5.46	4.60	0.00[a]	0.00[a]	0.00[a]
n-Butane	45.75	61.82	6.43	3.50	0.00[a]	0.00[a]	0.00[a]

[a]: The reason these values are not zero in the upgraders is that these components have been separated in the refinery and directed to the reformer and alkylation unit for gasoline production as shown in Fig. 3.5.

B.10 Default values in the model for combustion in vehicles

Table B. 5 lists the values used to estimate GHG emissions from the combustion of transportation fuels.

Table B.5 : Transportation fuels combustion emissions [35]

Fuel type	Combustion emissions	Unit
Gasoline	72.71	gCO_2eq/MJ of gasoline
Diesel	74.90	gCO_2eq/MJ of diesel
Jet fuel	72.80	gCO_2eq/MJ of jet fuel

B.11 Converting transportation emissions into $gCO_2eq./MJ$

In order to convert transportation emissions into $gCO_2eq./MJ$ of transportation fuels Equation B.24 is used.

Equation B.24: $E_{trans} = ((E_{dilbit} + (E_{diluent} * DR)) * \frac{1}{SCO\ yield}) + E_{SCO}$

where E_{trans} is the GHG emissions associated with crude transportation (g CO_2eq/bbl of crude), E_{dilbit} is the emissions in the transportation of dilbit (g CO_2eq/bbl of bitumen), $E_{diluent}$ is the emissions associated with diluent return to the extraction site (gCO_2eq/bbl of diluent), DR is the diluent ratio (vol %), and E_{SCO} is the emissions in the transportation of SCO from the upgrader to the refinery (g CO_2/bbl SCO).
The above equation is simplified into Equation B.25 in the direct bitumen refinery pathway.

Equation B.25: $E_{trans} = (E_{dilbit} + E_{diluent} * DR)$

B.12 Converting upstream refinery emissions into $gCO_2eq./MJ$

Equation B.26 is used to convert the upstream refinery emissions into gCO_2eq/MJ of transportation fuel.

Equation B.26: $E_{upstream} = ((((E_{extraction} + E_{trans} + E_{upgrader}) * \frac{1}{SCO\ yield})) * DBP) * \frac{1}{M_i * LHV_i} * \frac{(M_i * LHV_i)}{\sum_{i=1}^{3} (M_i * LHV_i)}$

where $E_{upstream}$ is the upstream GHG emissions prior to the refinery process (g CO_2eq/MJ

of transportation fuel), $E_{extraction}$ and $E_{upgrader}$ are the GHG emissions in the extraction stage and in the upgrading process, respectively, and both are in g CO_2eq/bbl bitumen, E_{trans} is the GHG emissions associated with transportation to the refinery (g CO_2eq/bbl of crude) (obtained using Equation B.24 or Equation B.25), *DBP* is the daily barrel production of bitumen, *i* is transportation fuel i (one of gasoline, diesel, and jet fuel), *M* is the daily mass production of the transportation fuel, and *LHV* is the lower heating value of the transportation fuel (KJ/Kg).

In the direct bitumen refinery pathway, the equation is simplified as follows: Equation B.27: $E_{upstream} = ((((E_{extraction}+E_{trans})*DBP)*\frac{1}{M_i*LHV_i}*\frac{M_i}{\sum_{i=1}^{3}(M_i*LHV_i)}$

where E_{trans} is the GHG emissions associated with the transportation of bitumen to the refinery (g CO_2eq/bbl of bitumen).

B.13 Life cycle impact assessment

CO_2, N_2O, and CH_4 are the greenhouse gases considered in this study. The global warming potential (GWP) factors used are with a 100-year time horizon and based on the Fifth Assessment Report of the Intergovernmental Panel on Climate Change (IPCC) [158].

B.14 Sensitivity analysis

The X-axis of the Morris plot represents the average deviation from the base value and the Y-axis shows the standard deviation of the changes [141]. Variables with a 1% average deviation from the output value were considered sensitive [12].

B.14.1 WTC sensitivity analysis results

As shown in the Morris plots in Fig.B.1-B.9, the air-to-oil ratio, interstage cooling, injected air pressure into the reservoir, amount of hydrocarbons and CO_2 in the produced gas, emission factor of electricity, pipeline target velocity, H_2 consumption in the upgraders, SMR feedstock and fuel, and the efficiency of the compressors, heaters, pumps, and reboilers were found to be sensitive to the production of all transportation fuels in all pathways. H_2 consumption in the reformer, NHT and HC units are sensitive parameters for the production of gasoline. Diesel production is sensitive to H_2 consumption in the HC and DHT. H_2 usage in the KHT unit is a sensitive input for jet fuel production in all pathways.

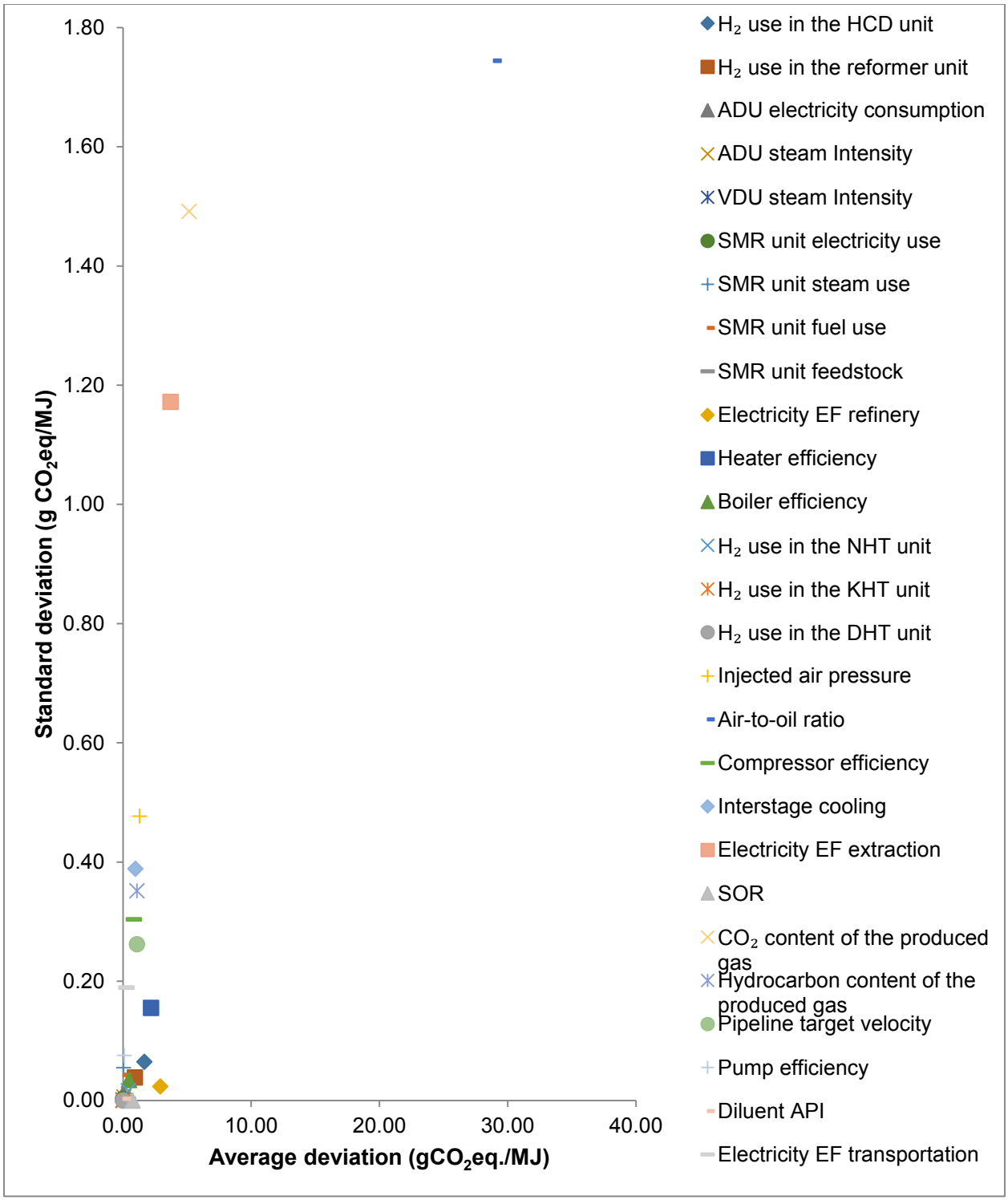

Fig. B.1. Morris plot of the WTC sensitivity analysis for the production of gasoline in pathway 1

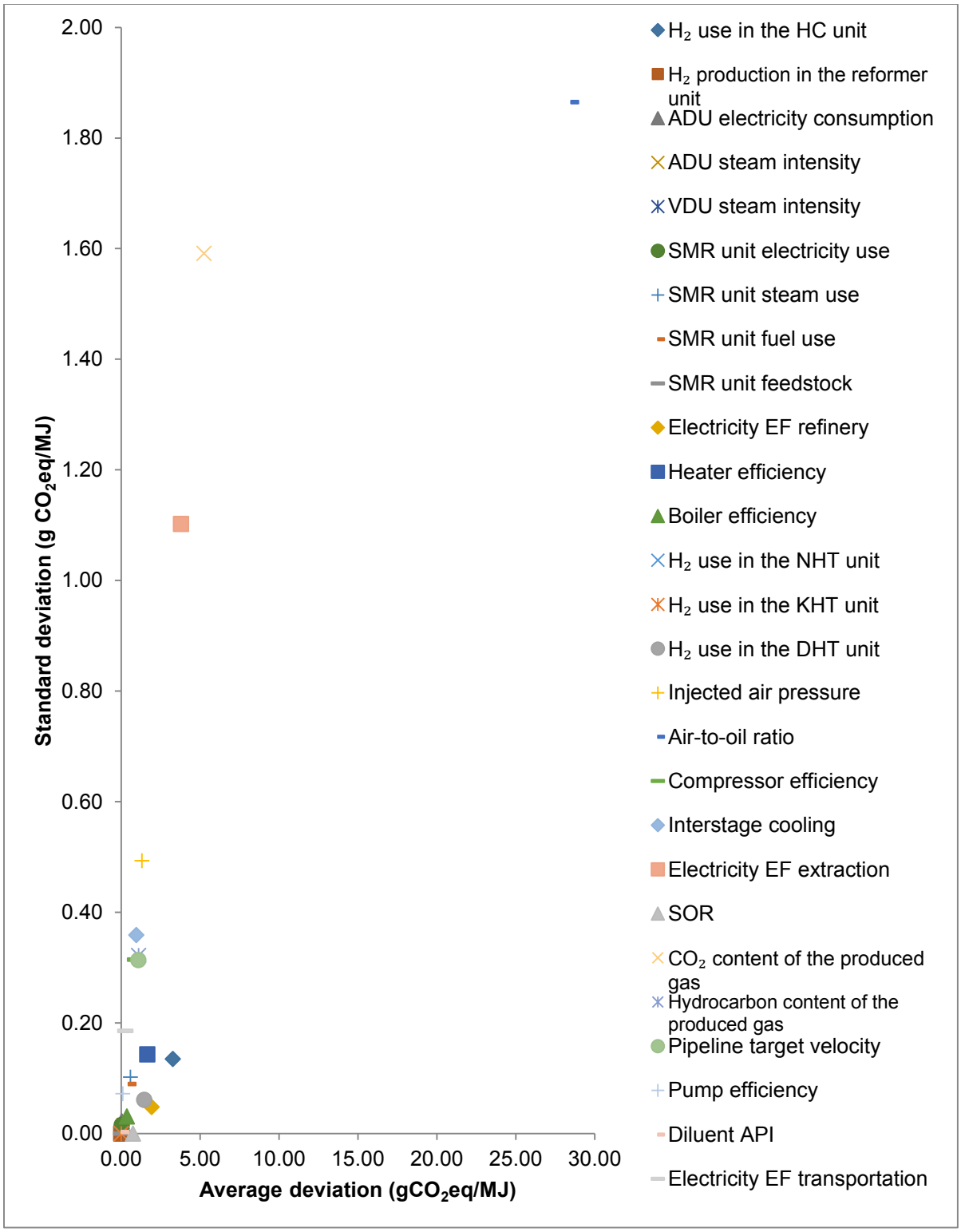

Fig. B.2. Morris plot of the WTC sensitivity analysis for the production of diesel in pathway 1

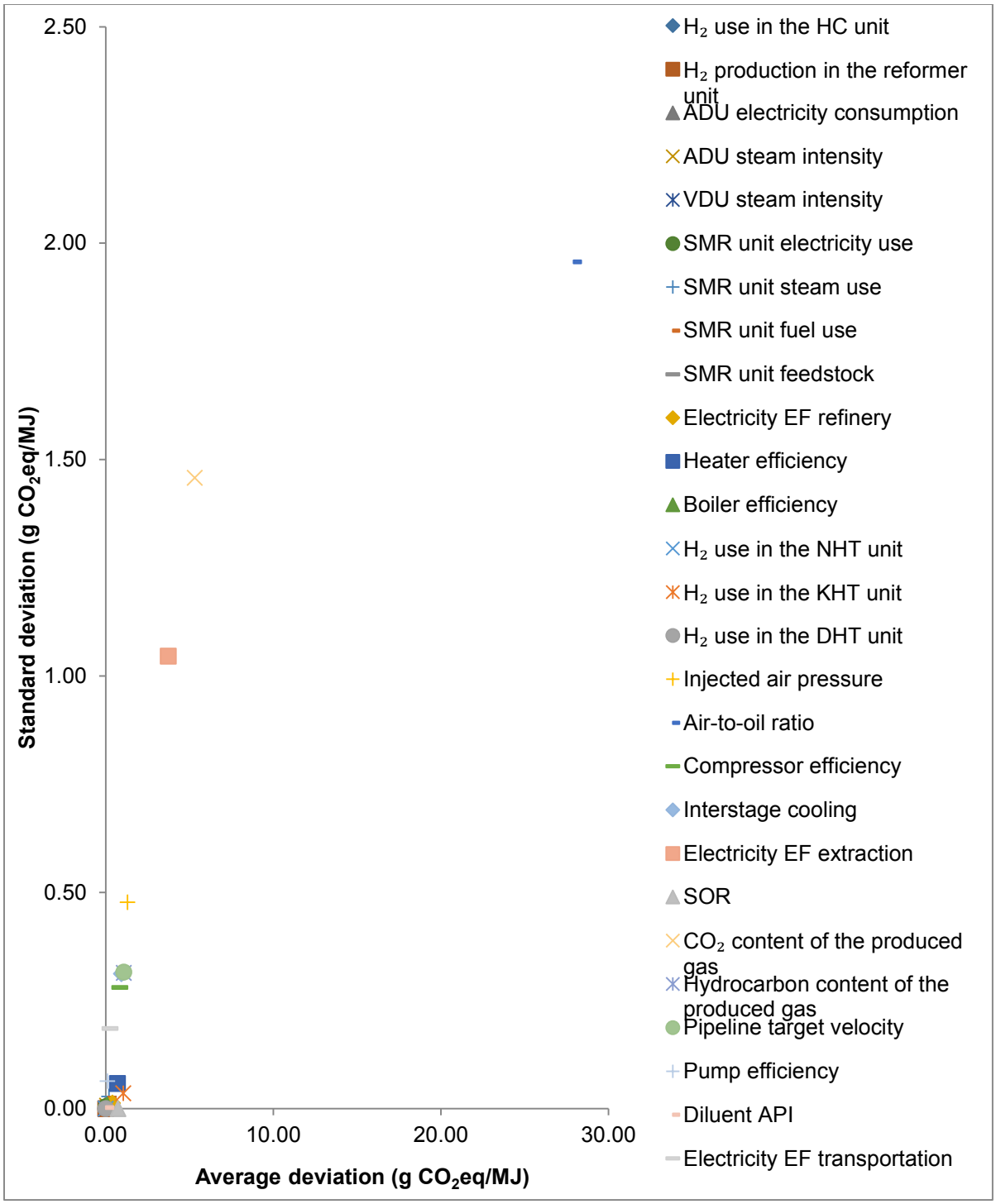

Fig. B.3. Morris plot of the WTC sensitivity analysis for the production of jet fuel in pathway 1

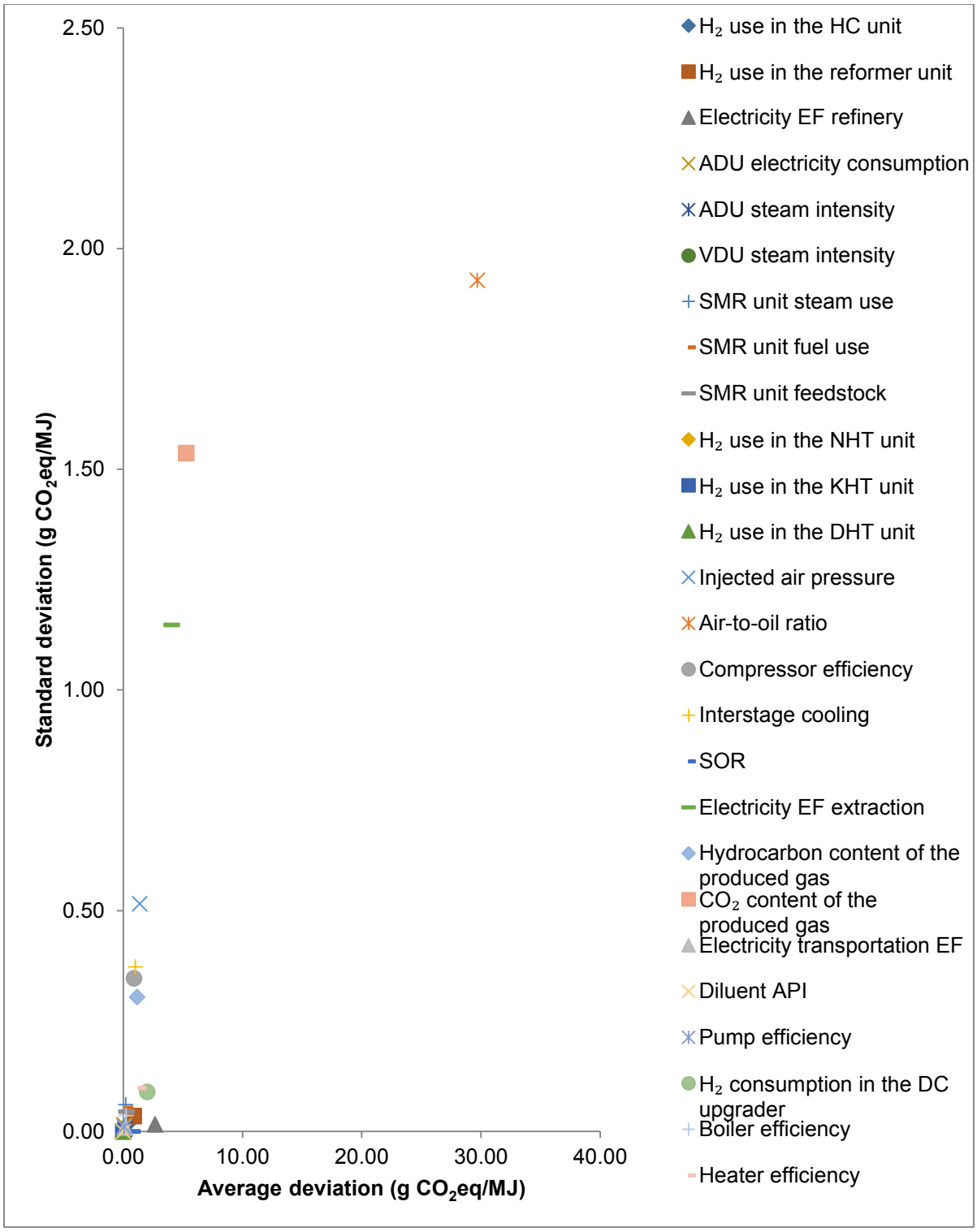

Fig. B.4. Morris plot of the WTC sensitivity analysis for the production of gasoline in pathway 2

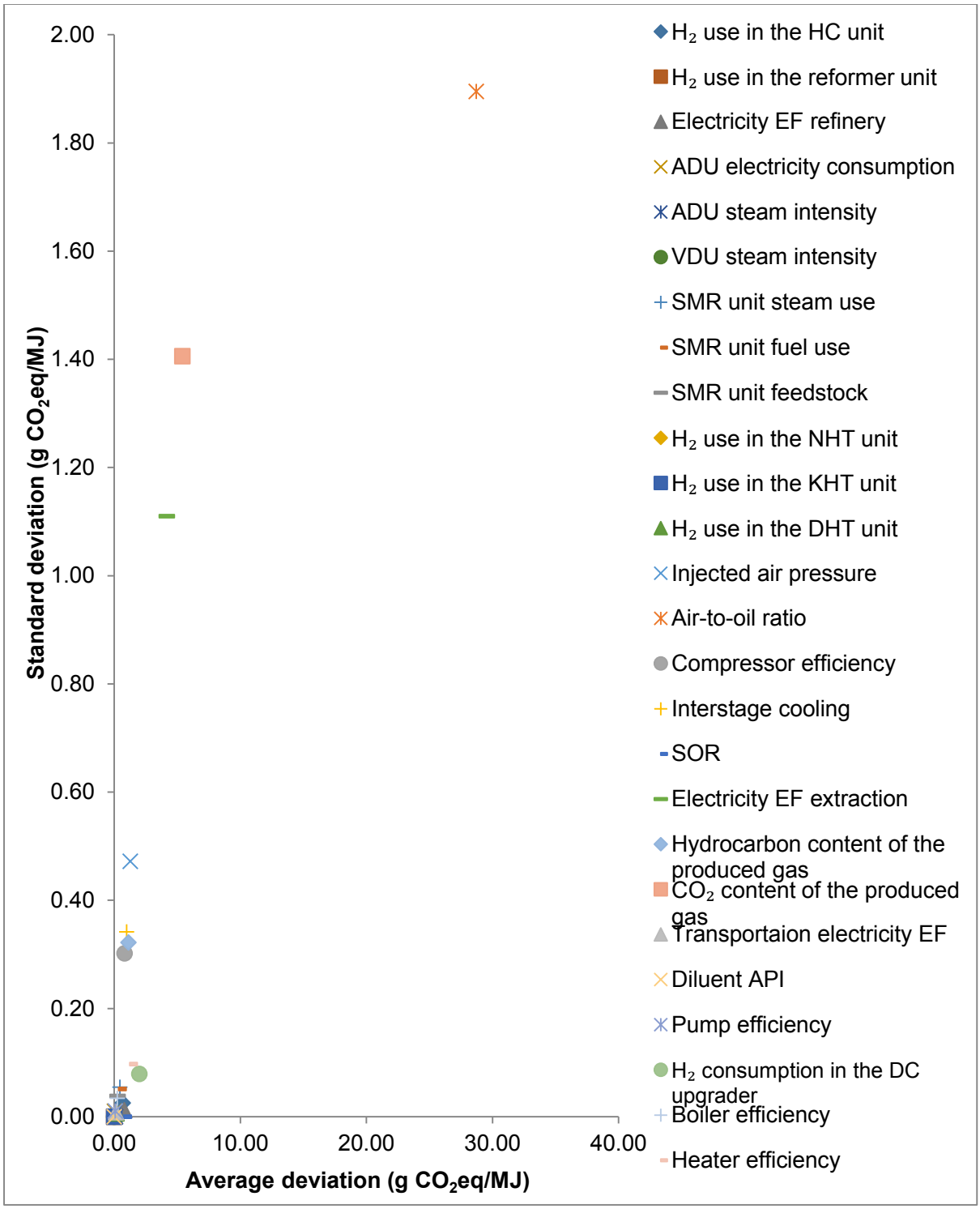

Fig. B.5. Morris plot of the WTC sensitivity analysis for the production of diesel in pathway 2

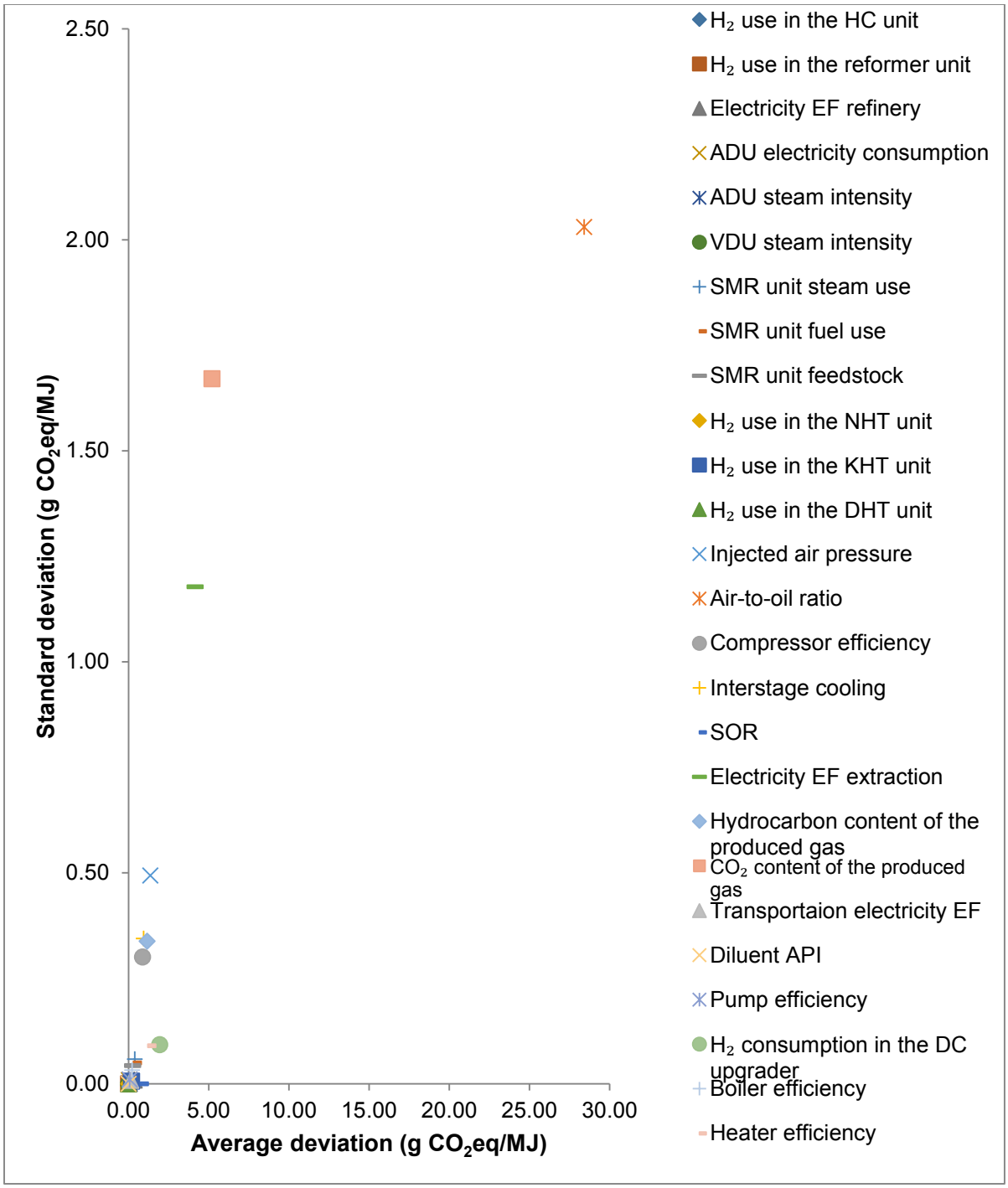

Fig. B.6. Morris plot of the WTC sensitivity analysis for the production of jet fuel in pathway 2

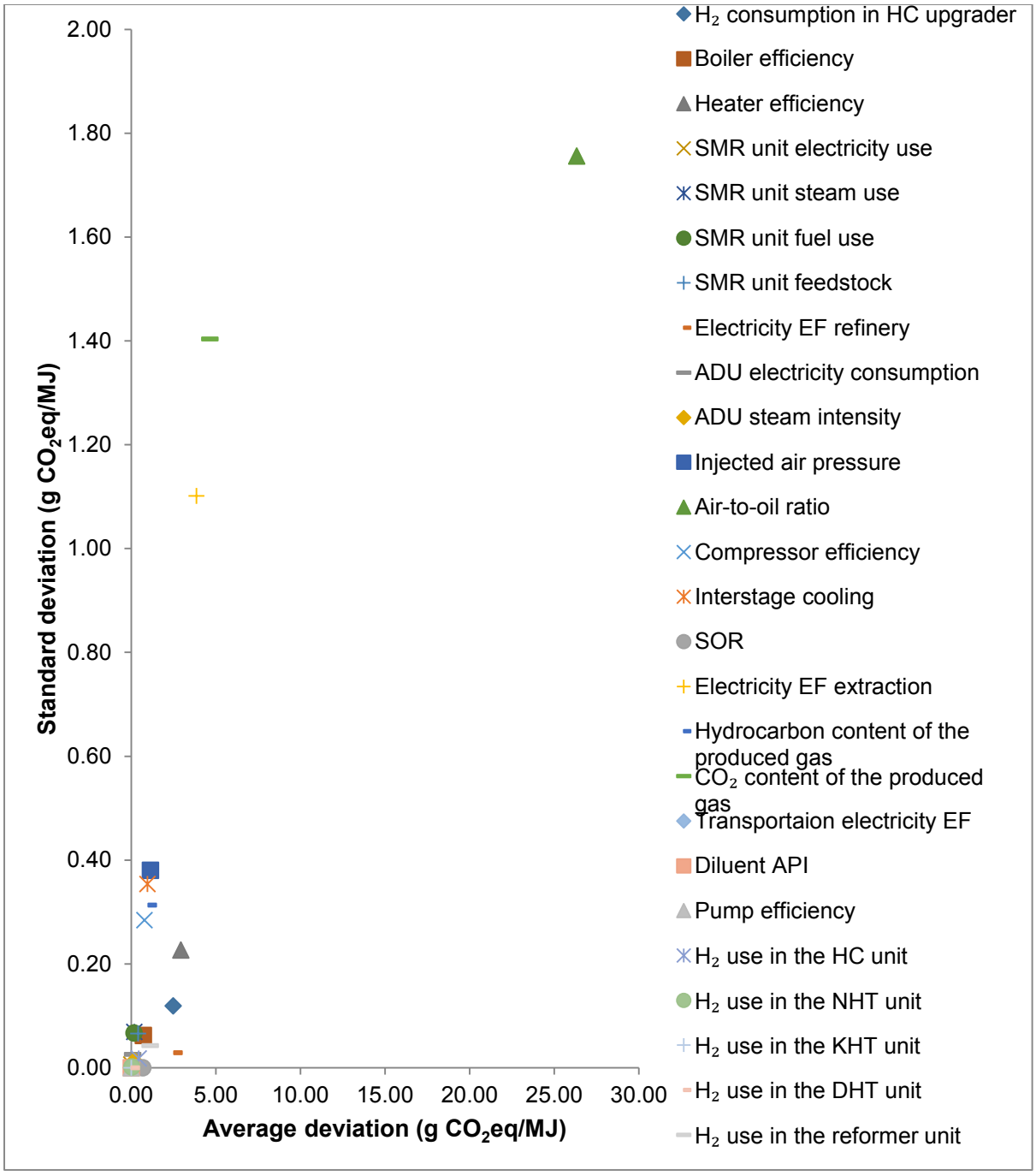

Fig. B.7. Morris plot of the WTC sensitivity analysis for the production of gasoline in pathway 3

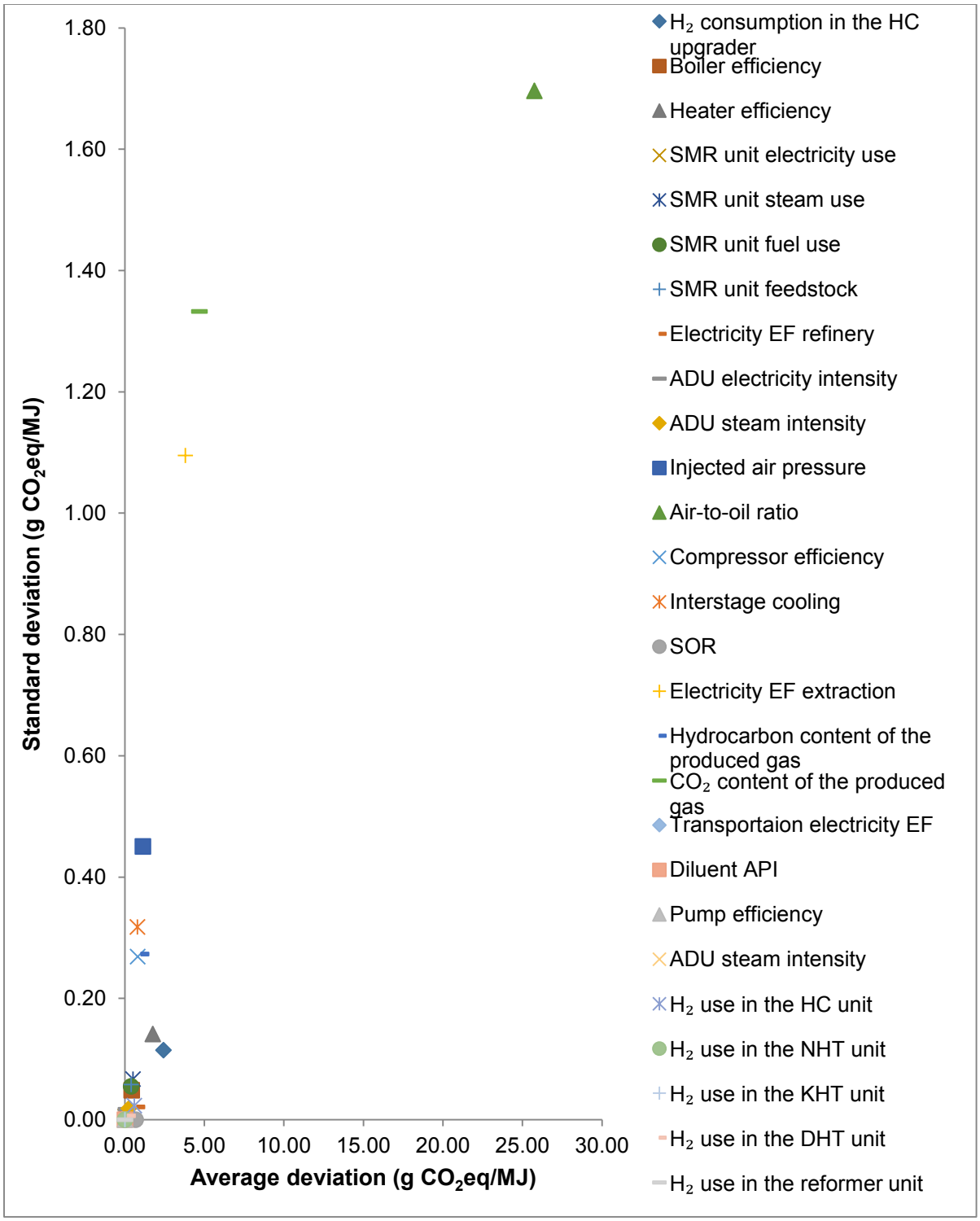

Fig. B.8. Morris plot of the WTC sensitivity analysis for the production of diesel (pathway 3)

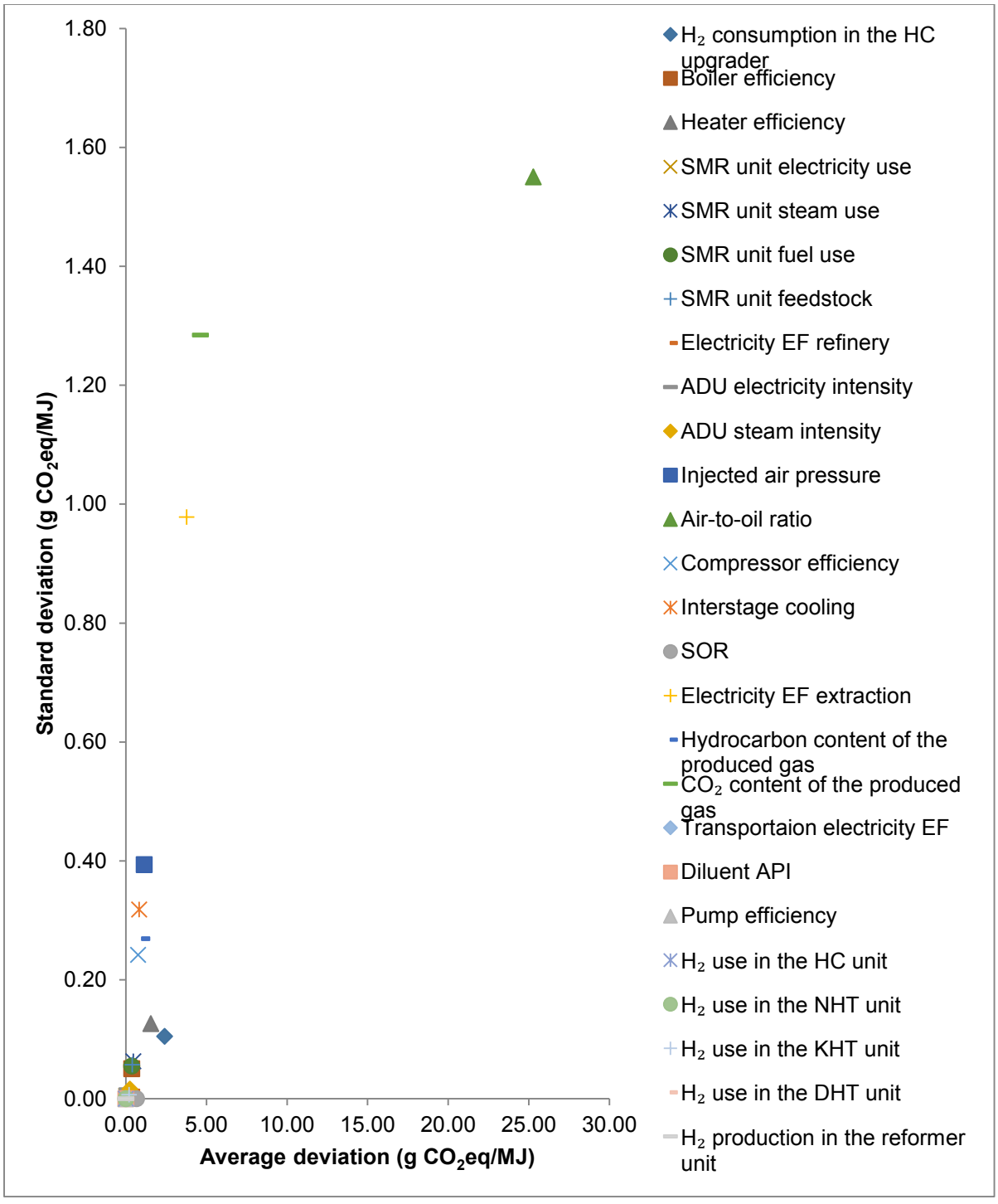

Fig. B.9. Morris plot of the WTC sensitivity analysis for the production of jet fuel (pathway 3)

15.0 WTC tornado plots for diesel and jet fuel production in different pathways

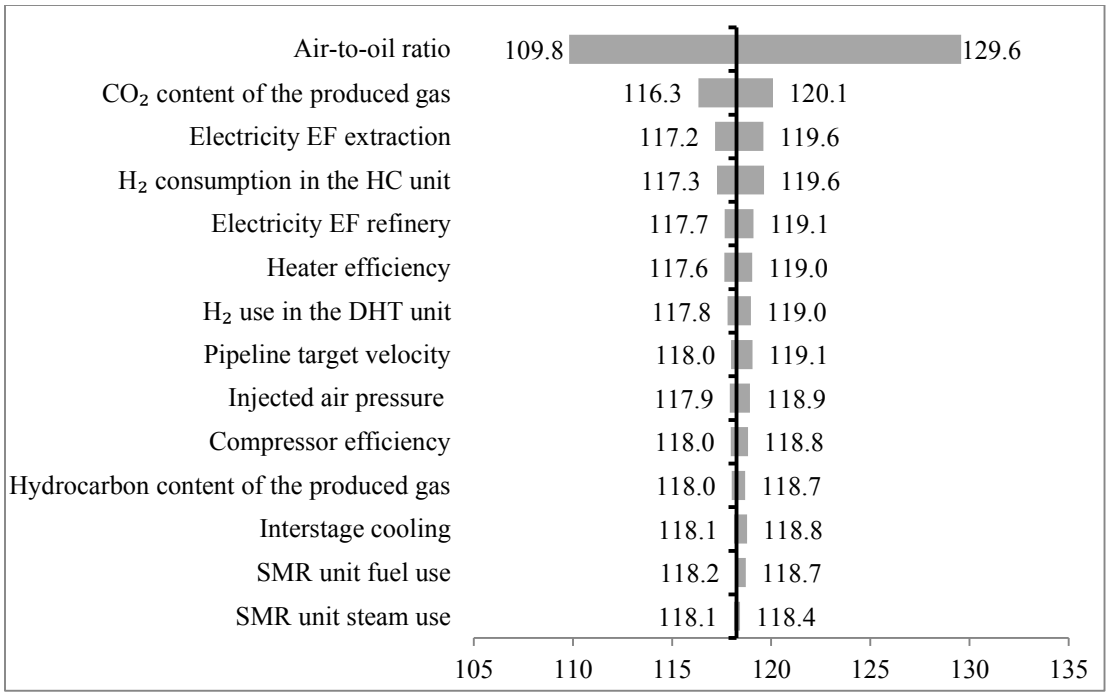

Fig. B.10. Tornado plot for the WTC GHG emissions for the production of diesel in the bitumen refinery pathway

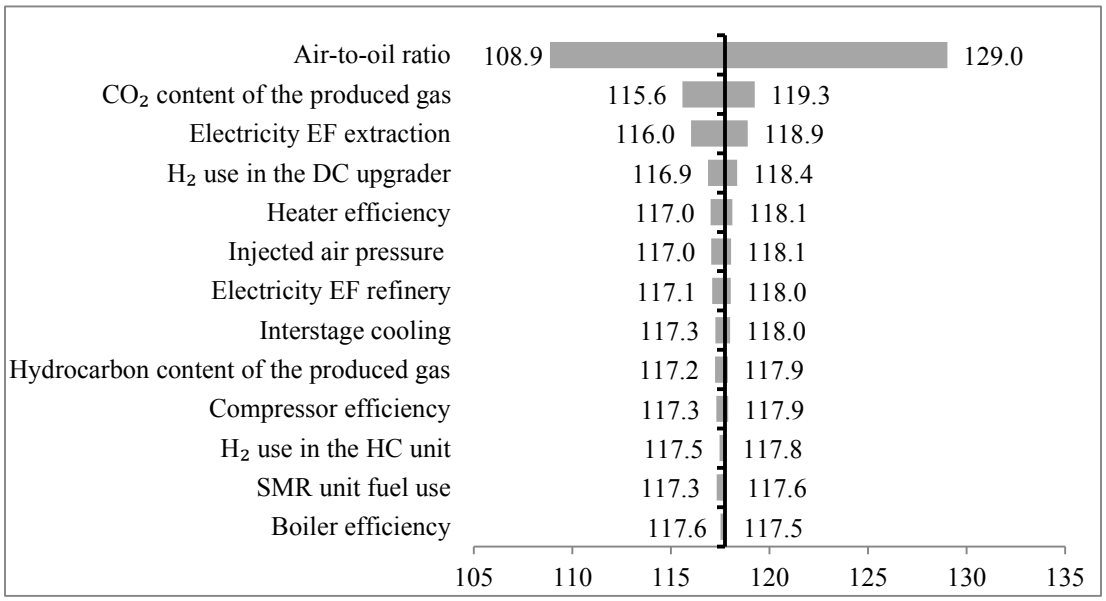

Fig. B.11. Tornado plot for the WTC GHG emissions for the production of diesel in the delayed coker pathway

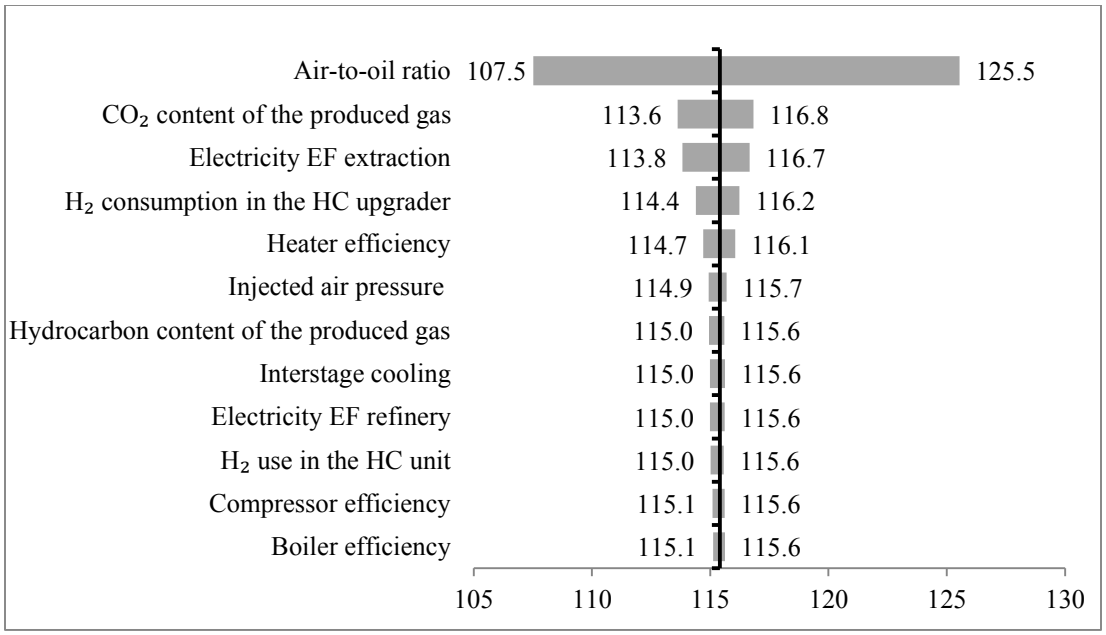

Fig. B.12. Tornado plot for the WTC GHG emissions for the production of diesel in the hydroconversion pathway

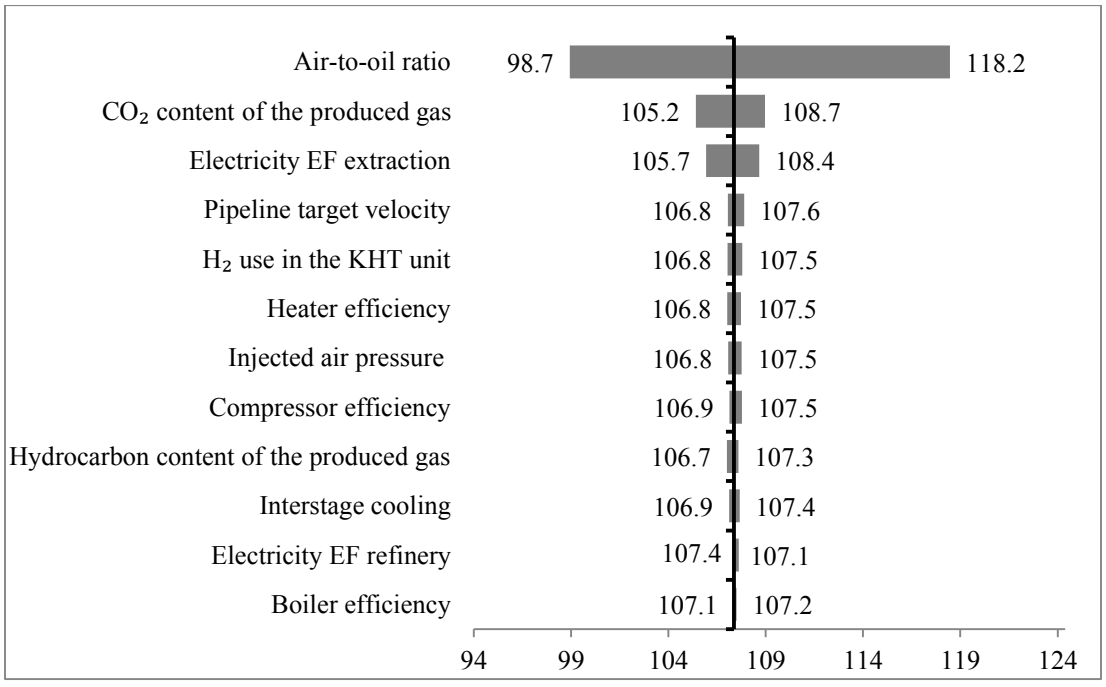

Fig. B.13. Tornado plot for the WTC GHG emissions for the production of jet fuel in the bitumen refinery pathway

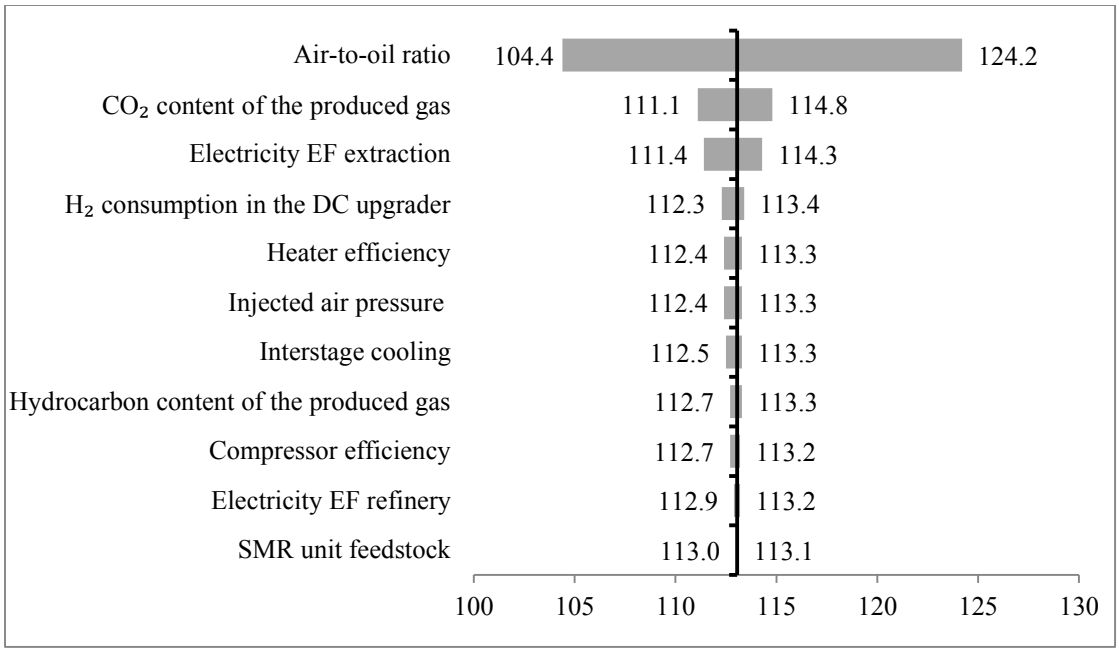

Fig. B.14. Tornado plot for the WTC GHG emissions for the production of jet fuel from refining the delayed coker SCO

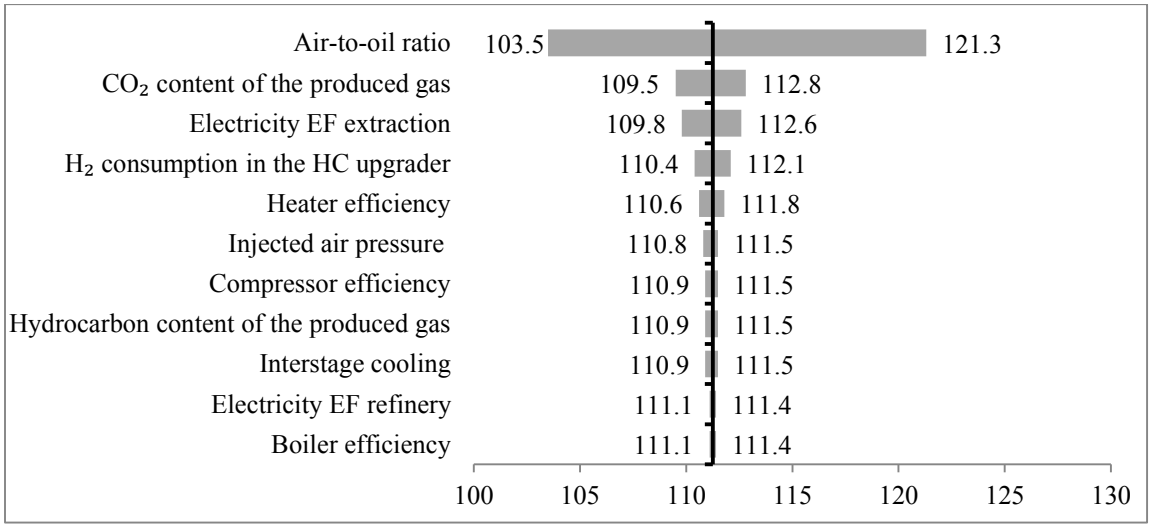

Fig. B.15. Tornado plot for the WTC GHG emissions for the production of jet fuel from refining the hydroconversion SCO

B.16 Equation for calculating the sampling error for the Monte Carlo simulation

The Monte Carlo sampling error is calculated using the following equation and illustrates the error between simulations [86]:

Equation B.28: $\bar{X}=\frac{Z^{*}\sigma}{\sqrt{n}}$

where $\bar{X}$ is the sampling error, n is the number of samples, σ is the standard deviation of the mean, and Z is 2.58 for 99% confidence interval simulations [86].

The number of simulations was determined in order to keep the simulation sampling error to less than 0.5 gCO_2eq/MJ for the well-to-combustion stages.